

AN ABSTRACT OF THE THESIS OF

Trevor M. F. Takaro for the degree of Master of Science in Mechanical Engineering
presented on June 3, 2015.

Title: Shocks and Awe: Damping Selection in Racecars to Maximize Grip

Abstract approved:_____

Dr. Robert Paasch

This thesis covers the use of a quarter car model to select damping rates for a Formula Student (FS) car, focusing on minimizing vertical tire force variation to improve grip. A 2 degree of freedom (DOF) quarter car model is cycled over the road frequencies of interest and the results compared with the 2 DOF optimum damping proposed by in references [1, 2, 3].

Using the Global Formula Racing (GFR) 2011 FS combustion vehicle, four different damper configurations are evaluated on FS style courses. Strain gauges on the suspension links are used measure all six tire forces and moments, compare between setups, and evaluate the relationship between vertical load variation and in-plane grip. Finally, the results of the simulation and physical tests are compared and the validity and utility of the 2 DOF quarter car model is assessed. Three standardized test tracks are utilized as well an artificial bump similar to that studied in reference [4].

©Copyright by Trevor M. F. Takaro

June 3, 2015

All Rights Reserved

Shocks and Awe: Damping Selection in Racecars to Maximize Grip

by

Trevor M. F. Takaro

A THESIS

submitted to

Oregon State University

in partial fulfillment of
the requirements for the
degree of

Master of Science

Presented June 3, 2015
Commencement June 2015

Master of Science thesis of Trevor M. F. Takaro presented on June 3, 2015

APPROVED:

Major Professor, representing Mechanical Engineering

Chair of the Department of Mechanical, Industrial and Manufacturing Engineering

Dean of the Graduate School

I understand that my thesis will become part of the permanent collection of Oregon State University libraries. My signature below authorizes release of my thesis to any reader upon request.

Trevor M. F. Takaro, Author

ACKNOWLEDGEMENTS

This paper is a collection of small part of my work on the Global Formula Racing team (GFR). Many people have played key roles in the success of the team, here I attempt to thank and acknowledge the people most influential in the ideas and work presented here.

Dr. Robert Paasch - IEs, organization, standing up for yourself

Dr. Christopher Patton - Tire modeling. MATLAB. Tire theory vs. practice.

Bill Murray - Focus on what you actually care about. Question everything.

Jeff Delany and Trenton Carpenter - Sometimes you just need to bite the bullet and work through it.

Chris Billings - Skip the frequency stuff - what is your damper actually doing? Go back to the actual forces.

Vehicle preparation: Bill Murray, Chris Patton, Alex Ursin, Clayton Wilson, Chris Billings

Driving: Phil Arscott, Doug Peterman

Photos: Robert Story, Jay Swift, Marshall Wagoner, Ankit Agarwal, FSG Photography team

Test location: Heather Sorenson, NW UAV

CONTRIBUTING AUTHORS

A popular adage in GFR is *No one of us is as smart as all of us*. As such much of the work done by the team is extremely collaborative. Three other GFR members were instrumental in the design and execution of the simulations and vehicle testing contained in this thesis. This section seeks to acknowledge their contribution to the work and results presented herein.

Chris Patton is responsible for many of the fundamental concepts used in the simulation and physical testing contained in this thesis. Chris came up with the idea of physical comparison of damping configurations and the artificial bump, as well as developed a plan of damper configurations, test types and analysis criterion. His work formed a first draft of the testing and simulation built on in this thesis. He also selected the final spring and damping rates for the physical test. His work in building a novel non dimensional tire model fit to FSAE Tire Test Consortium data laid the groundwork for what GFR's knowledge of tires and provides the data used in figure 1.5.

Bill Murray lead the design, development and implementation of the data acquisition system on the test vehicle. Together with the work of Alex Ursin they created one of the most instrumented cars in FSAE history without which this thesis could not be possible. Bill designed the full vehicle strain gauge calibration procedure and suspension link angle calculation based on suspension travel, allowing full vehicle forces to be measured, creating a logical approach to logging rate selection in the process. Bill created the *GFR Full Analysis V2* MoTeC project on which the author continued development for this thesis. Bill also heavily influenced the final test plan, contributing the idea of running the straightline and skidpads at two speeds to examine any speed dependency. Finally, Bill performed the tire vertical spring rate testing at a range of pressures. This data is used in the quarter car model.

Alex Ursin implemented the instrumentation on the test vehicle, critically the full

bridge strain gauges on each suspension link. Significant effort was put into the robustness of the system, allowing reliable operation years later.

Chris Billings and his Shock Shop allowed regular use of a shock dyno, tools and shock internals. Chris built the shocks used in this test and provided regular input and feedback on damper theory and test design.

Clayton Wilson performed the data acquisition system calibration before the test.

The 2011 GFR Team designed, and built the car.

TABLE OF CONTENTS

| | <u>Page</u> |
|---|-------------|
| 1. BACKGROUND | 1 |
| 1.1. The Formula Student competitions | 2 |
| 1.1.1 Global Formula Racing | 3 |
| 1.2. The objective of the FS car | 4 |
| 1.3. Tire Theory | 5 |
| 1.4. Load transfer | 8 |
| 1.5. Damper Theory | 9 |
| 2. MATERIALS AND METHODS | 14 |
| 2.1. Quarter Car Modeling | 14 |
| 2.1.1 Determining damping rates | 17 |
| 2.2. Physical Testing | 18 |
| 2.2.1 Onboard data logging system | 20 |
| 2.2.2 Damper builds | 23 |
| 2.2.3 Test tracks | 25 |
| 2.2.4 Test plan | 27 |
| 3. RESULTS | 29 |
| 3.1. Simulation | 29 |
| 3.1.1 Straightline without anti-roll bar | 30 |
| 3.1.2 Straightline with anti-roll bar | 34 |
| 3.1.3 Cornering with anti-roll bar | 35 |
| 3.1.4 Changes between straight line / cornering | 40 |
| 3.2. Vehicle testing | 40 |
| 3.2.1 Straightline | 40 |
| Straightline without bump | 41 |
| Straightline with bump | 46 |
| 3.2.2 Skidpad | 52 |
| Skidpad without bump | 52 |

TABLE OF CONTENTS (Continued)

| | <u>Page</u> |
|---|-------------|
| Skidpad with bump..... | 58 |
| 3.2.3 Asymmetric Oval | 64 |
| 3.2.4 Subjective Driver Evaluation | 70 |
| 3.3. Summary of system resonance | 71 |
| 4. DISCUSSION | 74 |
| 4.1. The “best” damper | 74 |
| 4.2. Validity of reducing vertical load variation | 75 |
| 4.3. Quarter car model..... | 75 |
| 4.4. Noise in data - cloudiness of conclusions | 78 |
| 4.5. Designing a new damping curve | 78 |
| 5. CONCLUSION | 81 |
| 5.1. Recommendations for FSAE teams | 82 |
| 5.2. Dampers for other applications | 83 |
| 5.2.1 Ride | 83 |
| 5.2.2 Aero platform..... | 84 |
| 5.3. Future work | 84 |
| 5.3.1 Further analysis of existing data | 85 |
| 5.3.2 Softer than baseline dampers..... | 85 |
| 5.3.3 On track damper selection | 85 |
| 5.3.4 Bilinear dampers..... | 86 |
| 5.3.5 Quadrilinear dampers and airshocks | 86 |
| 5.3.6 Inerters, mass dampers and other additional springing devices ... | 87 |
| 5.3.7 Expansion of data acquisition | 87 |
| Damper rod force..... | 87 |
| Sprung mass accelerations | 88 |
| Optical slip angle sensors | 88 |
| High speed video | 88 |
| 5.3.8 More advanced simulations..... | 89 |

TABLE OF CONTENTS (Continued)

| | <u>Page</u> |
|--|-------------|
| 5.3.9 Longitudinally interconnected suspensions | 89 |
| BIBLIOGRAPHY | 90 |
| APPENDICES | 93 |
| A APPENDIX A Quarter car model | 94 |
| A1 Equation Derivations | 94 |
| Equations of motion for 2 DOF system without tire damping..... | 95 |
| A2 1 DOF Sprung mass equations of motion | 98 |
| A3 Additional quarter car model output | 99 |
| B APPENDIX B Damper and Spring Force curves..... | 101 |
| C APPENDIX C Strain gauge calibration..... | 107 |
| D APPENDIX D Excerpts from logged data | 108 |
| D1 Driver comments..... | 108 |
| D2 Round 2 straight without bump FFTs..... | 109 |
| D3 Round 1 skidpad without bump FFTs..... | 110 |
| D4 Round 2 resonant frequency summary | 111 |
| D5 Damper speeds | 111 |
| D6 Driver inputs | 114 |
| E APPENDIX E Round 1 Test day photos..... | 115 |

SHOCKS AND AWE: DAMPING SELECTION IN RACECARS TO MAXIMIZE GRIP

1. BACKGROUND

If you have broken or malfunctioning legs, then you generally get around faster with some crutches. Likewise, most cars (racing or production) have very crudely designed “springing”, so they go a bit faster when given some crutches, err..., I mean dampers.

-Erik Zapletal

The goal of any racing vehicle is to complete the given race course in minimum time within given constraints. Differences in these constraints give each racing series or competition a unique set of competitive vehicles. We will examine the role of dampers in the vehicle suspension system, looking at their contribution to handling performance. Despite significant work in vehicle dynamics and handling, there is not significant agreement in literature about the importance of dampers in the system or how they should be used. Many of the race engineer’s first resources on vehicle design and setup such as the works of Carroll Smith in references [5, 6, 7], Racecar Engineering and Mechanics [8], Competition Car Suspension [9], or Learn & Compete [10] only scrape the surface of the damping problem, often leaving it as something to tune on track through lap times and driver feel.

This thesis seeks to explain through theory, simulation and testing the correct role of the damper in the race car suspension, and simple approaches to tune them for best

performance. Put simply, the damper's role in the suspension and how it should be tuned for best performance is not well understood and backed up with on track data. This investigation seeks to use simulation and testing to find the right damping in a suspension, starting with fundamental vehicle dynamics and following a logical engineering approach. Symmetric linear dampers are used to demonstrate these fundamentals so that more complex configurations can be evaluated with the same metrics and used should they show superior performance.

A Formula SAE car will be used as the basis for study there were already significant resources in place for study of vehicle behavior through the Formula SAE team at Oregon State University, known as Global Formula Racing.

1.1. The Formula Student competitions

Formula SAE and Formula Student are collegiate engineering design competitions which challenge students to design, build and test small, extremely high performance race cars. More than 450 universities around the world field teams to compete in nine official and numerous unofficial competitions. Of the 1000 points available in competition, 675 are scored in the 5 dynamic events, which test vehicle performance on track. In addition to proving the cars' performance on acceleration, skidpad and autocross courses, teams must defend the engineering, cost and marketability of their design to industry judges.

The relatively open rules set allows a variety of vehicle concepts to be competitive, with vehicles weighing from 140 to 220 kg with 250 to 610 cc engines competing together. Forced induction and aerodynamic devices are also legal and relatively minimally regulated. Although atypical for an autocross competition, FS competitions also award points for fuel efficiency and since 2010 have had classes for electric vehicles.

Although designed, assembled and in many cases fabricated entirely by college stu-

dents, the quality of cars produced is extremely high and performance of vehicles from top level teams exceed those of any production car, kart or motorcycle on FS courses. The educational aspect of the competitions in turn is popular with corporate sponsors and university research.

The three factors of open rule set, high vehicle performance, and strong research support allow huge potential for increased understanding of the fundamentals of vehicle performance.

1.1.1 Global Formula Racing

Global Formula Racing (GFR) is the collaborative FS team of students from Oregon State University in the USA and DHBW Ravensburg in Germany. Founded in 2010 the team has had considerable success, winning 13 FS competitions in 2010-2014, more than any other team. Recent vehicles have been built on a vehicle concept of a lightweight car with very high aerodynamic downforce. Two vehicles are produced each year, one combustion and one electric. Throughout this thesis the GFR 2011 combustion car (hereafter referred to as GFR11c) is used in both simulation and testing. This vehicle was chosen for its extensive data acquisition capabilities, further detailed in the methods section. Figure 1.1 shows two GFR cars from 2013 and 2014.



FIGURE 1.1: GFR13c at Formula Student Germany 2013, GFR14 in wet testing. Photo credit: Kroeger, Marshall Wagoner

1.2. The objective of the FS car

Formula Student is unlike many other forms of motorsport in the course design. FS courses are similar to Sports Car Club of America (SCCA) solo autocross courses, but scaled down for smaller cars and lower average speeds. The courses are primarily corners and slaloms with short straights connecting them. Average speeds in the autocross and endurance events are intended to be 48 kph and 57 kph respectively, with maximum speeds of 105 kph in the endurance event.[11] Figure 1.2 illustrates a typical FS endurance course mapped from onboard Global Positioning System (GPS) data.

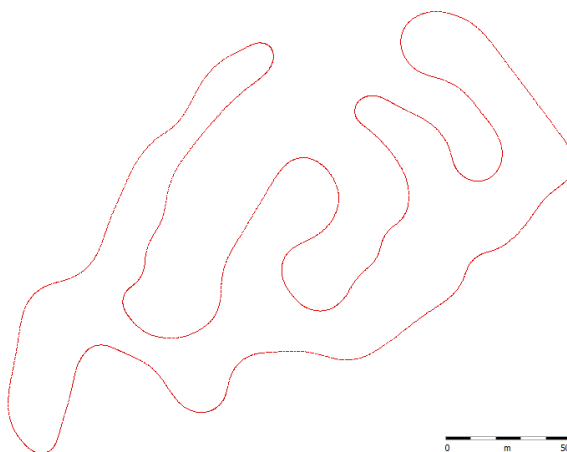


FIGURE 1.2: Formula Student Germany 2012 track measured by GPS

The course surface varies, but is typically run on sections of a full size race course or a large parking lot. While the granularity of the surface and elevation changes may differ between competitions, the cars rarely have to contend with bumps larger than pavement gaps or running over the small traffic cones used to mark the course. The infamous jump in the Formula Student Germany track and crossing of the curbing on courses run on full size racetracks are exceptions to this rule.

Suspension is assumed to be important to racecar performance, but the overall effect may appear to be less in FS than other series. FS events can be and have been won by

vehicles with effectively no suspension via the use of extremely high rate springs. Any conclusions at this level are clouded by the extremely varied field in both cars and driver capabilities.

1.3. Tire Theory

Minimizing time around the race track is achieved by maximizing the acceleration in the appropriate direction[12]. As race courses are primarily in a single planar surface, accelerations in the ground plane (XY plane in the vehicle axis system) are most important to performance. Figure 1.3 illustrates the vehicle axis system which will be used throughout this paper.



FIGURE 1.3: Vehicle and tire axis systems. Photo credit: Robert Story

Forces responsible for these accelerations fall into two categories, mechanical and aerodynamic, mechanical forces being those generated by the four tires in contact with the road surface, and aerodynamic forces being generated by wind gusts and aerodynamic reactions to the vehicle being pushed through the air. Tire reaction forces dominate x and y accelerations, while aerodynamic forces play a significant role in net forces on the vehicle in the x and z directions.

As such, in order to maximize the XY plane accelerations of the vehicle, performance

of the tires should be maximized. Tire performance is the force and moment output of the tire for a given set of inputs including but not limited to: vertical load, slip angle, slip ratio, pressure, temperature, inclination angle and contact surface factors.

Steady state tire behavior is commonly modeled using the empirical “Magic Formula”, which for lateral force has the form [13]

$$F_y = D \sin (C \arctan (B\alpha - E(B\alpha - \arctan B\alpha))) \quad (1.1)$$

where F_y is the lateral force, α is slip angle and B,C,D,E are coefficients which shape the curve. The characteristic shape of the magic formula is shown in the figure below for three vertical loads.

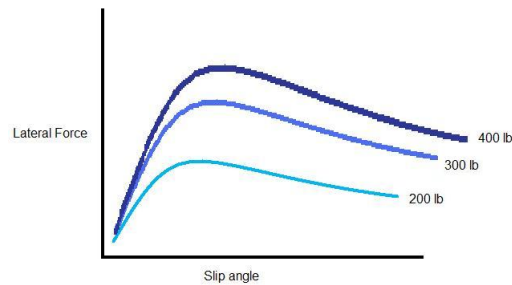


FIGURE 1.4: Lateral force vs. slip angle at three vertical loads for a hypothetical tire

The relationship we will focus on is that of vertical load and in-plane grip. Unlike many other engineering materials, tires and rubbers have a coefficient of friction that varies with vertical load. [12, 13, 14] Typically this is a reduction in coefficient of friction with increasing load, which can be seen in figures 1.4 and 1.5.

In steady state conditions this behavior is well understood and regularly used in setting the handling balance of the vehicle through load transfer distribution among the four contact patches[5, 12, 14]. In cyclic vertical loading conditions, this factor is partly responsible for a reduction in total grip relative to constant loading conditions[13].

In addition to this “steady state” factor, tires also exhibit transient effects of a time

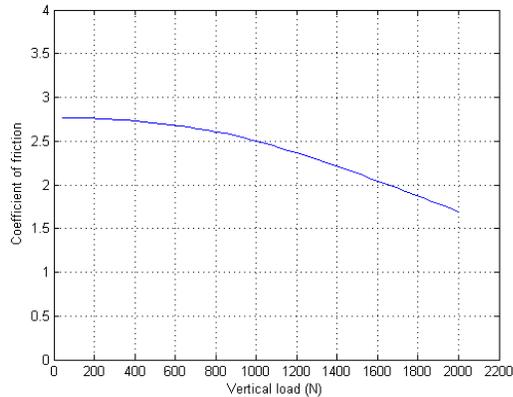


FIGURE 1.5: Coefficient of friction vs. vertical load for an FSAE tire

delay between a new operating condition of load [1, 13] or slip [1] and the corresponding change in grip. This delay is equal to the time it takes the tire to roll a certain *relaxation length*. [1, 13, 15]. In cyclic changes of vertical loading or slip the peak in-plane grip will always be less than the peak in-plane grip during steady state conditions [1]. In [15], Dixon asserts that forces develop exponentially converging on the steady state value, following the mathematical relationship

$$\frac{F}{F_{\infty}} = 1 - \exp^{-x/l} \quad (1.2)$$

where F is the force, F_{∞} is the steady state force, x is the distance rolled and l is the relaxation length which Dixon refers to as relaxation distance. Dixon also states that this relaxation length is approximately the circumference of the tire and not very sensitive to vertical load. Reference [14] discusses hysteresis and how it is generally higher in super soft race tires. This could mean that vertical load variation is more important to minimize for racecar handling than for road cars. The same book addresses the delay in strain vs stress in rubber samples loaded cyclically.

1.4. Load transfer

Vehicles of four or more wheels are over constrained or indeterminate systems, and the vertical load distribution between wheels is determined by the relative vertical positions of each wheel and stiffness through travel in response to various body motions.

In-plane accelerations cause transfer of vertical load between the suspension corners. In steady state cornering, lateral acceleration leads to lateral load transfer, a function of acceleration, mass, CG height and track width. The simplified formula is

$$LLT = \frac{a \times m \times CG_h}{t} \quad (1.3)$$

where LLT is lateral load transfer in newtons, a is acceleration in m/s^2 , m is mass in kilograms, CG_h is the height of the CG in m and t is the vehicle track width.

This simplified model of load transfer due to lateral acceleration is shown in figure 1.6. A similar equation applies for longitudinal acceleration, replacing the track width for the wheelbase. As load transfer greatly changes the vertical loading on the suspension, damping selection is impacted. The calculation is sometimes expanded to separate sprung and unsprung load transfers, which differ in how they are reacted by the suspension.

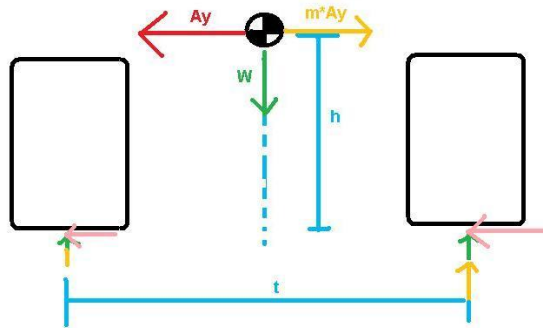


FIGURE 1.6: Steady state, single axle load transfer

1.5. Damper Theory

With a few rare exceptions such as karts, all road vehicles incorporate some form of suspension, isolating the frame and body of the vehicle from road irregularities and allowing the contact patches of the vehicle to conform to the road shape. This relative motion between the sprung and unsprung masses allows the suspension to absorb the energy of the road system, which must then be dissipated into heat in the damper, tire and other sources of friction and hysteresis. The typical system consists of a spring and damper between the outboard suspension and the chassis on each corner, and anti-roll bars connecting the two front corner suspensions and the rear two corner suspensions. Figure 1.7 shows a computer-aided design (CAD) model of a suspension corner.

The tire itself has both spring and damping properties by definition of being a viscoelastic material [14, 16], but the damping in the vertical direction is often neglected in simulation on the premise of being very small [1, 2]. The validity of this is somewhat debatable, particularly in FS where speeds are low; it is well acknowledged that vertical tire damping is maximum for a stationary tire and decreases with increasing speed [1, 16]. It is clear that tire damping has importance in some realm, as the energy absorption is fundamental to rubber friction and physically manifested in tire heating.

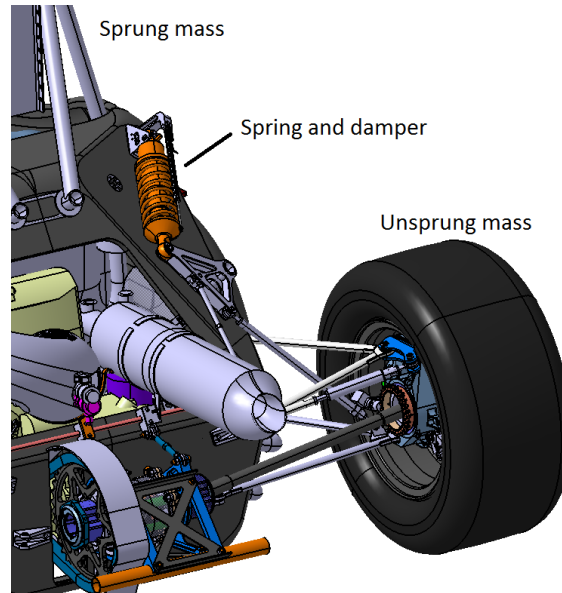


FIGURE 1.7: GFR11c rear suspension showing sprung and unsprung masses, spring and damper unit

Given a suspension spring rate established through other methods and a given tire rate, there are primarily three schools of thought on the role of dampers in the suspension system:

- Control sprung mass motion and vibrations [5, 17, 18, 19, 20]
- Tune transient vehicle balance via the rate of load transfer [5, 7, 14, 18, 21]
- Minimize vertical tire load variation [1, 2, 12, 19, 20, 22]

Additionally these tuning approaches may differ in their goals. Controlling the acceleration of the sprung mass is often done for ride comfort, but may be also be done for handling. Tuning transient vehicle balance and minimizing vertical tire load variation both seek to maximize handling performance in balance or overall grip respectively.

The most simple model of the vertical dynamics of a vehicle suspension is the quarter car model, and due to its simplicity is widely used in some capacity. One, two and three

degree of freedom (DOF) schematics are shown in figure 1.8 with sprung, unsprung and tire masses, suspension and tire springs and dampers, and cyclic road profile. These examples show linear springs with coefficient k and dampers c . Inerters, which give force proportional to acceleration, could also be modeled using this approach but are not shown.

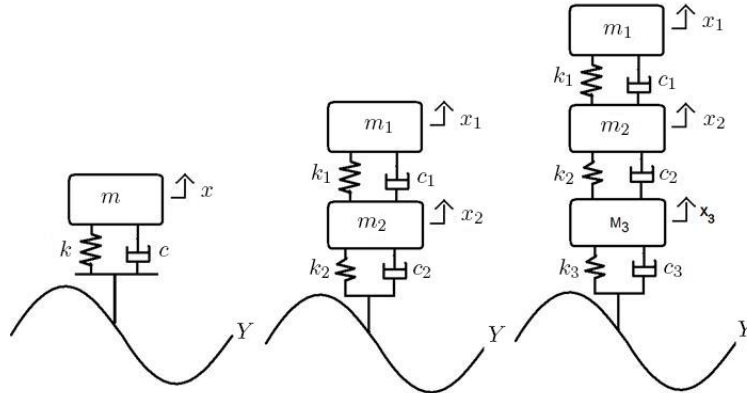


FIGURE 1.8: Quarter car models with 1, 2, and 3 DOF

References [21], [23] and many others suggest 70% of the critical damping for the 1 DOF quarter car model, usually with the justification that this gives faster response than critical damping with acceptable overshoot. This most simple form of analysis neglects the unsprung mass and so is not appropriate for study of high frequency vibrations beyond the range of the undamped natural frequency of the sprung mass [1, 2]. This approach is however, relevant to investigate due to its prevalence in literature and “tribal knowledge” of racers.

In [1], Genta introduces the concept of optimum damping for the 2 DOF quarter car model without tire damping:

$$C_{opt} = \sqrt{\frac{Km}{2}} \sqrt{\frac{P + 2K}{P}} \quad (1.4)$$

where K is the vehicle spring rate, m is the sprung mass and P is the spring rate of the tire.

This is an “optimum” aimed at minimizing the acceleration of the sprung mass [1] by setting a local maximum and thus zero slope at the first node in the frequency response diagram as shown in figure 1.9. This happens to also be very good at minimizing the area under the curve in the tire vertical load frequency response as well. Reference [2] also mentions this optimal damping as a comfort optimization and cites [3].

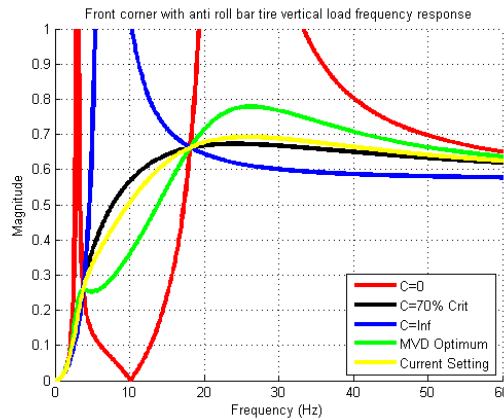


FIGURE 1.9: Tire force frequency response output of 2 DOF quarter car model

In [12], a road holding criteria is referenced from [24] for a 2 DOF quarter car model:

$$R = \frac{k_1}{(m_1 + m_2)g} \bar{\sigma} \quad (1.5)$$

where k_1 = vertical tire spring rate, m_1 = unsprung mass, m_2 = sprung mass, g = gravitational constant, and $\bar{\sigma}$ = root mean square of $X_0 - X_1$.

In speaking with Joe Gibbs Racing Engineers Bill Murray and Ross Kippenbrock, they suggested a grip metric:

$$Grip_{STD/RMS} = \frac{stdev(F_{zHPF})}{rms(F_z)} 100 \quad (1.6)$$

This metric gives lower values for higher grip levels and normalizes the variation by the rms of the vertical load.

In [25] Kowalczyk gives contact patch load variation as:

$$CPL = \frac{\Delta Load}{\Delta acc_{input}} \quad (1.7)$$

While substantially more complex suspension systems than the linear spring and damper exist including front-rear interconnected suspensions [26, 27], semi-active systems with magnetorheological damping [28], and active suspensions capable of adding energy, the fundamental issue remains that there is not an agreement on the goals of the damper in suspension tuning. It is the purpose of this thesis to assess the importance of vertical load variation on the tire. A simple conventional suspension is used to prove this point; more complex suspension systems could then be used to further improve performance with this goal in mind.

To give a clear goal to damper tuning a grip metric is proposed:

$$\text{Grip Factor} = \frac{avg(F_z)}{stdev(F_{z,filtered})} \quad (1.8)$$

Where F_z is the vertical load on the tire and $F_{z,filtered}$ is the vertical load passed through a high pass filter to attenuate signal content below 5 Hz. This cutoff frequency was selected to remove signal content from load transfer due to vehicle accelerations and found using Fast Fourier Transforms (FFTs) of driver inputs and vehicle accelerations. Removing the influence of load transfer due to vehicle accelerations allows comparison of grip factors over a full lap, where comparing solely the variation in vertical tire loading would show setups with higher accelerations and thus more load transfer to have a higher vertical load variation on the tires. There is stronger justification for a cutoff frequency related to the relaxation length of the tires used; bumps with a wavelength less than the relaxation length one would assume would have a much larger effect than those with wavelengths larger than the relaxation length. However, this is relegated to future work in this study.

An excerpt of logged data of driver inputs is shown in Appendix D.

In the time domain grip factor should be calculated over as long a duration as feasible. A minimum duration of 0.2 seconds is imposed, giving a minimum of 1 complete cycle of the minimum frequency in which we are interested.

In the frequency response of a linear system model, only the denominator of equation 1.8 has meaning. Thus maximizing the Grip Factor over a range of frequencies can be done by passing the curve in Figure 1.9 through the same high pass filter, then minimizing the enclosed area between it and the x axis.

Ride quality is not a significant concern in racing applications, particularly in FS where driving stints are extremely short, the longest being 11 km for each driver during the endurance event. Well organized teams may have a driver in the car for five times that in a long test day, so there is some validity to a quick look at ride comfort.

Typical ride comfort criteria are displacement[1], acceleration [29, 30, 31], or jerk of the sprung mass. Frequencies are often not evenly weighted as there is evidence that humans are more sensitive to specific frequencies. Reference [1] gives 1 Hz causing motion sickness, and resonant frequencies of major body parts in the 3 to 30 Hz range, with many specifics. ISO 2631 [31] assigns a weighting criterion which heavily attenuates vibrations over 16 Hz. For this investigation vertical suspension force transmitted to the body will be used to assess ride comfort. This is directly related to sprung mass acceleration in the quarter car model, and simple to measure in physical testing.

2. MATERIALS AND METHODS

2.1. Quarter Car Modeling

A 2-DOF quarter car without tire damping model was created in MATLAB. The simulation studies both the single bump behavior and cycles the model over a range of

road frequencies of constant amplitude. A sample tire vertical load frequency response plot is shown in figure 1.9. On this plot a range of damper configurations are shown, the red $C=0$ line representing the undamped system and the lower limit of system behavior. The upper limit is established by the infinite damping blue line. Between these two lines is the area we can influence with damping, any damping value will fall between these curves. *Motor Vehicle Dynamics* optimal damping (MVD optimal) and 70% of 1 DOF quarter car critical damping are included on the plot to show literature approaches.

The three peaks are the undamped natural frequencies of the 2 DOF system. From left to right they are: sprung mass vibrating on unsprung mass, both masses vibrating on the tire, and the unsprung mass vibrating between the sprung mass and the road.

Fast Fourier Transforms of vertical tire load were taken from logged data on previous GFR cars, and it was found most force activity was less than 40 Hz. As the quarter car simulation undamped natural frequencies occur at approximately 3, 8, and 24 Hz, a 0 to 40 Hz simulation captures all system behavior. This conclusions match those of previous authors[32]. A sample FFT can be seen in figure 2.1.

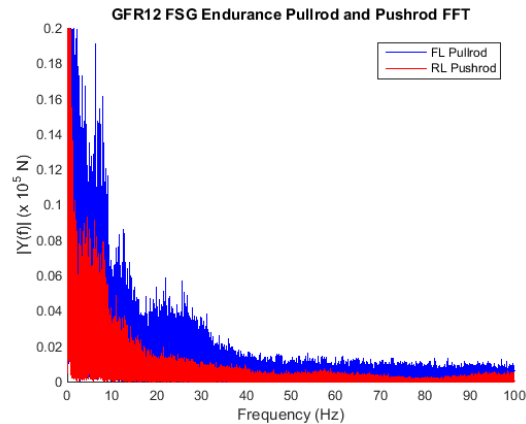


FIGURE 2.1: FFT of pullrod and pushrod forces from logged data

Damper forces were designed to be linear and symmetric. This simplified both simulation and physical implementation and is a reasonable first step in damper study

when we are trying to assess the validity of the model and damping tuning goals. Bilinear and quadrilinear damping curves were considered but left for future work. Figure 2.2 illustrates the three types of damper force curves.

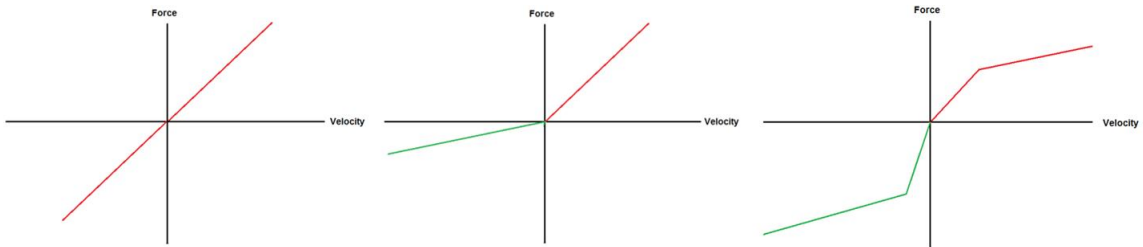


FIGURE 2.2: Damping curve types, from left to right: Linear, bilinear and quadrilinear

To study the effect of a single step input, the linear system can also be excited with the MATLAB *Step* command. This is not exactly like the a physical quarter car rolling over a step input bump due to the contact between the tire and the bump[4]. Example model output is shown in figure 2.3.

In [13], Pacejka suggests that if the wavelength of road studied is less than two or three times the contact patch length the point contact of the typical quarter car model is a large approximation. Reference [4] comes to a similar conclusion.

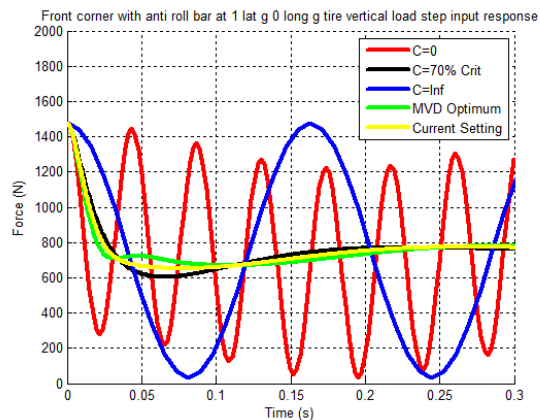


FIGURE 2.3: Quarter car model step input response

A load transfer model is used to calculate the change in the portion of sprung mass supported by the suspension corner which is being studied due to lateral and longitudinal accelerations. This allows the study of differing requirements for the inside and outside tires during a high g corner. As the model is linear, adding vertical load due to downforce has no effect on the system response. Anti-roll bar springs are also included in the model to evaluate their importance to the output. Model parameters such as masses and spring rates were obtained from measurements off the GFR11c car.

2.1.1 Determining damping rates

Damping rates were selected for the outside tires of the GFR11c car in a 2 g corner. As the effective sprung mass supported by a suspension corner differs dramatically between the inside and outside tires, and the outside tires have make a larger contribution to the total cornering force, particularly in FS, this is an appropriate approach. Figure 2.4 shows some example data illustrating the dramatic load difference. Notice how the vertical load on the FR tire is nearly zero, while the lateral force for the same tire is often negative, indicating the tire is being pushed into the corner by the car. We can safely say in corners like this the inside tires' contribution to vehicle cornering is very small or zero.

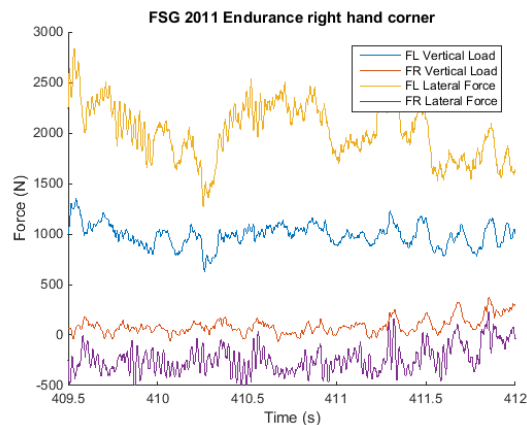


FIGURE 2.4: Vertical and lateral forces measured during a typical corner

With the unsprung mass supporting a sprung mass characteristic of these types of corners, the quarter car model was cycled over the 0-40 Hz road frequency range generating the output in figure 2.5. Damping forces which produce the Motor Vehicle Dynamics optimum damping in this plot produce curves quite similar to 70% critical damping in the straightline case. A build producing 42 lb @ 5 in/s is shown in yellow and was chosen as the baseline value for simulation and testing. Rigid damping and no damping configurations were also evaluated to explore the limits of system behavior. Finally a damper of 160% Baseline forces gives approximately 70% critical damping in a 2 G corner and is called *stiff* damping. Physical implementation of these damping rates is covered in section 2.2.2.

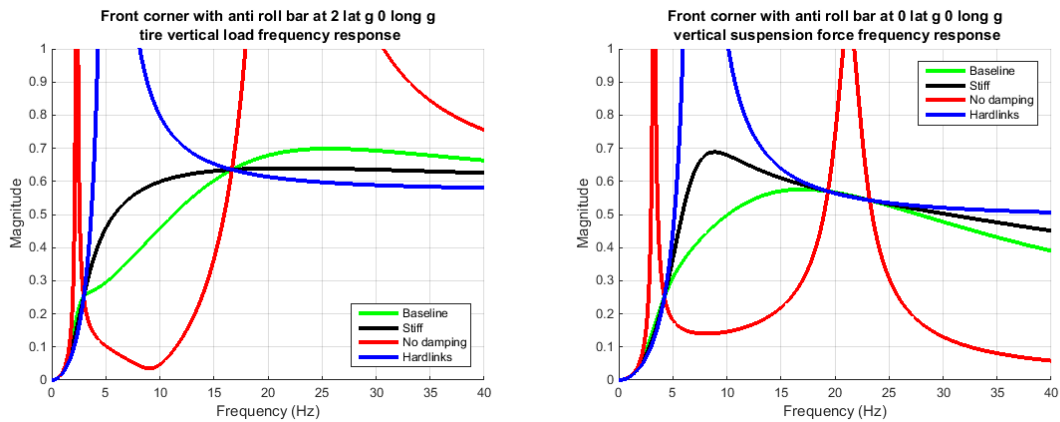


FIGURE 2.5: Quarter car model frequency response, cornering and straightline

2.2. Physical Testing

The 2011 GFR combustion car was used for physical testing. The vehicle was chosen because of the extensive data acquisition tools implemented including strain gauges on all suspension links between the outboard and chassis, and accelerometers on the left side outboard suspension.

The car competed in the 2011 FS season with an aerodynamic package consisting of front and rear wings and full length undertray, winning three international competitions.

As such, it is a good representation of the highest performing FSAE cars of the era and not far off current FS trends. This testing was performed without aerodynamic elements to ease in changing suspension settings and reduce impact of any aerodynamic performance differences on the results. Figure 2.6 illustrates.

The suspension setup used was appropriate for the car without wings. The relevant details are shown table 2.1.

| Parameter | Front | Rear |
|------------------------------------|--------------|-------------|
| Sprung corner mass (kg) | 40.83 | 69.84 |
| Unsprung corner mass (kg) | 7.71 | 8.62 |
| Wheel rate (N/mm) | 15.7 | 24.5 |
| Sprung mass natural frequency (Hz) | 2.98 | 3.51 |
| Roll stiffness (deg/g) | 0.69 | |
| % Reacted load transfer | 40 | 60 |

TABLE 2.1: GFR11c parameters in damper test configuration



FIGURE 2.6: GFR11c with and without aerodynamic elements, At left at FS Austria 2011, at right during Round 1 damper testing. The gold color on suspension links is heat shielding for the strain gauges on the links. Photo credit: Robert Story and Jay Swift

Although these springs and damping rates are not reflective of aero cars, the tire theory is the same and the results can be expected to translate for tire performance. Aerodynamic performance may have different results. See section 5.3., future work, for more information.

2.2.1 Onboard data logging system

Data was logged via the vehicle's onboard MoTeC data acquisition system. Four MoTeC Versatile Input Modules (VIM) received analog and differential data from the sensors and wrote the data to the CAN bus, off which it was logged by the MoTeC Advanced Central Logger (ACL).

The relevant sensors on the front left corner of the vehicle are:

- Suspension link strain gauges located on:
 - Upper a-arm front tube
 - Upper a-arm rear tube
 - Lower a-arm front tube
 - Lower a-arm rear tube
 - Tie rod
 - Pullrod
- Upright vertical accelerometer
- Wheel speed
- Infrared tire temperatures (3 - inside, center, outside)
- Damper position
- Chassis lateral, longitudinal acceleration
- Chassis yaw rate
- Chassis GPS position

A similar sensor list is used on the three other corners. Driver inputs were logged with sensors for:

- throttle position
- brake pressure
- steering rack travel.

Logging frequency was 1000 Hz for all pushrod and pullrod strain gauges inputs and 500 Hz for all other strain gauges. Damper position, necessary for the calculation of overall vertical and lateral forces, was also logged at 1000 Hz. To be able to calculate forces and moments between the outboard and the chassis, we assume all 6 links are two force members pinned at the end and therefore only transmit axial loads. This is not strictly true as the teflon lined plain spherical bearings had a small amount of friction, the a-arm tubes form a welded joint, and the pullrod and pushrod attachments to the front upper and rear lower a-arm respectively do not occur exactly at the balljoints. Additionally the angles of the suspension links in 3D space must be known. The position of all suspension points were measured in the CAD model at model ride height, then the angle of all links relative to the ground plane was measured as a function of wheel travel from this position. A setup sheet value called the *kinematic ride position* is set during suspension setup and defines the distance the suspension must travel from full droop to the ride height position defined in CAD. This distance is measured as a linear distance of damper travel, then converted to suspension travel through the damper motion ratio. Suspension travel is zero at full droop, so the kinematic suspension position used in a-arm angle calculation is:

$$\text{Kinematic Suspension Position} = \text{Suspension Position} - \text{Kinematic Ride Position} \quad (2.1)$$

Each strain gauged link uses 4 strain gauges in two T configurations and wired in full bridge configuration such that link axial strain is measured and bending and thermal expansion are rejected. Links were calibrated individually off car and the full car accuracy measured. Figure 2.7 shows the full car error measurement in progress for lateral forces. The complete full car error measurement data record sheet can be seen in appendix C.

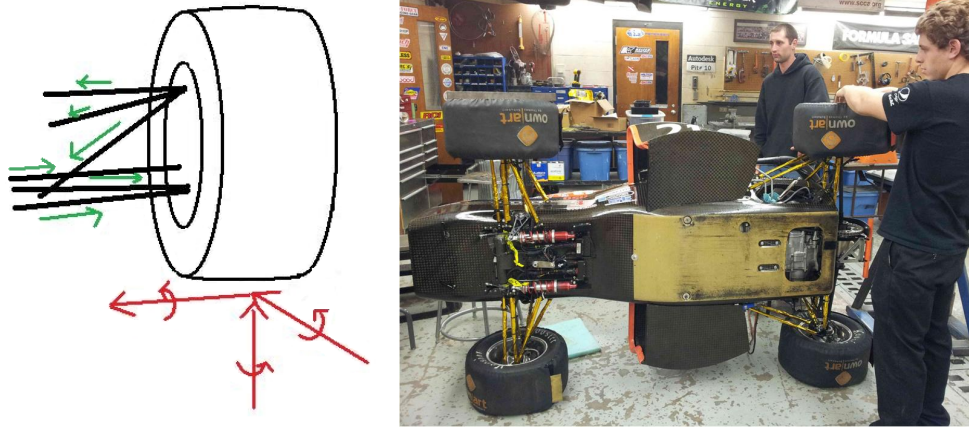


FIGURE 2.7: Visualization of 6 suspension link forces used to calculate 6 forces and moments between the outboard and body, GFR11c during full car strain gauge error measurement

With these sensors, the goal was to measure the vertical load on each tire and the lateral force on the vehicle from the tire. The vertical load measured by the suspension links differs from the vertical load seen by the tire due to the inertial forces of the outboard including upright, wheel and tire. Upright vertical acceleration was used in conjunction with the suspension link strain gauges to calculate vertical load on the tire.

$$F_{t,z} = F_{s,z} + m_2 \ddot{x}_2 \quad (2.2)$$

where $F_{t,z}$ is vertical tire load in N, $F_{s,z}$ is vertical suspension force in N, m_2 is the unsprung mass in kg and \ddot{x}_2 is the vertical acceleration of the unsprung mass in $\frac{m}{s^2}$. Figure 2.8 illustrates.

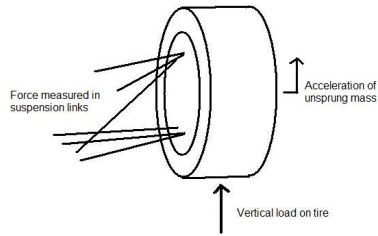


FIGURE 2.8: Suspension link forces vs vertical load on tire

Additional load cells or strain gauges on the shock shaft were considered but ultimately not implemented due to the additional implementation work required to allow fitment of the load cell and the poor resolution of data from strain gauges on the solid damper shaft. Reference [32] explains the data acquisition system used in more detail and other vehicle dynamic uses of the system.

2.2.2 Damper builds

Four damping configurations matching those of the simulation were tested. Their common names and forces at 5 in/s damper travel are shown in table 2.2.

| Number | Trace color | Damper | Force at 5 in/s |
|--------|-------------|----------------|-----------------|
| 1 | Green | Baseline | 42 lb |
| 2 | Black | Stiff | 68 lb |
| 3 | Red | No damping | 3 lb |
| 4 | Yellow | Baseline run 2 | 42 lb |
| 5 | Blue | Hardlinks | “Rigid” |

TABLE 2.2: Damper test order

Baseline, stiff and no damping were physically implemented through tuning of three sets of Penske 7800 quarter midget dampers. The 7800 is a single tube gas shock intended for use in quarter midget racing, an wingless oval track genre of racing for young drivers from 5 to 16 years old. Cars typically weigh 250 to 340 lb with driver and use kart size tires. To adapt the damper to use on GFR cars, damper valving is changed and a droop

limiter installed to reduce travel to 55 mm.

Baseline and stiff sets were tuned by replacing internal shims and verifying forces on a shock dynamometer. The no damping set simply had all shims removed. While this does not truly give zero damping due to the resistance of the fluid passing through the piston holes, the piston, fluid and gas pressure were left intact to avoid damage to the damper due to dry friction on the seals or cocking of the shaft in the body when only supported by the single shaft bearing.

Rigid damping was implemented using a hardlink usually used for suspension setup of leveling and balancing cross weights. While technically the hardlinks are very high rate spring with proportionally low internal damping, this is an acceptable implementation compromise versus building a damper similar to the other sets with the highest forces possible, at which point the damper would be locked at anything over glacially slow speeds. The Baseline damper configuration was run twice to allow comparison between runs which should be identical and thus give an indication of changing experimental conditions. Figure 2.9 shows an example of the dampers and hardlinks used, while figure 2.10 shows the damper internals used to tune damping forces.



FIGURE 2.9: Penske 7800 damper on left, “Hardlink” installed for rigid damping setup on right. Photo credit: Author, Ankit Agarwal

Dampers were built by Chris Billings at Shock Shop in Portland, OR. Damping forces were measured on a SPA BTP 2000 crank damper dynamometer. Force - velocity outputs of the dyno runs for the baseline and stiff dampers are shown in figure 2.11.

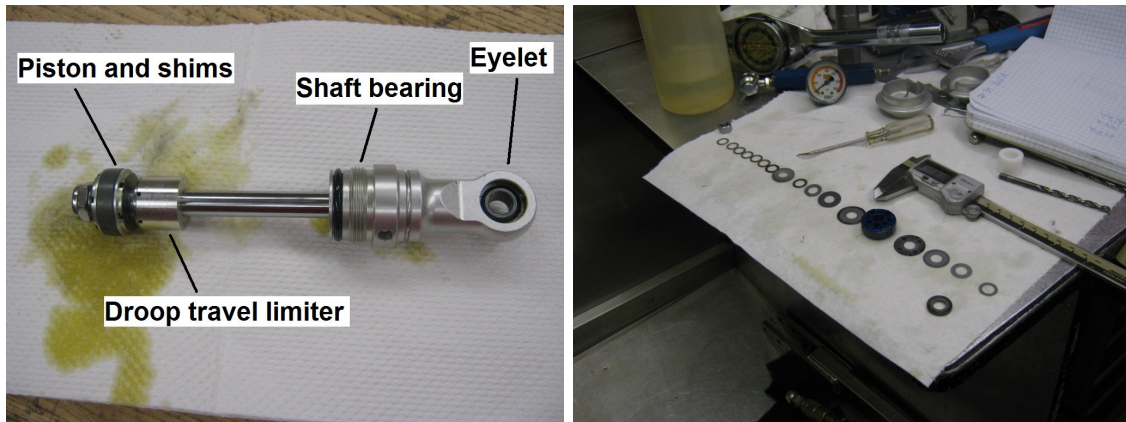


FIGURE 2.10: Left: Penske 7800 shaft assembly showing piston and shims. Right: Shims and piston laid out during damper assembly

Positive forces are compression, negative are extension. Velocity is always shown positive, making these figures a “folded” or reduced size version of those shown in figure 2.2.

Full page force plots of all dampers and springs tested are shown in appendix B.

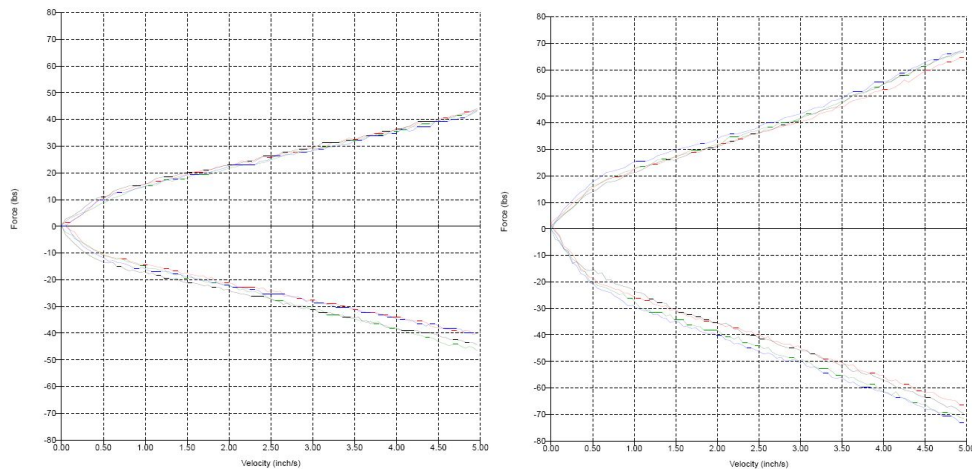


FIGURE 2.11: Baseline and stiff damper force - velocity plots. Full page plots of these dampers and no damping can be seen in appendix B

2.2.3 Test tracks

Each damper configuration was run on three test tracks: A straight line, a 21 m diameter skidpad and the Asymmetric Oval, a test course designed by GFR. These courses

allowed both isolation of vehicle performance in straight line and cornering situations as well as an estimate of performance on full FSAE course. The Asymmetric Oval was designed to give vehicle performance similar to that of a typical FS course, but in a smaller, simplified track layout to ease fast and repeatable setup, minimize the time for a driver to learn the course and have a short lap time to maximize the number of laps done for statistical analysis. Reference [32] details the use of each course for vehicle performance analysis and compares the Asymmetric Oval with 2011 season FS courses in several metrics.

The purpose of each course is:

- The straight line course is used to isolate the vertical load response;
- The skidpad course is used to examine the coupling of vertical load with lateral grip;
- An artificial bump was also used in straightline and skidpad tests to introduce a known disturbance into the system; and
- The asymmetric oval assesses the effect on complete vehicle performance on an FS track.

A GPS trace of these three tracks during round 1 testing is shown in figure 2.12. The tracks are placed so that the same section of ground with the removable bump is hit by both the straightline and skidpad courses.

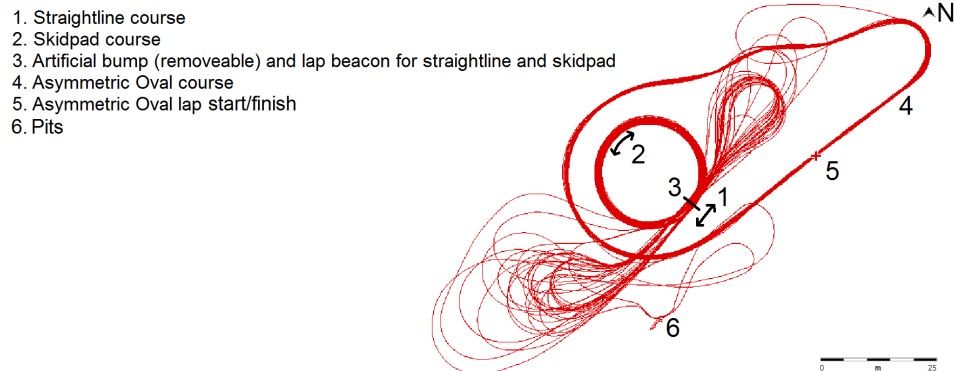


FIGURE 2.12: GPS trace of test tracks used, showing straight line, skidpad and Asymmetric Oval

2.2.4 Test plan

Physical testing was completed in two test days a year apart, which will be referred to as Round 1 and Round 2. Round 1 took place on November 17th 2012 under light rain conditions and a 1/4" (6.35 mm) high by 1.5" (38.1 mm) long artificial bump was used. Phil Arscott drove the car on Hoosier LC0 slicks hand grooved for rain use. Round 2 took place October 20th 2013 with dry conditions and a 1/2" (12.7 mm) high artificial bump. Doug Peterman drove the car on Hoosier LC0 slicks. The asymmetric oval runs were omitted to save time during the second test, and the test order was changed, switching the hardlinks for the second baseline run to give a better indication of condition change over the test day. These differences were intended and to our knowledge the only differences between the tests.

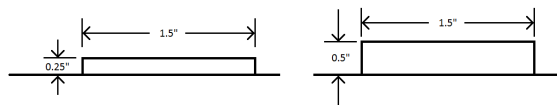


FIGURE 2.13: Artificial bumps used

To introduce a known disturbance to the suspension, an aluminum artificial bump with non-slip tread tape was bolted to the track surface with concrete anchors. The effect

is similar to running over a corner of a track cone during competition events, a common enough occurrence that it should be considered in damping selection. The bump of known shape allows more direct comparison with the computer model and the same straight line and skidpad courses were run with and without the bump to have a direct comparison and evaluation of the bump's effect. The bump used in round 1 testing is shown in figure 2.14.

| Test number | Damper | Track | Speed | Direction | Bump |
|-------------|----------|-----------------|-------|-----------|------|
| 1 | Baseline | straight | high | - | no |
| 2 | Baseline | straight | low | - | no |
| 3 | Baseline | skidpad | high | ccw | no |
| 4 | Baseline | skidpad | high | cw | no |
| 5 | Baseline | skidpad | low | ccw | no |
| 6 | Baseline | skidpad | low | cw | no |
| 7 | Baseline | straight | high | - | yes |
| 8 | Baseline | straight | low | - | yes |
| 9 | Baseline | skidpad | high | ccw | yes |
| 10 | Baseline | skidpad | high | cw | yes |
| 11 | Baseline | skidpad | low | ccw | yes |
| 12 | Baseline | skidpad | low | cw | yes |
| 13 | Baseline | Asymmetric Oval | high | ccw | no |
| 14 | Baseline | Asymmetric Oval | high | cw | no |

TABLE 2.3: Round 1 test plan for baseline damper configuration. Test plan for other dampers is identical. Round 2 test plan eliminated the Asymmetric Oval tests and switched the order of the skidpads and straights.

The test plan for each damper consisted of running the straight line and skidpad tracks at low and high speed, with and without the bump. Both ccw and cw directions were run so that both performance of both in the inside and outside suspension corner could be assessed. Drivers were instructed to always drive the left tires through the artificial bump location whether or not the bump was present. This was done as the upright accelerometers were only present on the left side of the vehicle and to always present the vehicle with the same section of pavement. As noted in the results section this was not always achieved.

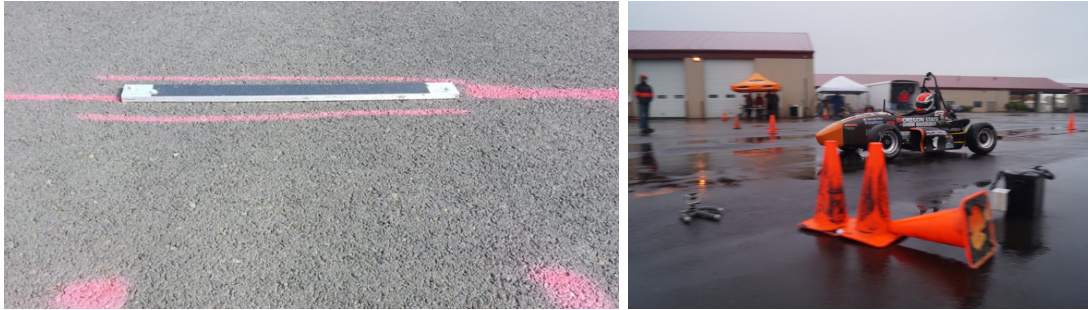


FIGURE 2.14: Left: 1/4” artificial bump bolted to track. Right: Lap beacon in front of cones marking location of bump. Photo credit: Jay Swift

3. RESULTS

In this section, results from the quarter car MATLAB model and vehicle test data are examined. Data from each test is looked at individually, with conclusions across multiple tests discussed in section 4.: Discussion.

3.1. Simulation

For a given vehicle configuration of masses and spring rates, any damper we simulate will fall between the performance of no damping and rigid damping on a frequency response plot such as in figure 3.1. This performance envelope is shown for vertical tire load and sprung mass acceleration; similar plots can be created for other simulation state variables. Whenever the no damping and rigid damping curves cross a node is formed through which all damping configurations must pass.

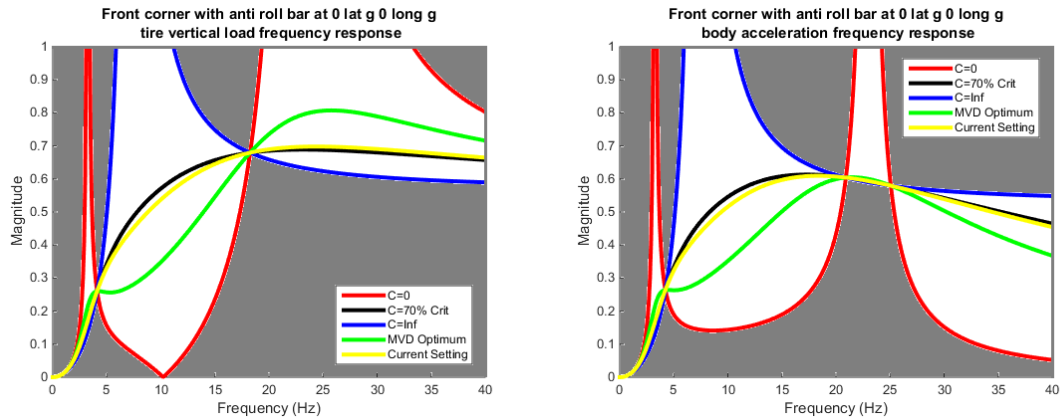


FIGURE 3.1: Simulation frequency response plots. Area of possible outputs shown in white, grayed off areas are not possible with this vehicle configuration

Figure 3.1 shows the theoretical limits of system behavior. However, as noted in section 2.2.2 the physical implementation of no damping retained some force and the baseline and stiff dampers are not exactly equal to literature values. As such simulation performance is a bit different.

3.1.1 Straightline without anti-roll bar

The most simple implementation of the model does not incorporate any anti-roll bar or load transfer due to vehicle accelerations. This is representative of straightline driving both front wheels moving together such that the front anti-roll bar does not change wheel loading.

With a 1/4" (6.35 mm) step input representing the artificial bump, the response in figure 3.2 is similar to the example output in figure 2.3 with the large difference of the attenuation of the no damping response. This is due to the aforementioned simulation of the physical dampers produced, which in the case of the no damping set produces a small amount of damping as the empty piston moves through the fluid. No damping has two clear oscillation frequencies of approximately 3 and 22 which clearly appear in the FFT of the response in figure 3.3.

The baseline and stiff dampers have visually similar performance, with the baseline dampers having quicker initial response, smaller peak and longer oscillation than the stiff dampers as we would expect of the lower damping. Both dampers overshoot steady state as the tire is undamped, with the stiff dampers converging to steady state slightly quicker.

With no tire damping and rigid suspension, the hardlinks quarter car continues to vibrate on the tire after excitation without attenuating any energy of the bump as is expected for a simple harmonic oscillator. This behavior obviously results in a very poor Grip Factor.

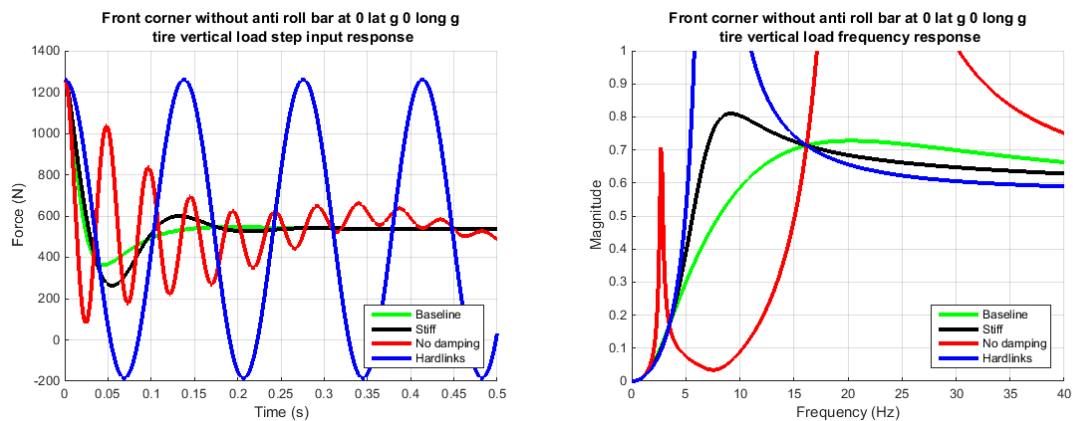


FIGURE 3.2: Straightline without anti-roll bar vertical tire load, step input and frequency response

The frequency response of the system too looks similar to example output such as figure 3.1, but with a more damped behavior of the *no damping* curve, leading to a smaller peak at 2.7 Hz range and slightly more force around 7 Hz, not touching a zero point. Over the 0-40 Hz range the baseline dampers have the smallest enclosed area as is expected, minimizing the magnitude of vertical tire load oscillation in this frequency range of the four configurations studied.

If this simulation case were the only one in consideration, it appears that damping between baseline and no damping could enclose a smaller area than the other configurations. In particular, both baseline and stiff are more damping than the *optimal* curve in

figure 3.1. Visually there appears to be substantial room from reduction in the 4 to 16 Hz range. Table 3.1 shows how each damping configuration compares to literature values and performs in step input and frequency sweep cases. *Critical frac.* and *Optimal frac.* refer to the fraction of literature critical and optimal damping, while *Grip Fractor* is the Grip Factor seen in the step input simulation, and *Freq. resp. area* is the enclosed area in the frequency response plot.

| Damper | Critical frac. | Optimal frac. | Grip Factor | Freq. resp. area |
|------------|----------------|---------------|-------------|------------------|
| Baseline | 0.791 | 2.14 | 5.27 | 23.11 |
| Stiff | 1.28 | 3.46 | 4.51 | 23.70 |
| No damping | 0.0565 | 0.153 | 3.15 | 38.52 |
| Hardlinks | ∞ | ∞ | 1.15 | 40.04 |

TABLE 3.1: Straightline simulation performance

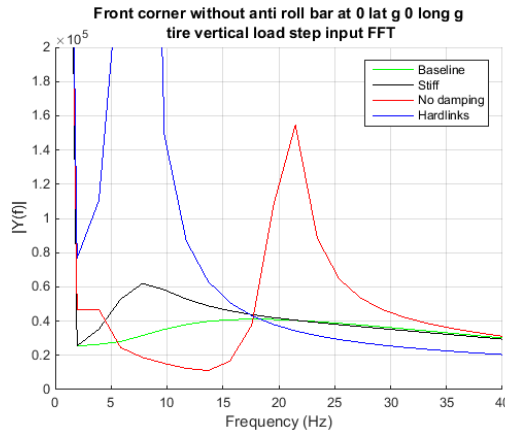


FIGURE 3.3: Straightline without anti-roll bar tire force step input frequency breakdown

As we would expect, vertical suspension force and sprung mass vertical acceleration are the same results, differing only by the sprung mass. These are both shown in figure 3.4. This is relevant because from a quarter car model perspective we only need to look at vertical suspension force to understand both channels. This differs from more complex models or physical testing where the sprung mass is supported by four suspension corners and thus has additional degrees of freedom in pitch and roll. Because they do not offer

any additional information and cannot be directly compared with physical test data, the sprung mass vertical acceleration plots will not be investigated further.

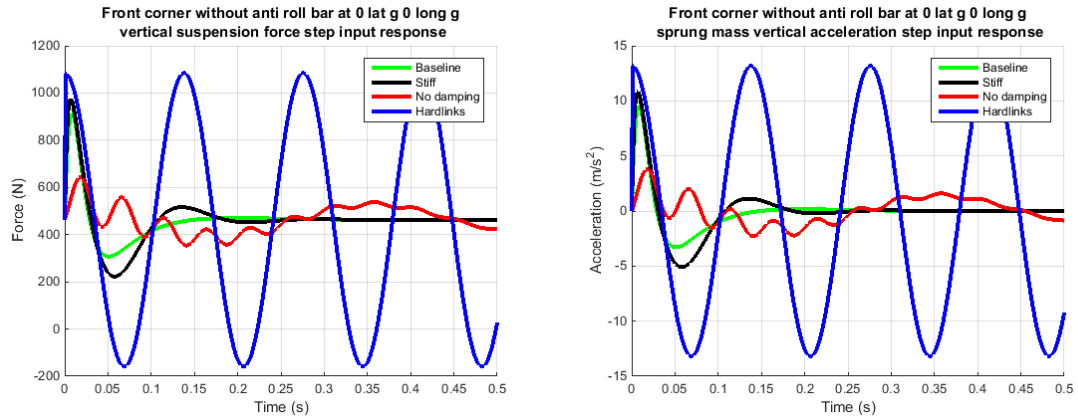


FIGURE 3.4: Straightline without anti-roll bar vertical suspension force and sprung mass acceleration, step input

The frequency response of vertical suspension load is fundamentally the same shape (figure 3.5), differing most in the higher frequencies as the importance of the unsprung mass inertia, the sole difference between the tire vertical load and the suspension vertical force as shown in equation 2.2.

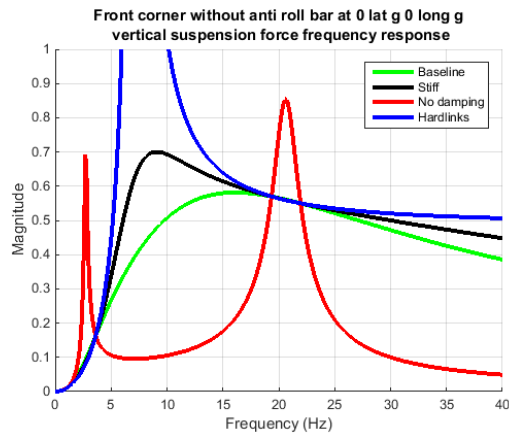


FIGURE 3.5: Straightline without anti-roll bar vertical suspension force frequency response

3.1.2 Straightline with anti-roll bar

Any difference in vertical travel of the left and right wheels of the front or rear axle of the car causes the anti-roll bar(s) to twist, giving an anti-roll moment which attempts to level the two wheels. A single wheel hitting a bump thus engages the anti-roll bar, which manifests itself in the quarter car model as an additional vertical suspension spring rate. The results however, are very similar in both step input Grip Factor and frequency response area as seen in figure 3.6 and table 3.2.

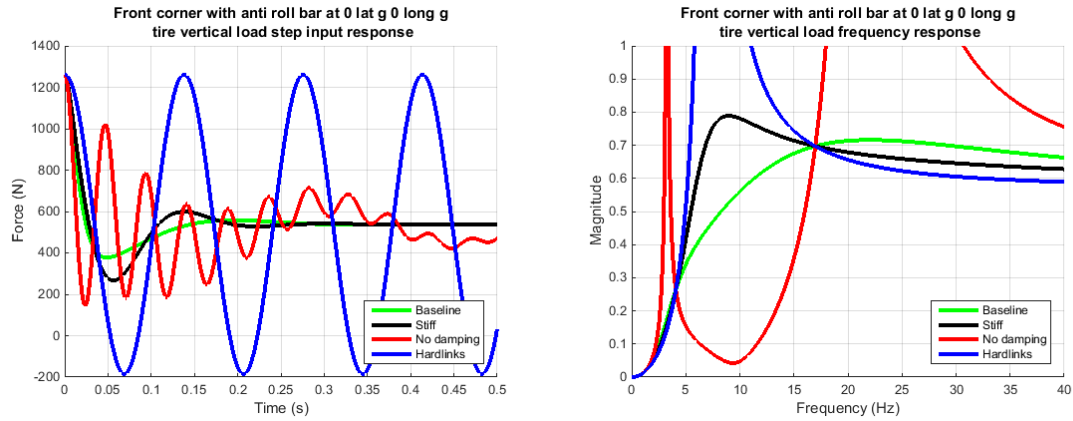


FIGURE 3.6: Straightline step input tire vertical load

| Damper | Critical frac. | Optimal frac. | Grip Factor | Freq. resp. area |
|------------|----------------|---------------|-------------|------------------|
| Baseline | 0.642 | 1.65 | 5.31 | 22.84 |
| Stiff | 1.04 | 2.66 | 4.53 | 23.55 |
| No damping | 0.0459 | 0.118 | 3.25 | 37.18 |
| Hardlinks | ∞ | ∞ | 1.15 | 40.03 |

TABLE 3.2: Straightline with anti-roll bar simulation performance

FFT of the step input response too are similar, with the addition of the anti-roll bar slightly increasing response of baseline and no damping in the less than 5 Hz range (figure 3.7).

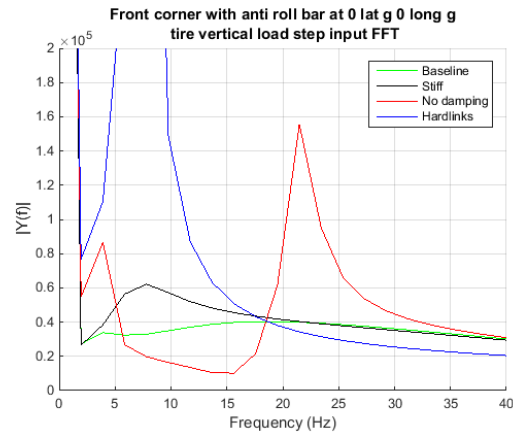


FIGURE 3.7: Straightline tire vertical load step input frequency breakdown, vertical suspension force

In any case, the presence of the anti-roll bar does not change the damper selection as baseline damping continues to have the highest Grip Factor and lowest frequency response area. Figure 3.8 illustrates similar behavior of vertical suspension force to simulations without the anti-roll bar.

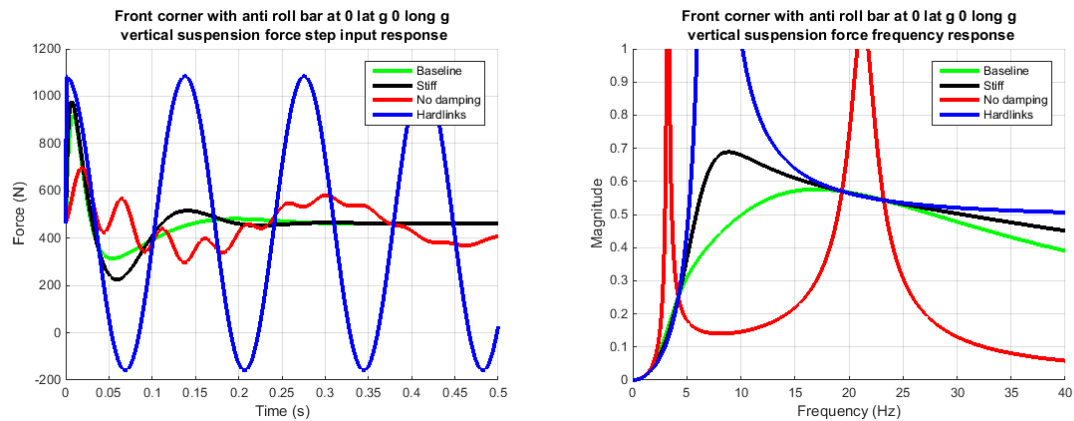


FIGURE 3.8: vertical suspension force step input and frequency response

3.1.3 Cornering with anti-roll bar

At 1.1 lateral G as seen in round 1 test conditions (see section 3.2.2) the model response is similar, differing due to the increased effective sprung mass from load trans-

fer. As addressed in section 2.1.1 the outside tires contribute substantially more to the overall cornering forces on the vehicle and thus will be the focus of this investigation. In comparison to the straightline case, the step input response at this cornering attitude has higher grip factors, primarily due to the higher total load on the tire due to load transfer. Figure 3.9 and table 3.3 illustrates.

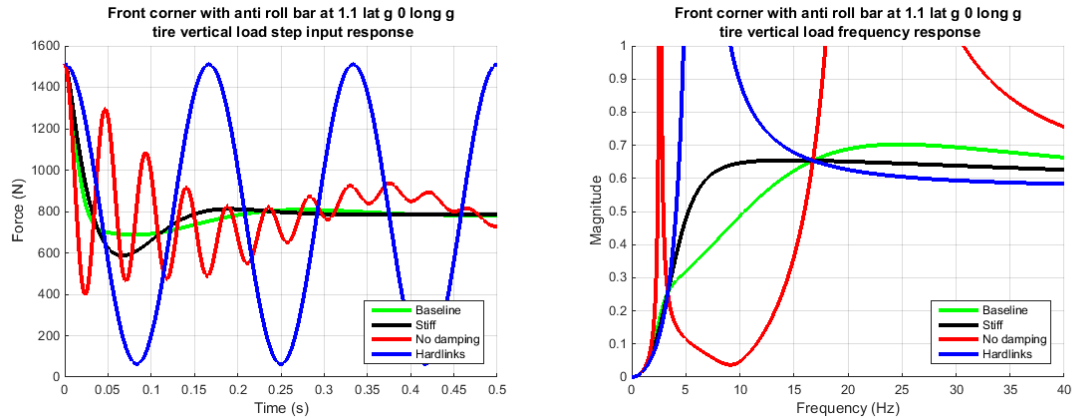


FIGURE 3.9: Cornering with anti-roll bar

| Damper | Critical frac. | Optimal frac. | Grip Factor | Freq. resp. area |
|------------|----------------|---------------|-------------|------------------|
| Baseline | 0.531 | 1.33 | 8.22 | 21.98 |
| Stiff | 0.860 | 2.15 | 7.16 | 22.34 |
| No damping | 0.0380 | 0.0948 | 4.86 | 37.26 |
| Hardlinks | ∞ | ∞ | 1.92 | 258.7 |

TABLE 3.3: Cornering with anti-roll bar simulation performance

In the FFT of the response shown in figure 3.10 it can be seen that the vertical load response of the baseline, stiff and hardlinks is reduced from the straightline case in the 5 to 15 Hz range, while the no damping response is higher in these areas. At 20 Hz and higher frequencies the response of the baseline, stiff and hardlinks is increased.

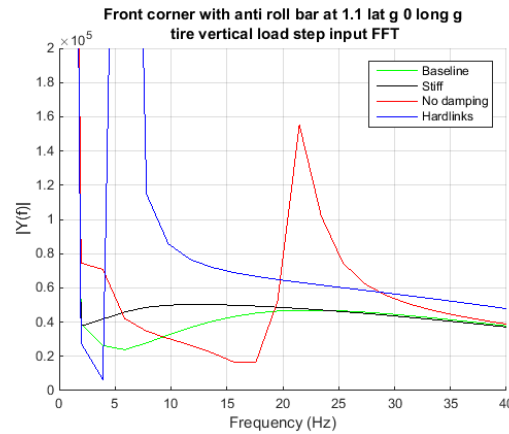


FIGURE 3.10: Cornering tire vertical load step input frequency breakdown.

Comparing the frequency response at 1.1 lateral g versus the straightline case we can see both the baseline and stiff curves have lowered significantly in the 4-18 Hz range, indicating less vertical load variation and matching the result of the step input response. Vertical suspension force in both step input and frequency response is similar to that of straightline simulations and can be found in appendix A3.

The performance at 2 lateral g, the design condition and peak cornering for non-aero cars is very similar to the 1.1 g cornering case in both output (figure 3.11) and Grip Factors. In the frequency response, we see lower tire force from both stiff and baseline in the frequencies below 15 Hz. The slope of the baseline curve through the node at 3 Hz is nearly zero, indicative of the damping approaching the MVD optimal damping, as can be seen in table 3.4. It can also be seen that the enclosed area under the frequency response curve is closer than ever between the baseline and stiff dampers. Vertical force transmitted through the suspension appears nearly identical to the 1.1 g case, so plots are included with the others in appendix A3.

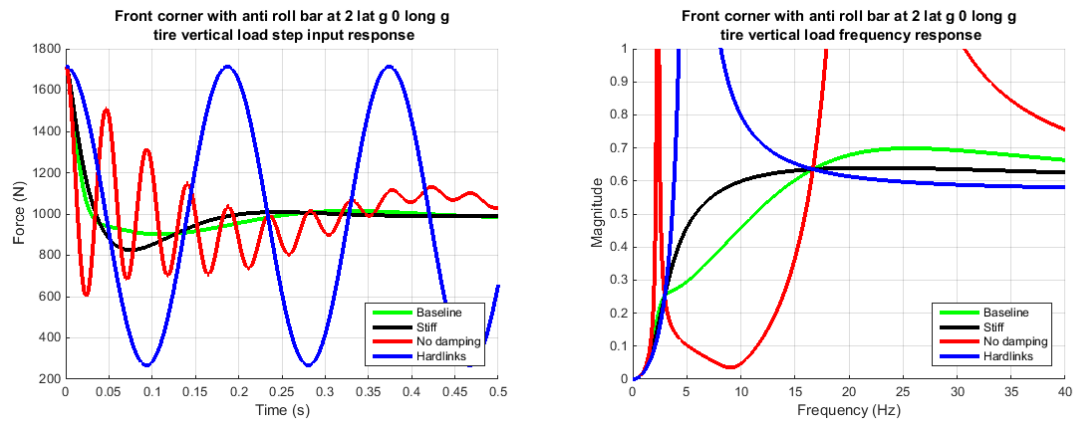


FIGURE 3.11: Cornering at 2 g step input and frequency response tire vertical load

| Damper | Critical frac. | Optimal frac. | Grip Factor | Freq. resp. area |
|------------|----------------|---------------|-------------|------------------|
| Baseline | 0.474 | 1.16 | 10.6 | 21.61 |
| Stiff | 0.767 | 1.89 | 9.37 | 21.81 |
| No damping | 0.0338 | 0.0836 | 6.10 | 37.29 |
| Hardlinks | ∞ | ∞ | 2.57 | 32.37 |

TABLE 3.4: Cornering at 2g simulation performance

A frequency breakdown of the step input response (figure 3.12) gives us the same conclusion as the frequency response plot, similar output to 1.1g cornering, with reduced variation in vertical tire load in the lower frequencies, particularly noticeable for stiff damping around 5-8Hz.

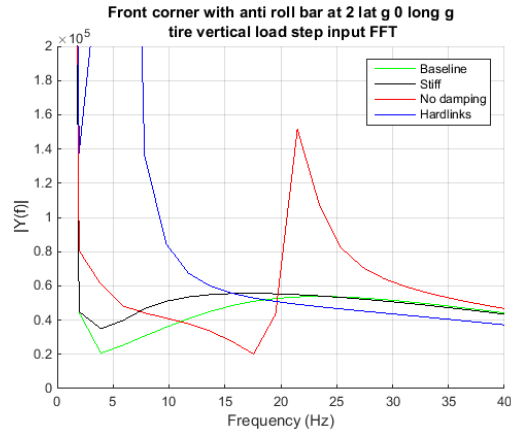


FIGURE 3.12: Cornering at 2 g tire vertical load step input frequency breakdown

As longitudinal performance of the of the vehicle too is important, it would be appropriate to also consider the behavior of the quarter car model under pure longitudinal and combined lateral-longitudinal accelerations. However, as vehicle accelerations are only manifested in the quarter car model as an apparent change in the sprung mass, the behavior will be very similar to the lateral cases already studied and identical to the lateral case with load transfer giving the same apparent sprung mass. As the simplified equation for longitudinal load transfers differs from the lateral load case (equation 1.3) only by substitution of the wheelbase for the track width, it should be clear

$$\frac{\text{longitudinal load transfer}}{\text{lateral load transfer}} = \frac{\text{wheelbase}}{\text{track}} \quad (3.1)$$

and thus with the quarter car model:

$$\text{longitudinal acceleration} = \frac{\text{lateral acceleration} \times \text{track}}{\text{wheelbase}} \quad (3.2)$$

which give the two investigated lateral cases as also representing braking cases of 0.81 and 1.5 g.

3.1.4 Changes between straight line / cornering

In addition to the load transfer effects studied, vertical spring rate of the tire will also change due to vertical load and contact patch lateral and longitudinal motion.

There is a recognized reduction in tire vertical spring rate with lateral force, largely due to the lateral motion of the sidewall [21], a significant contributor to vertical spring rate. Figure 3.13 illustrates.

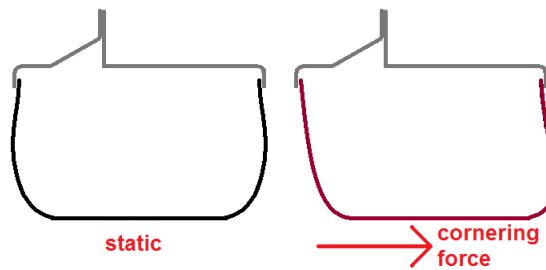


FIGURE 3.13: Sidewall deformation due to cornering force

3.2. Vehicle testing

Analysis of physical test data was started looking at the basic isolated tests and working up in the tests with more factors at work. The intent was to understand the most simple tests first and make conclusions about vertical dynamics before investigation of the resulting lateral effects.

3.2.1 Straightline

The straightline tests were run at two speeds - approximately 48kph and 32 kph, which we will refer to as high and low speed. The natural track surface was run with and without the artificial bump. In both cases we look at a window of 0.1 seconds before of the beacon and 0.5 seconds after, ensuring capture of sufficient behavior for analysis.

The first impression of the vertical tire load on the straightline track without the

artificial bump is that the track is anything but flat, as illustrated in figure 3.14. The test site is a former RV sales parking lot, and contains both large wavelength bumps and macro and microscale surface roughness. Appendix E contains photos of the pavement.

Because of the noisy nature of physical test data, comparison between data may not always be clear cut. Two sample t-test tools in MATLAB are used to conclude whether the difference is statistically significant, ie due to a true difference rather than the result of sampling error. The terms suggestive, moderate and convincing evidence are used in this paper exclusively to report the statistical evidence against the null hypothesis of two populations of data being the same either in mean or variance as detailed. Whenever these terms are used they are accompanied by the p-value of the test. When a statistical test is not used, these words are not be used, instead terms such as some, much, or strong.

Straightline without bump

As noted, there is substantial tire vertical load activity on the natural track. While looking at tire vertical load in the time domain illustrates the chaotic nature for all dampers, it is difficult to make any conclusions at this level of analysis. Figure 3.15 condenses this data, showing the vertical load variation on for each damping configuration with the standard deviations printed out. Hardlinks clearly have the largest variation in vertical loads in all rounds with statistically convincing evidence of a difference in standard deviation to all other configurations. Unfortunately for clarity of conclusions, with select exceptions, all configurations have a statistically significant (p-val <0.00694) difference in standard deviation from other configurations. The exceptions are between stiff and no damping with no evidence of a difference (p-val = 0.425) in round 1 high speed, between baseline 1 and no damping in both rounds at high speed with no evidence of a difference (p-val <0.727) and between baseline 1 and stiff in both rounds at low speed with no and moderate evidence (p-val = 0.382 and 0.0382 respectively).

As we would expect, the load variation is higher among all configurations in the

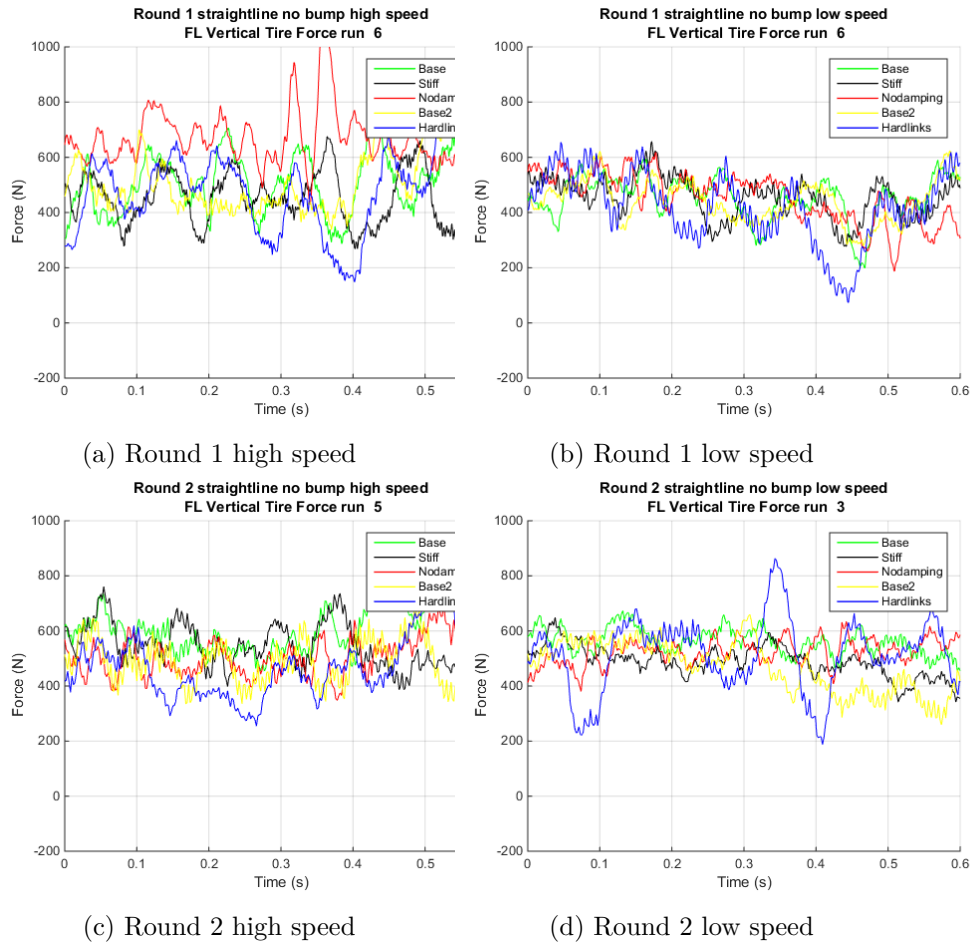


FIGURE 3.14: Straightline without bump FL vertical tire force

high speed runs, and also higher in round 1 than round 2. Average speeds are nearly identical between round 1 and 2 so it is possible this difference is due to the difference in tire vertical spring rate in the different weather conditions. Round 1 was in colder, damp conditions which could increase tire spring rate.

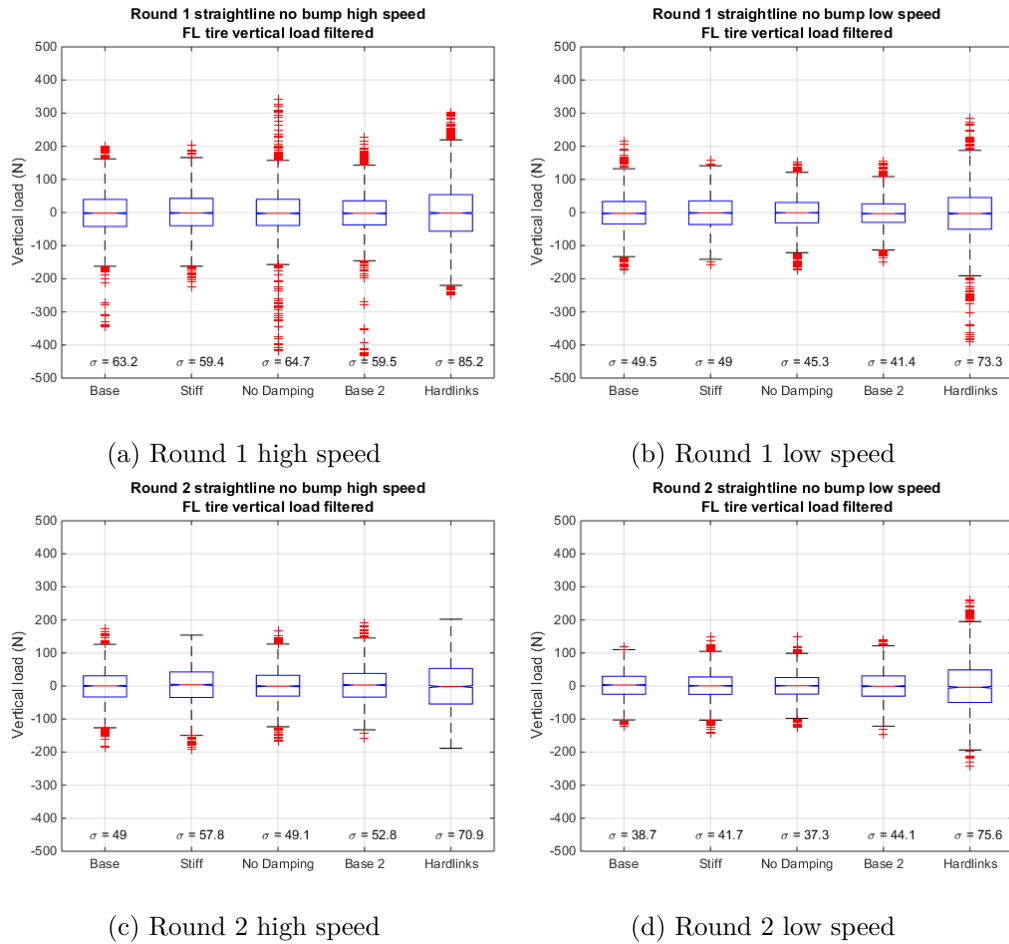


FIGURE 3.15: Straightline without bump FL Tire vertical load distribution

Figure 3.16 shows a summary of the Grip Factors for each round with the mean displayed. Hardlinks clearly have the lowest Grip Factor with convincing evidence (p -val < 0.00891) of a difference in mean to all other configurations save for stiff damping in round 2 high speed, where there is moderate evidence (p -val = 0.0123). In round 1 high speed there is no evidence of a difference (p -val > 0.132) between any of the damping configurations except for the hardlinks, for which there is convincing evidence as noted. In round 1 low speed there is convincing evidence between the base runs (p -val = 0.00764), which makes conclusions difficult. There is convincing evidence between base 2 and stiff

(p-val = 0.00106), suggestive evidence between stiff and no damping (p-val = 0.0585), and suggestive evidence between base 1 and no damping (p-val = 0.0754).

In round 2 high speed there suggestive evidence between base runs (p-val 0.0814) and moderate evidence between base 1 and stiff (p-val 0.0280). There is no evidence between stiff, no damping and base 2.

In round 2 low speed there is convincing evidence between base runs (p-val 0.00472) no evidence between all others except hardlinks, where there is convincing evidence (p-val <0.00320) to all other dampers. The spread of Grip Factors between configurations is the largest of the tests, and each damper has very large spreads. This is probably indicative of poor experimental control, with 5 runs for each configuration, although not bad speed control of each run. Although the variances make it difficult to see, there seems to be evidence that no damping may have the best Grip Factor overall, with baseline 2 runs within uncertainty. There is stronger evidence that stiff has worse Grip Factors and it is clear hardlinks fare the worst in that regard. The cause of the not insignificant differences between the baseline runs, but could be due to driver and vehicle warm up.

FFTs of filtered vertical tire load let us break down the frequency composition of the signal (figures 3.17 and 3.18). The plots are very similar at both speeds in both rounds, with more activity in the higher speed data, matching the time domain plots. Peaks in the FFT give us indication of the system natural frequencies. There is a substantial peak at approximately 10 Hz in both base runs and the hardlinks, but this peak shifts down to about 8.5 Hz with the stiff dampers and is dramatically reduced for no damping. A second, substantially smaller peak appears at around 32 Hz for both base runs and hardlinks. This peak is slightly lower for the stiff dampers and part of a more continuous response distribution for no damping. These should be a function of the physical geometry of the system so it is expected that there is not a speed dependency. We can see the prominence of these peaks is reduced in the baseline and stiff damper data indicating a more even

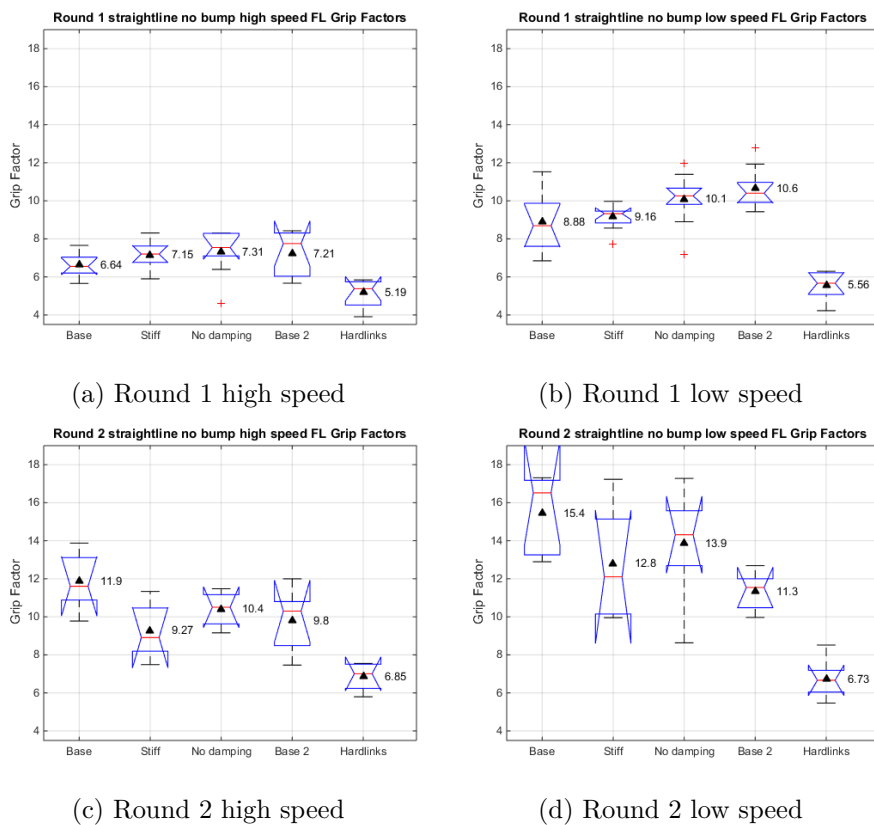


FIGURE 3.16: Straightline without bump FL Grip Factors

response to road disturbances.

Round 2 data is similar, but with smoother roll off in force magnitude with increasing frequency. Stiff, baseline 2 and hardlinks again have a strong peak at 10 Hz, but the secondary peak is not visible. No damping again has an fairly even distribution with minimal peaks. These plots are shown in appendix D2.

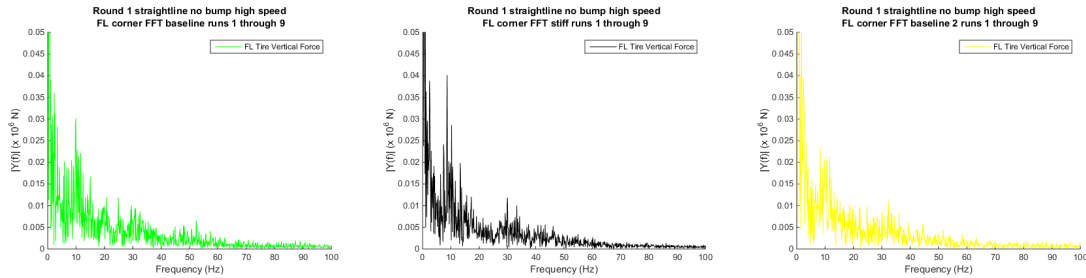


FIGURE 3.17: Round 1 straight no bump high speed FFTs

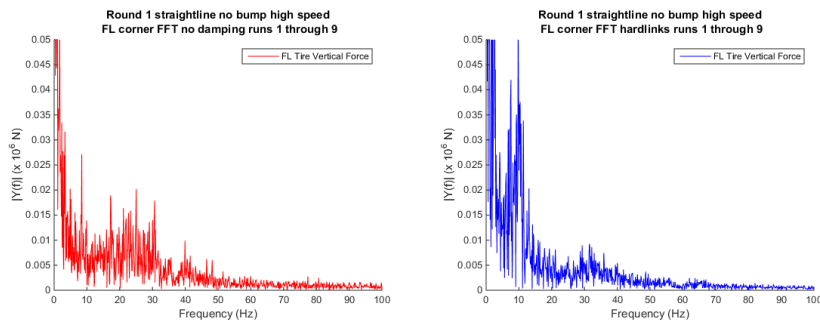


FIGURE 3.18: Round 1 straight no bump high speed FFTs

Straightline with bump

Looking at the runs with the bump, we can see how each damper responds to large scale inputs. As we would expect, we see an obvious peak in the tire vertical loads for all dampers as the bump is hit. Figure 3.19 shows an example of each round at both speeds.

It is clear the peak force on the tire is not a function of speed, but very clearly higher in round 2 data with the larger bump. The following negative force trough however, is similar in both rounds and speeds, just hitting zero vertical load, indicating the tire is off the ground. In both round 2 plots the baseline 2 trace is clearly offset from the others (figure 3.20), illustrating a data error that was traced back to all round 2 with bump data. For this reason baseline 2 data from round 2 with bump testing will be excluded in further analysis.

Figure 3.21 summarizes the tire vertical load data. The data is passed through the

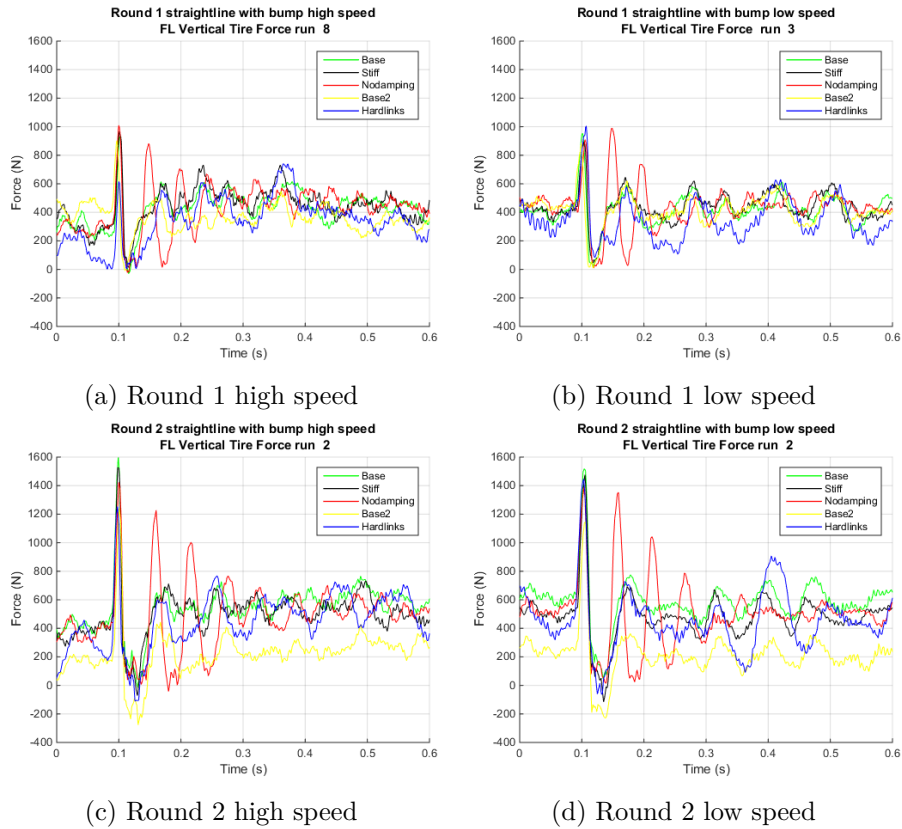


FIGURE 3.19: Vertical load variation on FL corner, straight line with artificial bump

low pass filter and so it centered around zero force.

Presumably due to the dramatic load oscillation no damping sees over the bump, no damping has the largest variation in tire vertical load over the bump in both rounds and speeds, the opposites result of the straightline tests without the artificial bump.

Baseline and stiff are similar, with the baseline runs generally having marginally less variation in load. There is convincing evidence (p-val 8.07×10^{-7}) of a difference between stiff and baseline 2 at both speeds in round 1, convincing evidence (p-val = 0.00742) between stiff and baseline 1 in round 1 low speed, and moderate evidence (p-val = 0.028) in round 2 low speed. Elsewhere this is no evidence of a difference, so we can conclude there is evidence that baseline dampers have less vertical load variation amidst the data

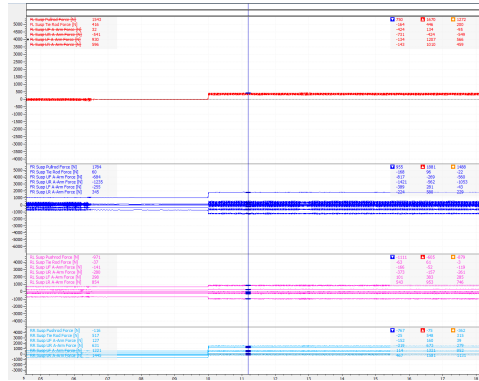


FIGURE 3.20: Round 2 baseline 2 data shift error

noise. This “noise” or other clouding factors in the data is illustrated by the differences in baseline runs. Comparing the baseline runs in round 1 testing, there is convincing evidence of a difference (p-val = 0.0482) at high speed and moderate evidence (p-val = 0.0108) at low speed.

Comparing the hardlinks and no damping, there is suggestive (p-val = 0.0521), convincing (p-val = 6.03×10^{-8}), convincing (p-val = 2.08×10^{-13}), and no evidence (p-val 0.146) of a difference in standard deviation in round 1 and round 2 testing at high and low speed respectively. We can safely say that both configurations have more vertical load variation than the other configurations, and no damping has more variation than hardlinks.

Looking at Grip Factors should give the same information, but in a different visualization, number of datapoints and statistical results. Figure 3.22 illustrates Grip Factors of each configuration over the bump. As expected and matching the vertical load variation results, baseline and stiff configurations are similar, and markedly separated from the hardlinks and no damping which are somewhat similar. Between the four datasets there appears to be minimal speed dependency, but the size of the bump does appear to have an effect. In round 1 testing the baseline runs are similar in performance to the stiff dampers, with no evidence (p-val >0.394) of a difference between them in round 1 high

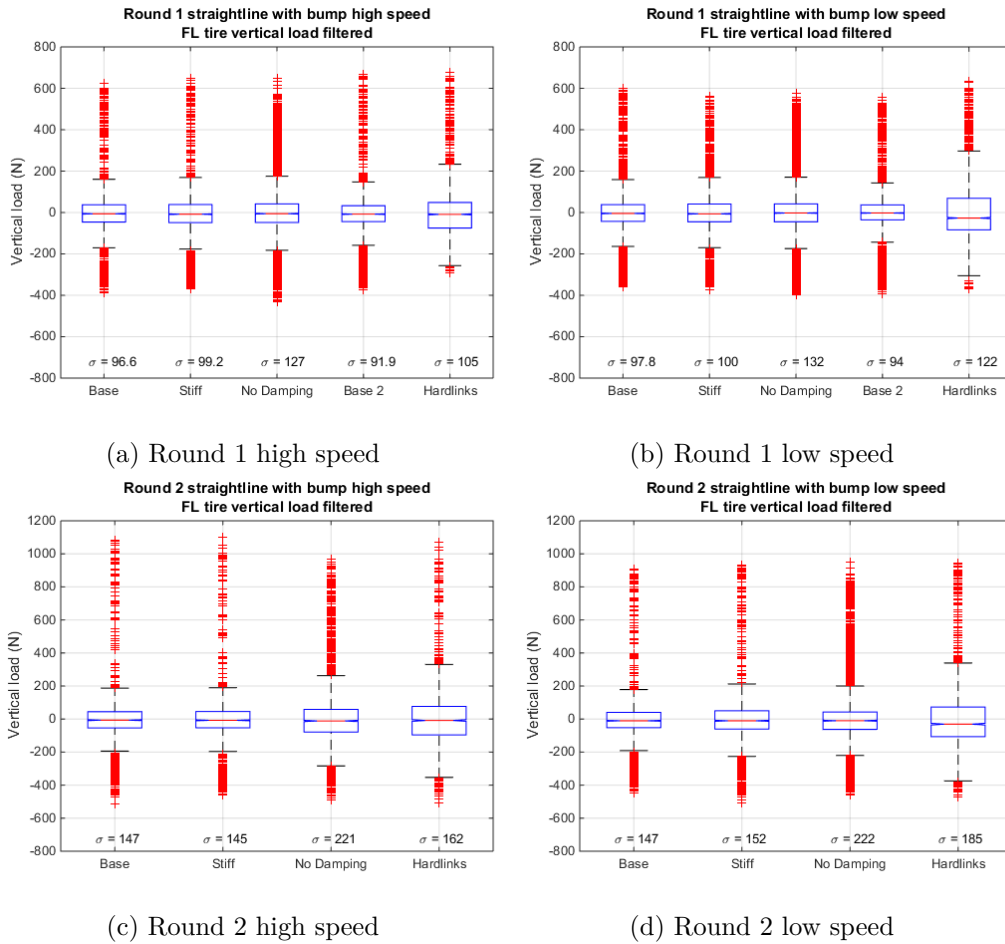


FIGURE 3.21: Straightline with bump FL Tire vertical load distribution

speed, and moderate (p-val = 0.0304) and no evidence (p-val 0.205) between stiff and baseline 1 and 2 respectively at low speed. In round 2 testing the result is much more conclusive, with convincing evidence of a difference between baseline and stiff at both speeds (p-val <0.000104).

As expected from the visual difference in Grip Factor, there is convincing evidence (p-val <0.00156) between all baseline and stiff runs and both no damping and hard links.

Between no damping and hardlinks the relationship is less clear, with no evidence of a difference in round 1 high speed (p-val = 0.747) and round 2 low speed (p-val = 0.133),

and convincing evidence in round 1 low speed ($p\text{-val} = 0.00650$) and round 2 high speed ($p\text{-val} = 3.13 \times 10^{-5}$)

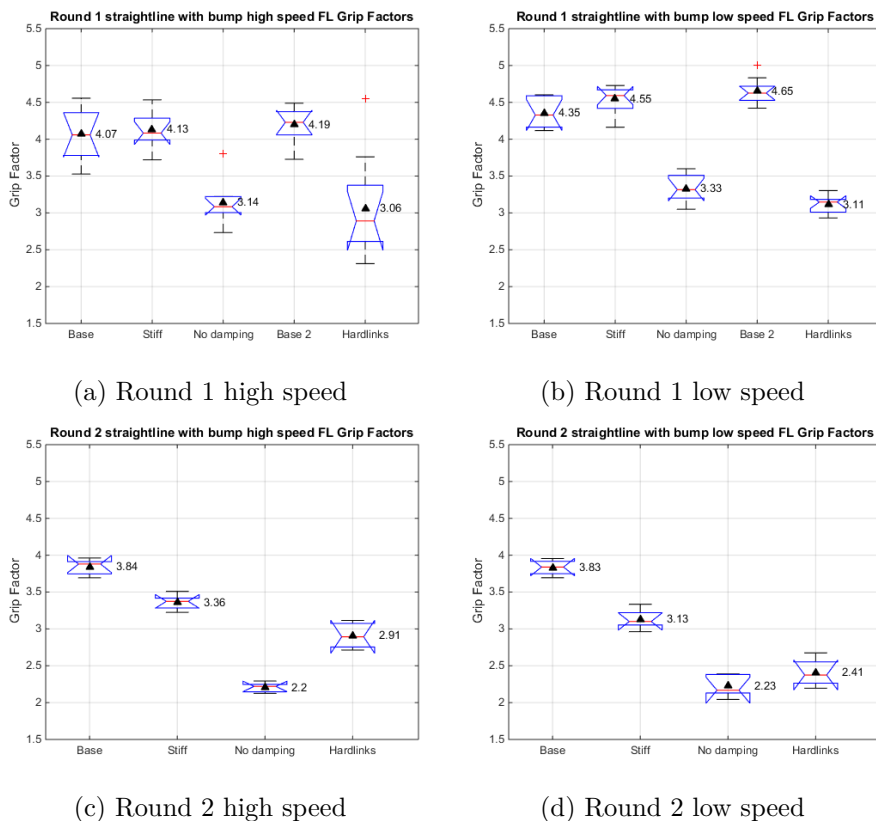


FIGURE 3.22: Straightline with bump FL Grip Factors

Interestingly unlike the natural track without the bump, no damping has a worse Grip Factor than the baseline runs. This is perhaps due to the continued oscillations of vertical tire load after the bump, occurring at about about 23 Hz in round 1 and 18 Hz in round 2. Figure 3.23 shows the frequency content of the no damping runs. The shift of the 20 Hz peak towards the lower frequencies and emergence of the 36 Hz peak in the round 2 data is interesting, perhaps due to the larger bump, since there appears to be little if any speed dependency in both rounds.

Vertical tire load response with the hardlinks is very evenly spread across the 0-40

Hz range in the high speed runs, but there is a more focused response in the low speed runs as seen in figure 3.24 with strong response at 10 Hz and 29 Hz.

Excitation due to the artificial bump is in the much higher frequencies, at 48 and 32 kph the frequency of hitting the leading and trailing edge of the artificial bump is 350 and 233 Hz respectively.

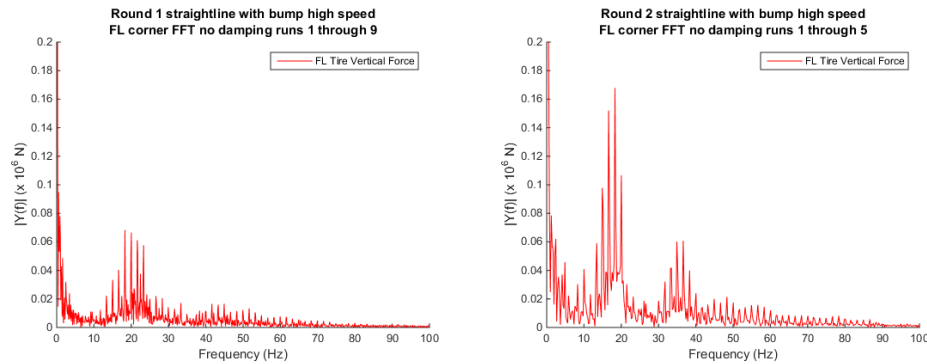


FIGURE 3.23: Frequency content of vertical tire load, no damping

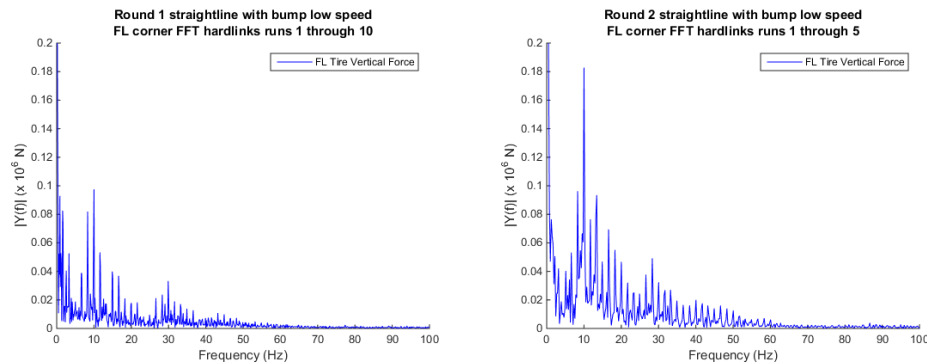


FIGURE 3.24: Frequency content of vertical tire load, no damping

Looking at the vertical force in the suspension can tell us about the ride quality of each damper configuration. In figure 3.25 we can see that the hardlinks have the highest vertical load transmission to the body, while no damping has the least and the first baseline run and the stiff dampers fall somewhere in between. Damper speeds are shown in inch units for easier reference to dyno plots in Appendix B. Round 2 data follows the same

trends as that in figure 3.25, but with vertical suspension force reaching 1200 N for the hardlinks and damper speeds reaching 13 in/s for no damping and 5 in/sec for the other dampers.

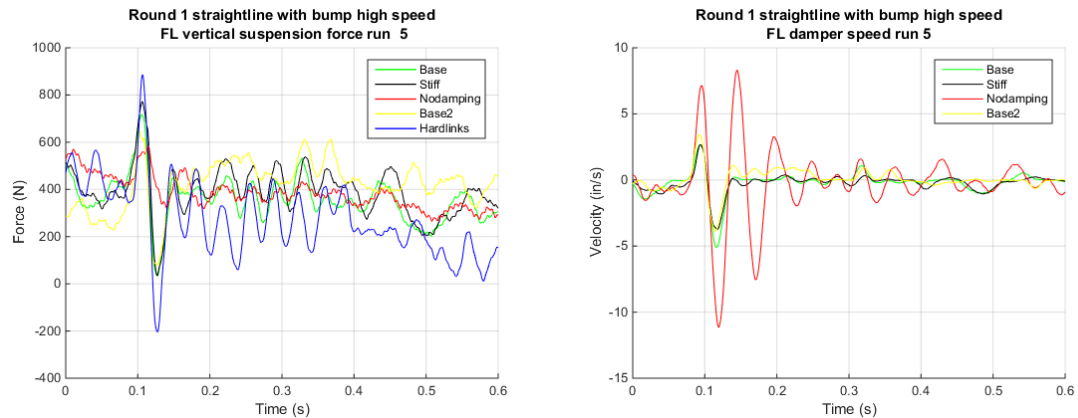


FIGURE 3.25: Vertical suspension force and damper speed over the artificial bump

3.2.2 Skidpad

Data from the skidpad track lets us look at typical forces during a cornering event. In round 1 data the wet track and cold temperature limited lateral acceleration to about 1.1 G, while 1.5 G was achieved in round 2 testing. A typical plot of vertical and lateral forces over a lap is shown in figure 3.26. As with the straightline case, a window of 0.1 seconds before the bump location (whether or not it is present) and 0.5 seconds afterward is examined.

Skidpad without bump

We can clearly see that as in the straightline case, the track is anything but smooth. This leads to lateral forces which vary considerably in what we would call steady state cornering. Tie rod forces, though not shown look very similar in shape to the lateral force while being a magnitude smaller and often reversing direction.

Differences between dampers are best seen when the data is condensed into boxplots as in figure 3.27. We can clearly see the largest variation in vertical load of the Hardlinks,

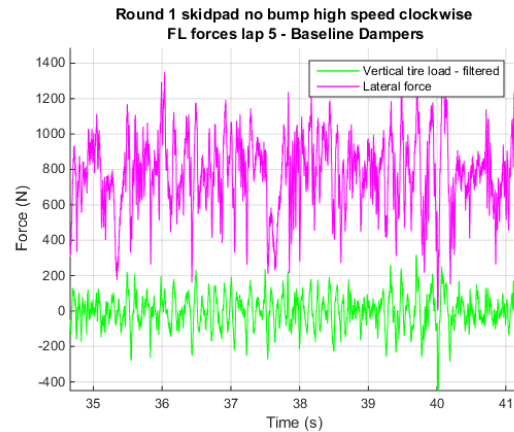


FIGURE 3.26: FL corner forces skidpad

while no damping has the smallest variation. Visually, it is difficult to see a difference between the baseline runs and the stiff setup. The same can be said for the Grip Factors in figure 3.28.

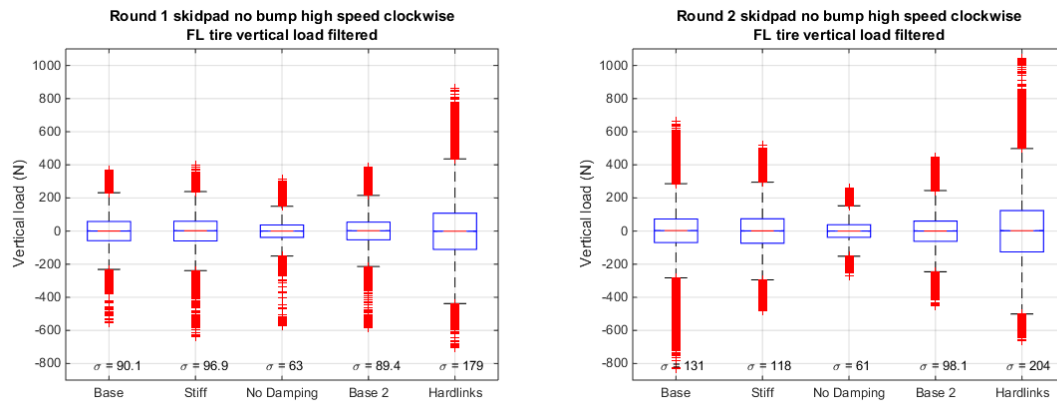


FIGURE 3.27: Vertical tire load filtered, for each damping configuration

There is convincing evidence of a difference ($p\text{-val} < 4.56 \times 10^{-11}$) between all dampers in both rounds of testing. Unfortunately the t tools do not tell us anything about the size of the differences, but looking at the standard deviations, it is clear the as expected the baseline and stiff dampers are most alike, with larger differences to no damping and hardlinks.

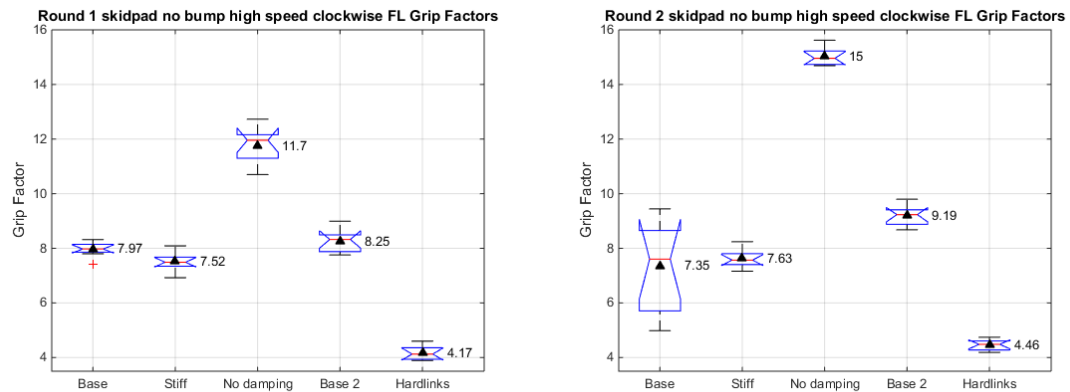


FIGURE 3.28: FL Grip Factors

Looking at Grip Factors, in round 1 there is convincing evidence ($p\text{-val} < 0.00817$) between all runs except for the baseline runs, where there is no evidence ($p\text{-val} = 0.111$).

In round 2 there is convincing evidence ($p\text{-val} = 0.00325$) between all runs except for baseline 1 and stiff, where there is no evidence ($p\text{-val} = 0.608$) of a difference. In both rounds no damping has the best performance while hardlinks has the worst, matching the conclusion from vertical load variation.

In the skidpad tests, a good measure of performance is the purely the lateral or cornering force. Figure 3.29 summarizes lateral force for each damper. In both round 1 and round 2 testing there is convincing evidence ($p\text{-val} < 2.82 \times 10^{-5}$) of a difference between all configurations. As no damping had the smallest standard deviation in vertical load and the largest Grip Factor in both rounds, a similar performance delta is expected in lateral force. This difference is not as clear however. In round 1 no damping has the the largest mean and a tighter distribution of lateral forces, but in Round 2 is outstripped in mean by stiff and baseline 2, while maintaining the smallest range of loads. The relationship between vertical load variation or Grip Factor and lateral force can be examined more closely in figures 3.30 and 3.31.

These two figures in the end are different visualizations of the same information.

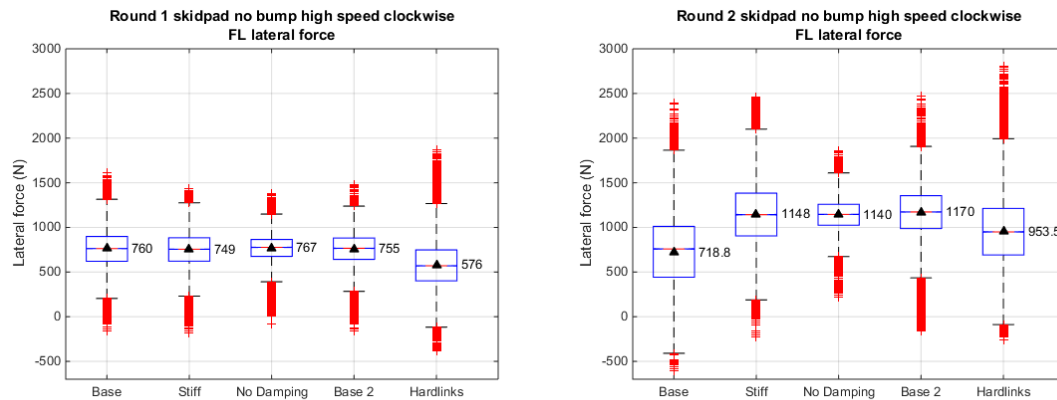


FIGURE 3.29: Skidpad lateral performance

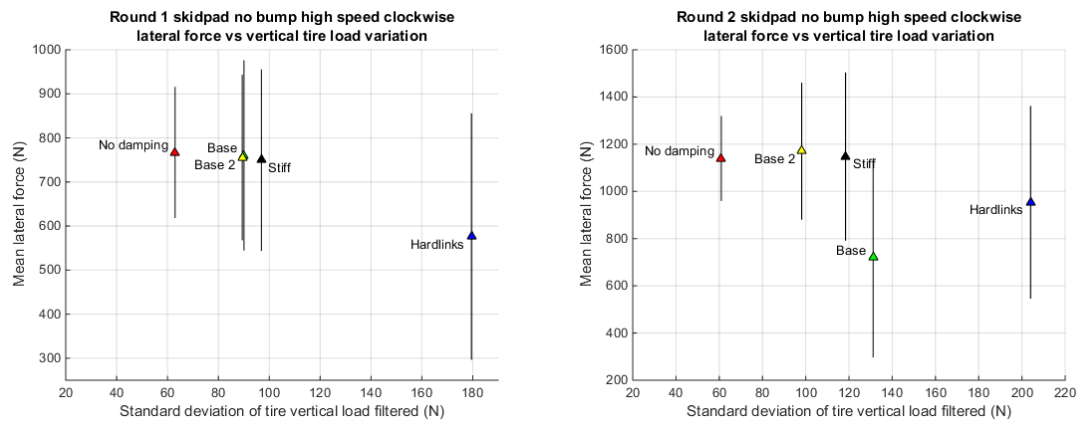


FIGURE 3.30: Skidpad without bump vertical and lateral force coupling

Figure 3.30 plots the standard deviation of lateral force over the whole run for each damper, giving a single value summary of the performance. Lateral force is plotted as a single mean value for each damper, with error bars of 1 standard deviation in each direction. A cursory look at round 1 data finds a slight relationship between vertical tire load variation and lateral force, with more load variation reducing lateral force. This is much less clear in round 2 data, where baseline 1 has substantially less lateral force than expected, the lowest of any damper tested.

Figure 3.31 gives another visualization of the same information, plotting lateral force

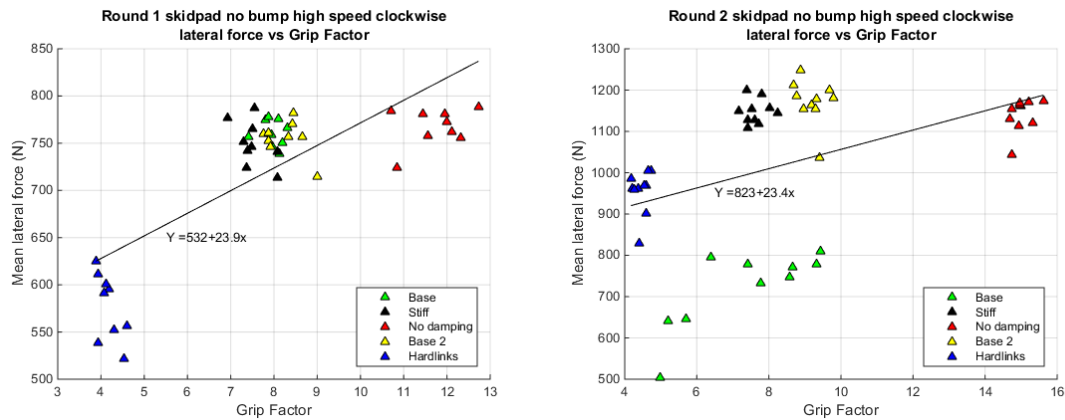


FIGURE 3.31: Skidpad without bump vertical and lateral force coupling

against the Grip Factor of each lap. The point clouds give a better representation of how each individual lap differs in both axes. Best fit (minimum residuals) linear trendlines are shown on each plot to give some indication of the overall trend of the data, though the fit is poor at best with R-square values of 0.588 in round 1 and 0.214 in round 2. Baseline 1 data is likely the cause of the particularly poor fit in round 2, again as it does not match well with the other data.

Ultimately, lap times are the final measure of overall performance. Lap time data was only obtained for round 1 testing as a logging failure in GPS for the stiff dampers in round 2 testing limited its utility. Round 1 times are shown in boxplot form in figure 3.32.

There is convincing evidence of a difference in lap time between the baseline runs ($p\text{-val} = 0.00162$) and the large difference in means between the two makes conclusions with other dampers difficult. Baseline 2 has both the lowest mean and single fastest lap time among all dampers; perhaps the second slowest mean lap time of baseline 1 can be explained by a driver warming up to the course. Other than to baseline 2, there is no evidence of a difference in lap time between baseline 1 and any other damper.

There is however, moderate evidence ($p\text{-val} = 0.0489$) evidence of a difference be-

tween baseline 2 and no damping, moderate evidence ($p\text{-val} = 0.0385$) to stiff damping, and convincing evidence to the hardlinks ($p\text{-val} = 0.00875$);

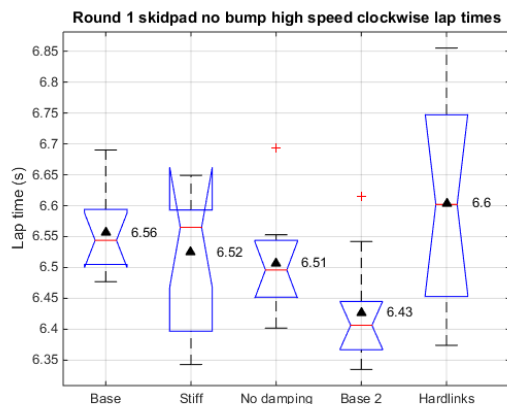


FIGURE 3.32: Skidpad lap times without bump

FFTs of vertical tire load are similar to those of the straightline case, but with more activity due to the longer laps, a clearer picture of system response can be seen in figures 3.33 and 3.34. Lateral force response echos that of vertical load, but with a strong peak at 32 to 36 Hz, larger in round 2 than round 1. Plots from round 1 can be found in appendix D3.

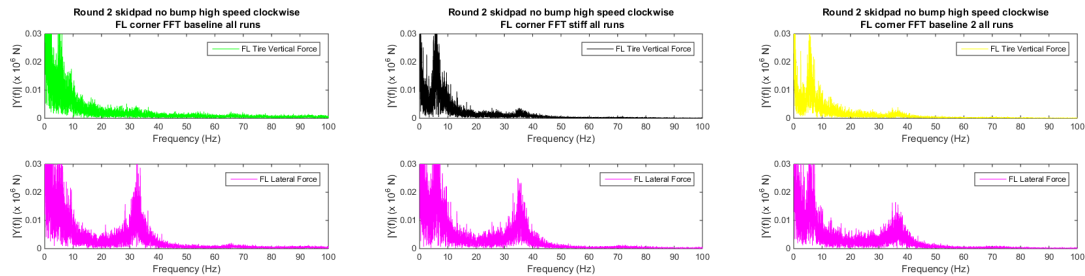


FIGURE 3.33: Round 2 skidpad FFT

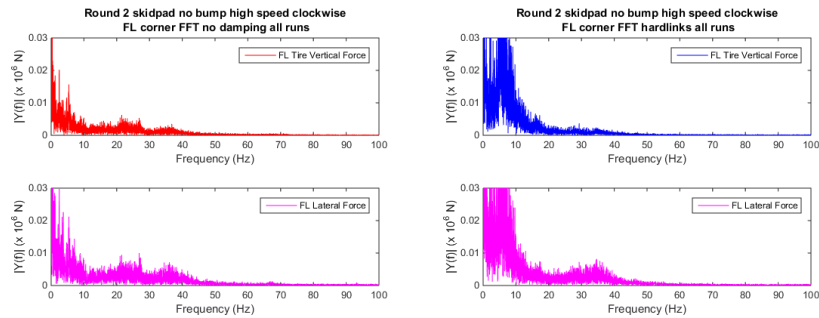


FIGURE 3.34: Round 2 skidpad FFT

Skidpad with bump

As with the straightline tests, an artificial bump was also used in skidpad to evaluate the vehicles response. A sampling of the FL suspension channels hitting the bump can be seen in figure 3.35. All channels shown are in units of N force, except for upright acceleration, expressed in Gs acceleration times 100. In high speed tests the driver was instructed to drive at the limit and the bump was placed such that a driver taking the inside line in a clockwise skidpad would hit it with the left side tires. Speeds were 41kph on average during round 1 testing and 46.6 kph in round 2 testing, being slightly higher for baseline runs and lower for hardlink runs.

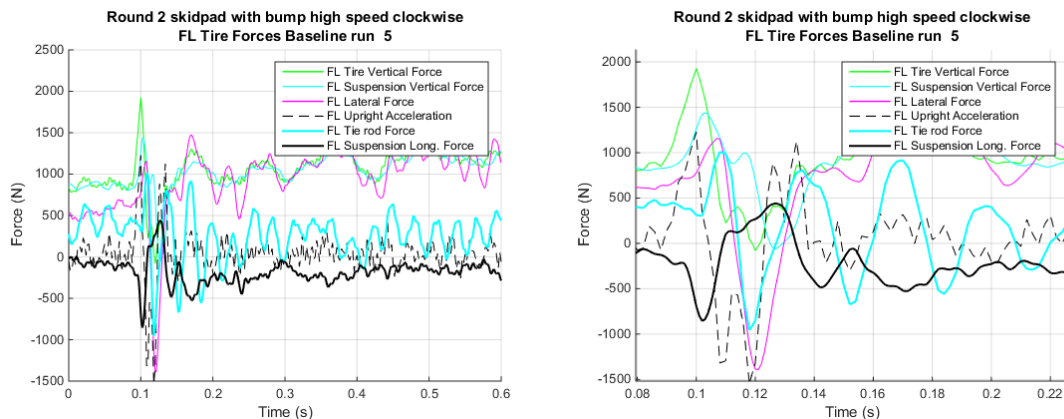


FIGURE 3.35: Left: FL corner hitting bump in skidpad. Right: detail of same plot

The tire vertical force trace give the best indication of the start of the bump, spiking to 1900 N in figure 3.35 before dropping to zero and then recovering. Round 2 data is shown here to illustrate the worst case bump behavior, with both the high speed and larger hight bump. All channel activity over the bump is lower in round 1 data.

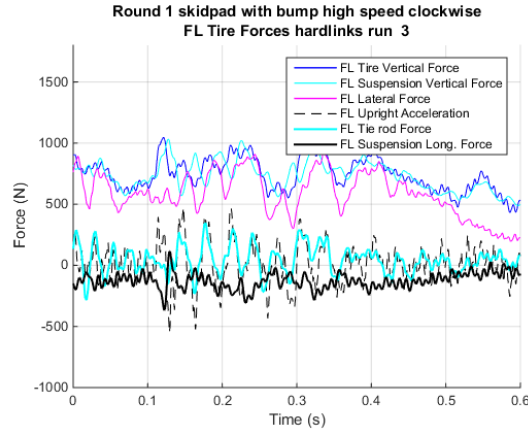


FIGURE 3.36: Example of driver not hitting bump with hardlinks

In 2 of the 10 hardlinks runs the driver was not able to hit the bump as seen in figure 3.36. In all other runs, every channel shows a complete oscillation hitting the bump, including lateral force and tie rod force. This means the wheels temporarily push the car out of the corner as the steering wheel force felt by the driver reverses.

Looking at the timing of each channel oscillation, we can see there is measurable delay in some channels. Suspension vertical load is the next channel to show bump behavior after tire vertical load. For the baseline dampers this delay averages to 0.71 m in round 1 and 0.98 m in round 2. The difference between the rounds could be due to the higher speed or larger artificial bump in round 2. An example plot can be seen in figure 3.37.

As seen in the straightline tests, no damping sees continued oscillation of the vertical load for two or more cycles. Hardlinks produce a similar phenomenon with more cycles and two more visibly distinct frequencies. These correspond to the vibration of the sprung

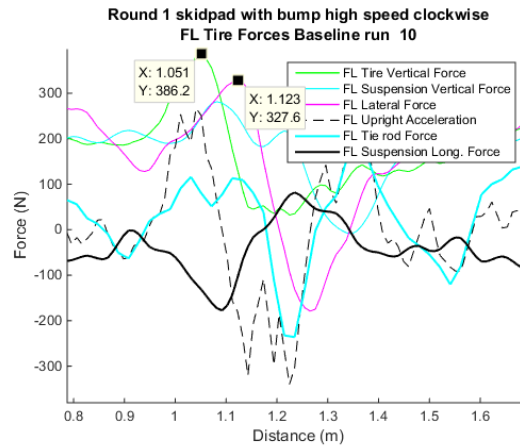


FIGURE 3.37: Delay between suspension vertical and lateral loading

and unsprung masses respectively. Plots of both no damping and hardlinks are shown in figure 3.38.

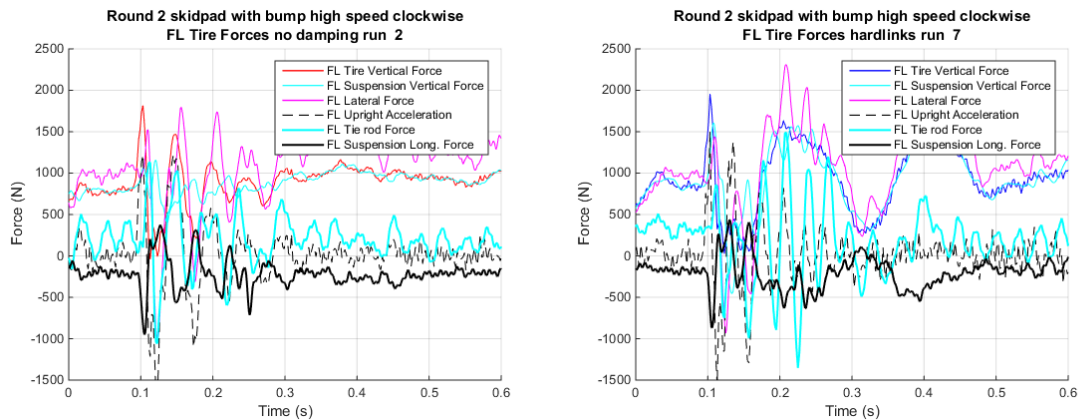


FIGURE 3.38: Continued oscillation of vertical tire load with no damping and hardlinks

Looking at FFTs, the frequency content of the baseline and stiff runs is fairly even from 0 to 40 Hz (figure 3.39), while both the no damping and hardlinks both have very definitive peaks in vertical tire load occurring at 22 Hz for no damping and 6 and 29 Hz for the hardlinks (figure 3.40).

In both rounds of testing the drivers had difficulty hitting the bump on every lap.

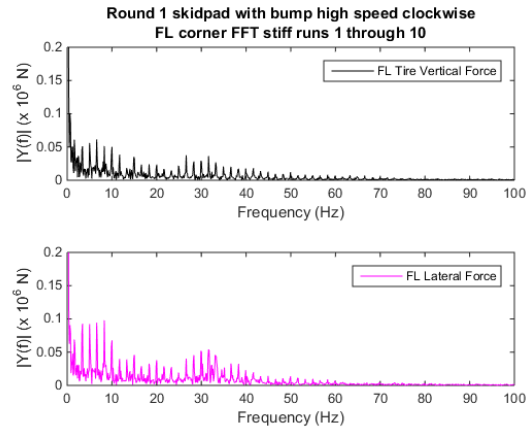


FIGURE 3.39: Frequency content of tire forces - skidpad with bump

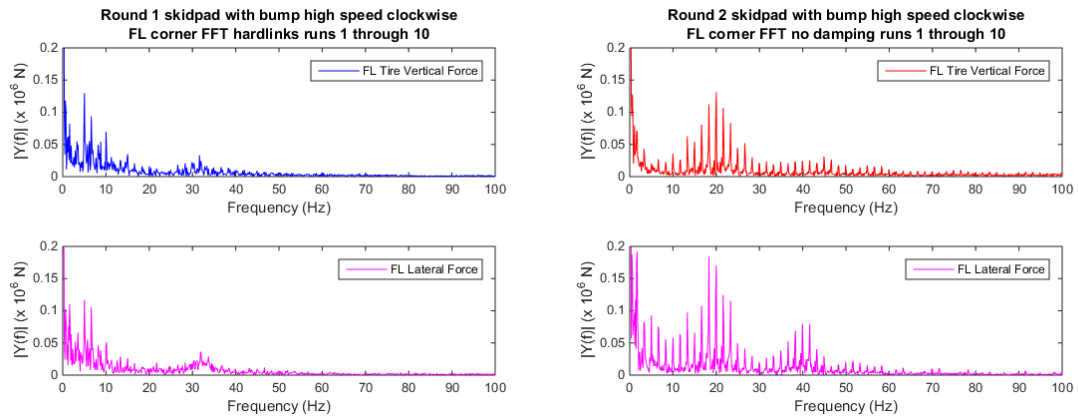


FIGURE 3.40: Frequency content of tire forces - skidpad with bump

These laps can be clearly seen as outliers in the data with significantly higher Grip Factors and the absence of spikes in suspension vertical load and upright acceleration, occurring three times in the first round and once in the 2nd round. The last run of many of the damping configurations was also not representative of steady state skidpad performance over the bump, with the driver reducing steer angle and increasing speed after the bump. Both these outlier types have been removed from the data in figures 3.41, 3.42, and 3.43.

Looking at boxplot summaries of tire vertical load filtered, vertical load control of each damper can be more easily compared. Figure 3.41 illustrates.

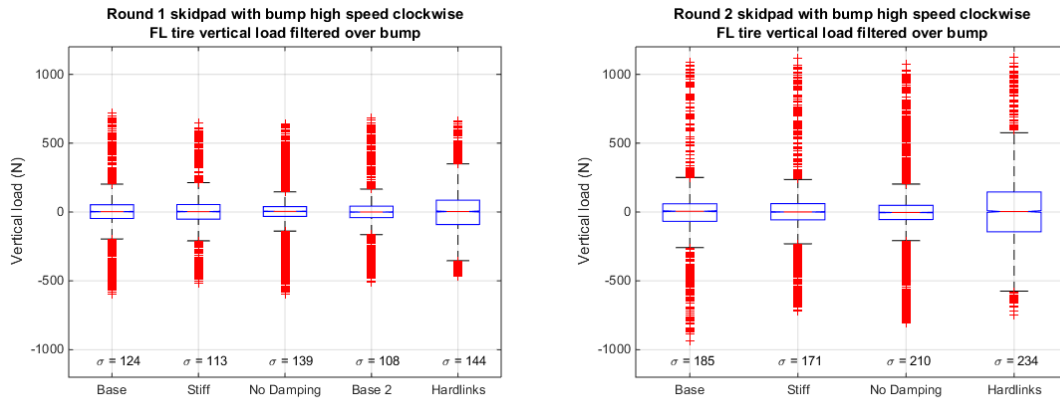


FIGURE 3.41: Vertical tire load filtered over bump

In both rounds of testing there is some evidence between baseline 1 and stiff, with no evidence ($p\text{-val} = 0.380$) in round 1 and moderate evidence ($p\text{-val} = 0.01738$) in round 2. There is convincing evidence ($p\text{-val} = 1.62 \times 10^{-10}$) of a difference between baseline 2 and stiff in round 1, but the previously mentioned logging error means the same comparison cannot be made in round 2.

In both rounds no damping appears to have a larger standard deviation than baseline 1, but there is no evidence ($p\text{-val} = 0.686$) in round 1 and convincing evidence ($p\text{-val} = 0.000954$) in round 2. This is perhaps due to the larger bump, causing more oscillation in no damping in round 2, while having a less significant impact on the other dampers.

Hardlinks again have the largest standard deviation, with convincing evidence ($p\text{-val} < 3.97 \times 10^{-53}$) of a difference to the other dampers in both rounds.

Grip Factors are a different representation of the same information, but useful as it is easier to interpret a difference in means than a difference in spread (figure 3.42).

With the exception of stiff and baseline 2 in round 1 where there is moderate evidence ($p\text{-val} = 0.0133$), there is convincing evidence ($p\text{-val} < 0.00726$) of a difference in Grip Factor between all dampers in both rounds of testing.

In lateral force (figure 3.43) there is convincing evidence ($p\text{-val} < 0.00270$) between

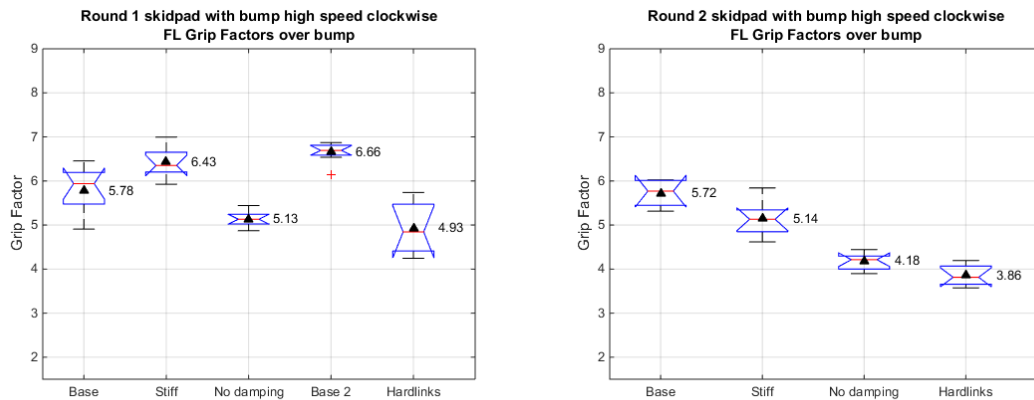


FIGURE 3.42: Skidpad high speed clockwise Grip Factors over bump

all dampers except for round 1 between stiff and no damping with moderate evidence ($p\text{-val} = 0.0429$) and round 2 between baseline 1 and hardlinks ($p\text{-val} = 0.0356$).

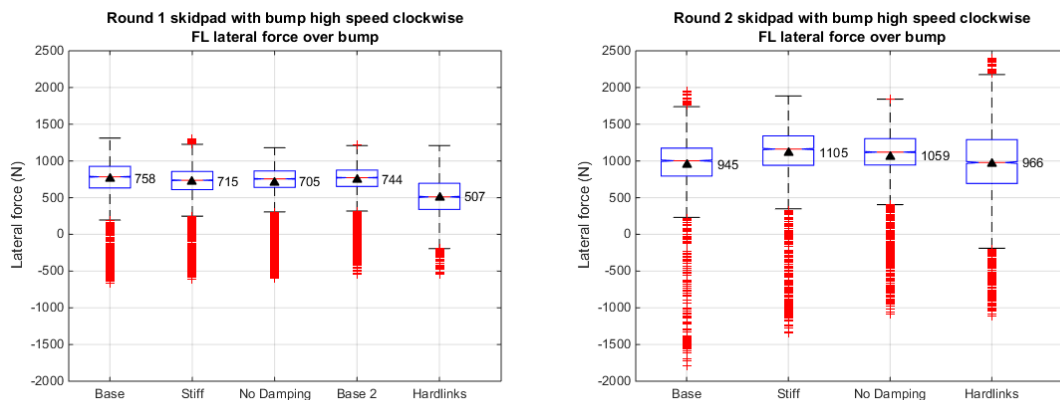


FIGURE 3.43: Lateral force over bump

Again we can look at the relationship between Grip Factor and lateral force, shown in figure 3.44. The relationship is weaker than the full lap data without the bump, but may still be present. R-square values are indicative of a trendline which does not well explain the variation in the data, at 0.315 in round 1 and 0.0368 in round 2. The relative lack of lateral force in round 2 baseline data can again be seen here.

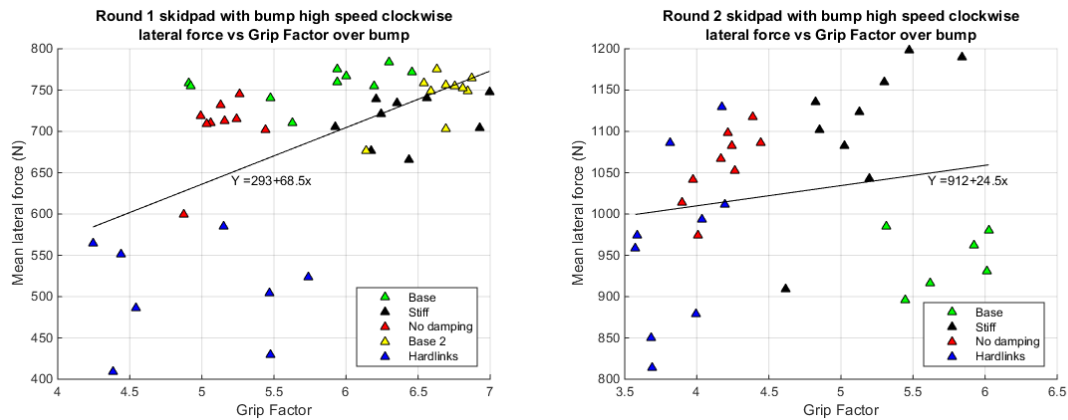


FIGURE 3.44: Lateral force vs Grip Factor over bump

3.2.3 Asymmetric Oval

Analysis of the Asymmetric Oval data reinforces the need to filter the vertical load data when using vertical tire load variation to compare damper configurations. As the course incorporates both left and right hand turns as well as acceleration and braking zones, vertical load change due to load transfer should not be accounted for as noted in section 1.5.. Vertical load variation and grip factors are shown in figure 3.45.

As with the other tests without the artificial bump, no damping has the smallest standard deviation in vertical load, and hardlinks have the largest. Baseline and stiff are similar, with both baseline runs having less variation than stiff and all closer in behavior to no damping than to the hardlinks. There is statistically convincing evidence of a difference between each damper, including the baseline runs, indicating changing conditions or a driver which is improving. The situation is similar, though easier to visualize when looking at Grip Factors.. There is convincing evidence ($p\text{-val} = 2.6 \times 10^{-7}$) of a difference in mean Grip Factor between the baseline runs which we would expect to be the same, indicating a difference in track or vehicle condition between the runs and clouding our inference of conclusions with other dampers. There is statistically convincing evidence of a difference from the the first baseline run to no damping and the hardlinks as well ($p\text{-val} = 0.0079$

and 3.8×10^{-15} respectively), but no evidence of a difference to the stiff dampers.

The second baseline run had the highest grip factor, with statistically convincing evidence ($p\text{-val} < 8.0 \times 10^{-6}$) against all other dampers except for no damping, where there is only suggestive evidence ($p\text{-val} = 0.079$). The hardlinks are again clearly the worst of the configurations, with convincing evidence ($p\text{-val} < 8.7 \times 10^{-11}$) and of a difference between the hardlinks and all other configurations.

We can say from a full track Grip Factor perspective, there is evidence to support at selection of no damping or baseline as the best choice.

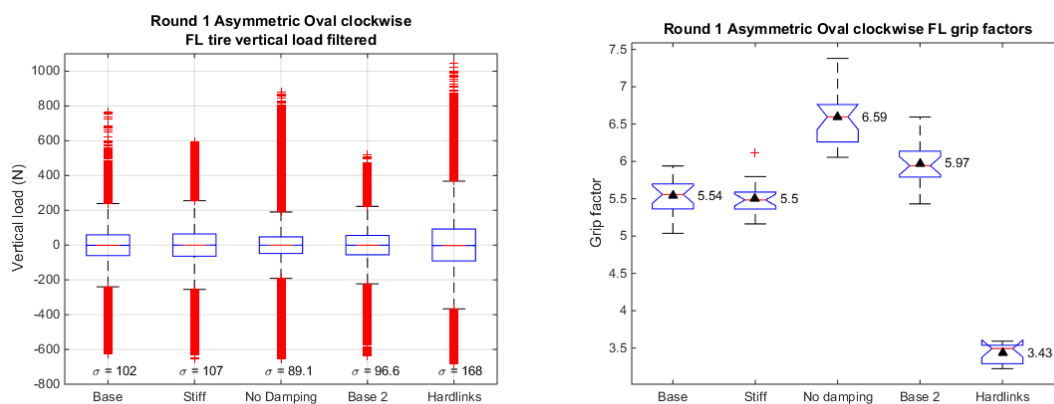


FIGURE 3.45: Vertical load and Grip Factors on Asymmetric Oval clockwise

Analysis of the lap time results shown in figure 3.46 lets us assess the total effect on our primary performance metric: how much faster is the car overall on a FS course? In general the data is difficult to read because the differences are very small and the ranges of each dataset is very large. Additionally, there were fewer runs of the hardlinks on the Asymmetric Oval because the driver felt the experience was particularly painful and it was affecting his ability to drive. This makes the sampling size fairly small at 10 runs counterclockwise and 11 runs clockwise. In addition the driver stopped the car on track to have the car checked two laps into the clockwise run, splitting the data physically and in the driver's mind.

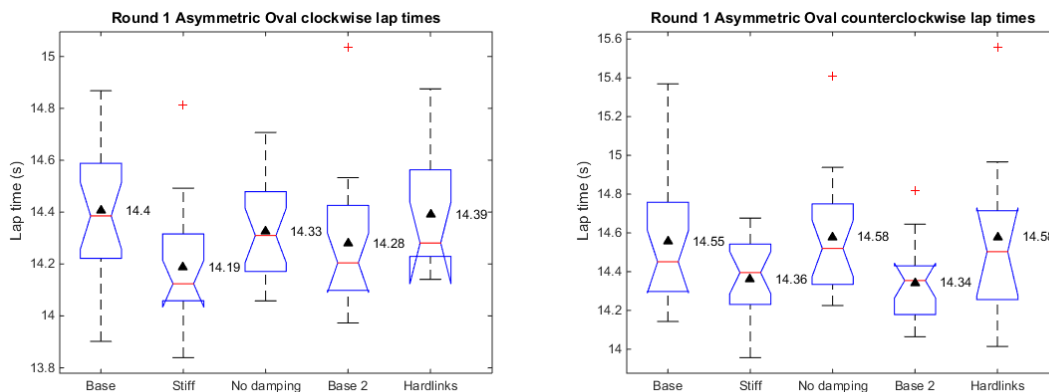


FIGURE 3.46: Asymmetric Oval lap times

The counterclockwise laps were run first, but we will examine the clockwise data first to compare it with the Grip Factor data taken from the left side of the car, making the clockwise run more relevant.

In the clockwise direction the most statistically significant difference is between the first baseline run and the stiff dampers. There is convincing evidence ($p\text{-val} = 0.009$) that the stiff dampers have a lower mean lap time. In fact stiff was the only damper configuration with any statistical difference in mean to any other damper, with moderate evidence ($p\text{-val} = 0.040$ and 0.029) to no damping and hardlinks respectively. There was no evidence of difference to the second baseline run which had the second fastest mean time.

In the counterclockwise direction there is moderate evidence of a difference ($p\text{-val} = 0.025$) of a difference between the baseline runs. Here the second baseline run is marginally faster than the stiff dampers, with statistically no evidence of a difference in mean between them. Likewise there is no evidence of a difference between the first baseline run, no damping and hardlinks. However the difference between these two groups is not clear cut, there is only suggestive evidence ($p\text{-val} = 0.054$ and 0.076) between the hardlinks and the second baseline run and stiff dampers respectively. The only statistically convincing

evidence ($p\text{-val} = 0.0061$) is between no damping and the second baseline run.

In both directions stiff damping has the fastest single lap time and lowest or second lowest mean time. From a purely lap time perspective stiff damping is likely the best choice.

It is surprising however, how well the hardlinks fare in terms of mean and standard deviation of lap time. In all tests hardlinks fare very poorly in Grip Factor, and in all tests before the oval also lag behind the other dampers in lateral force (with lower mean) and in lap time (with higher mean and larger standard deviation). In mean alone, Hardlinks are 1.41% and 1.69% slower than the fastest run in clockwise and counterclockwise respectively. This is a fairly small difference, considering the difference between first and second place finishers in the endurance event at FSAE Michigan 2014 were separated by 0.755%, with the third place finisher behind 3.36% from the leader. The teams, GFR, TU Munich, and the University of Stuttgart respectively, are arguably the best combustion FS teams in the world, all with international wins.

As with the skidpad tests, the relationship between vertical load variation or Grip Factor and in-plane performance can be evaluated; figure 3.47 illustrates. The relationship appears to be weak at best, with large variations in lap time for each damper, even as Grip Factors may be more clearly distinguished. The R-square value of 0.00210 affirms that there is little relationship. The poor correlation in this test may be due to the combination of track sections rewarding good steady state performance (the large corner and straight) and sections rewarding good body control (the slalom and hairpin corner). Testing with and without the artificial bump has shown the two situations favor different dampers.

FFTs of vertical tire load and lateral force shown in figures 3.48 and 3.49 illustrate system response similar to that seen in other tests, again indicating the Asymmetric Oval cycles the system in similar ways. The large peak around 7 to 10 Hz for baseline and stiff is characteristic of runs without the artificial bump, while no damping is similar to runs

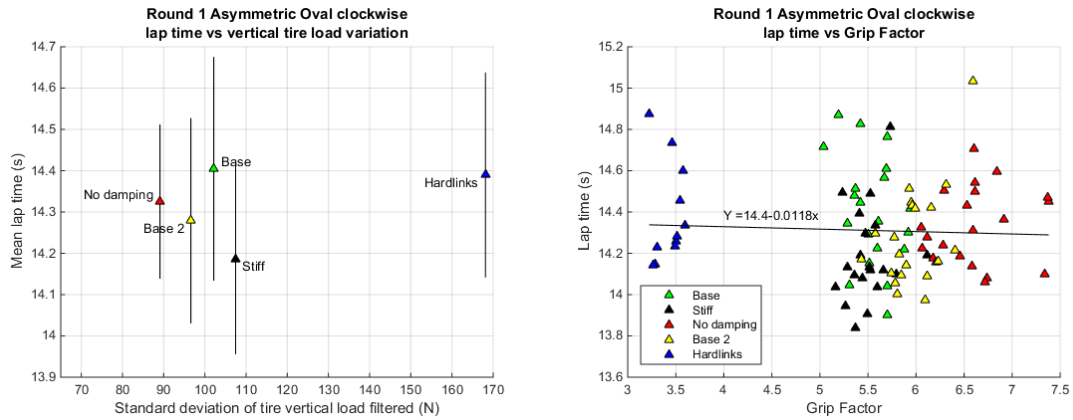


FIGURE 3.47: Lap times vs tire load variation and Grip Factor

with the bump, having a significant peak at 20 Hz.

As seen in the skidpad tests, there is a significant peak in lateral force at about 35 Hz for all dampers, but minimal if any peak in vertical load at the same frequency. Strong peaks in vertical load are also reflected in lateral force, with the end result of more “peaky” or resonant behavior for lateral force than vertical load.

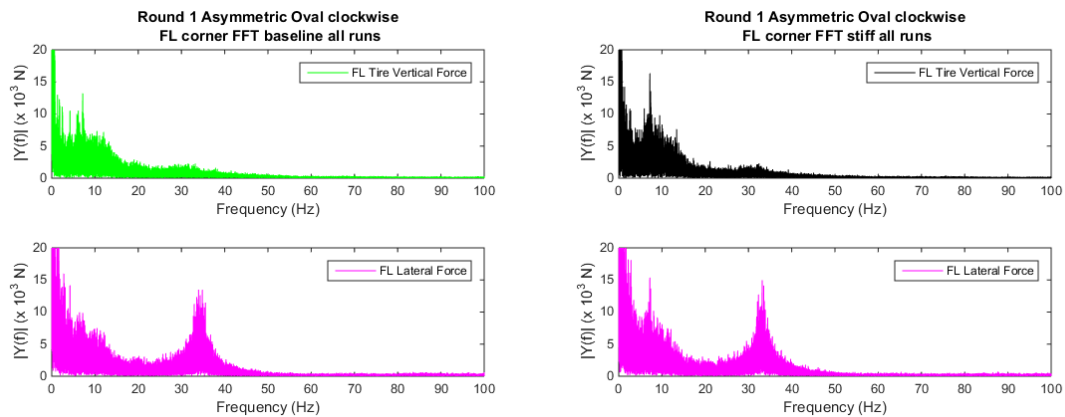


FIGURE 3.48: Tire force frequency response - baseline and stiff dampers

Looking at ride quality, the response of vertical suspension force (shown in figure 3.50) is similar to vertical tire load, differing only around 20 to 22 Hz where the unsprung mass is vibrating between the sprung mass and the road. From a vertical suspension

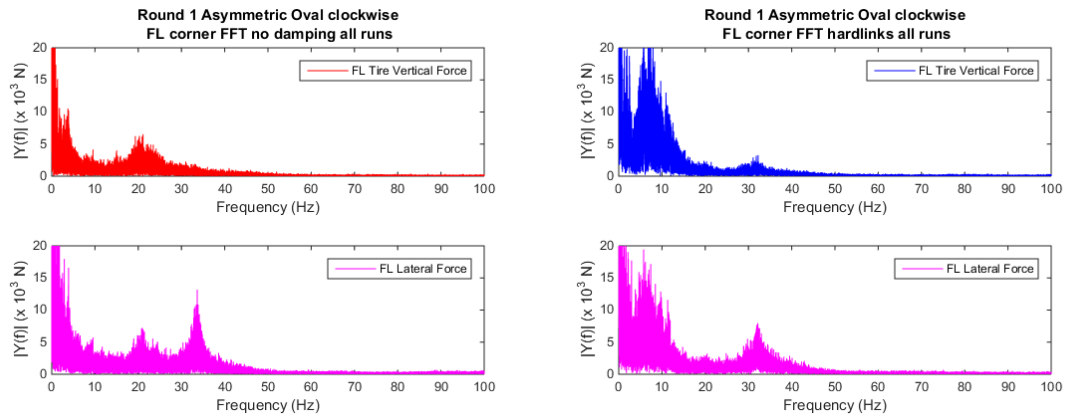


FIGURE 3.49: Tire force frequency response - no damping and hardlinks

force perspective, no damping actually appears to have better ride quality than baseline dampers, but suffers from large oscillations of damper position, likely indicative of the driver comments of sprung mass oscillation. FFTs of damper position are shown in figure 3.51. Hardlinks naturally did not have any appreciable travel, and vertical suspension force is thus clearly the harshest as expected. The extremely high peak at about 8 Hz explains the drivers complaints about a painful ride and the test session for the hardlinks was cut short accordingly.

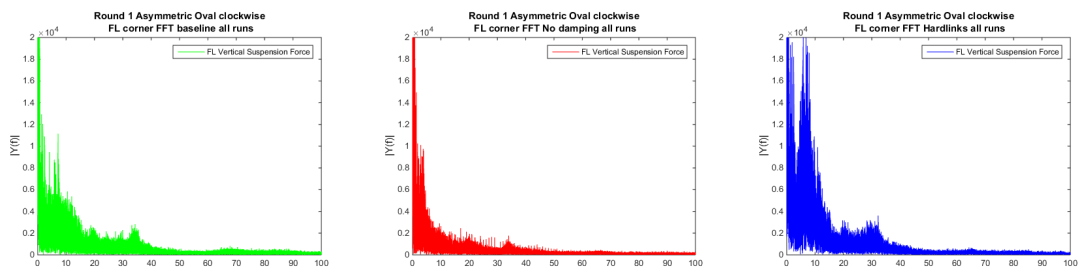


FIGURE 3.50: Vertical suspension load frequency response

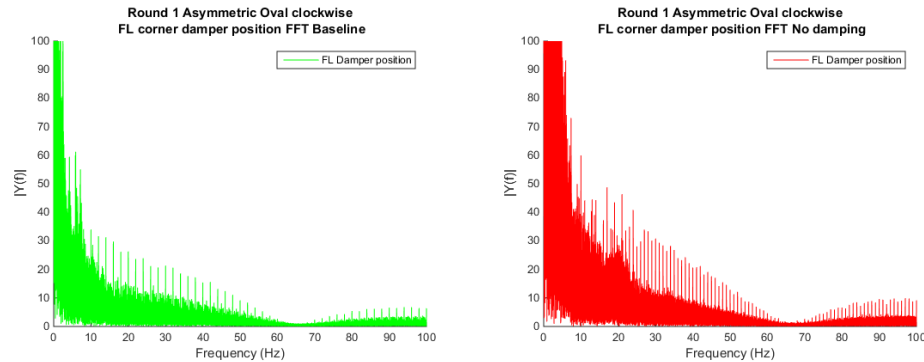


FIGURE 3.51: Damper position frequency response

3.2.4 Subjective Driver Evaluation

To aid in interpretation of the logged data and give additional data not captured on car, driver comments were taken after each run during the second test. An example of the driver comments logged is shown in table 3.5, with the complete comments in Appendix D. Figure 3.52 shows the numeric ratings plotted. We can see that the driver felt very little difference between the baseline and stiff damper sets, but found much less performance from the hardlinks. This is not surprising, since with hardlinks the vehicle is much stiffer than other suspension-less vehicles such as karts, leaving the only appreciable spring in the system to be the tires at $115\frac{N}{mm}$ ($650\frac{lb}{in}$). Interestingly the no damping configuration rates nearly as well as the other dampers, despite the driver comment *“Felt like the whole car was on a trampoline...”*. This is indicative of good steady state cornering and high frequency vertical motion behavior but poor body control in the low frequencies. In runs without the bump no damping rated the same as stiff and better than the baseline dampers in overall handling, but worse in lateral grip than either while matching the baseline and bettering stiff in direction change.

In all cases the driver was not told which dampers were going on the car, although the hardlinks looked distinctly different from the dampers which were all valved internally and so looked virtually identical on the outside.

| Damper | Bump? | Overall handling | Lateral grip | Direction change | My driving | Comments |
|----------|-------|------------------|--------------|------------------|------------|--|
| Baseline | N | 7 | 7 | 8 | 9 | slow skidpad was easy to stay consistent. Easier to go left (outside lane) on skid pad cause you have more room. Track felt better the more laps I ran. Will try to be more consistent next run. |

TABLE 3.5: Example driver comments collected during round 2 testing

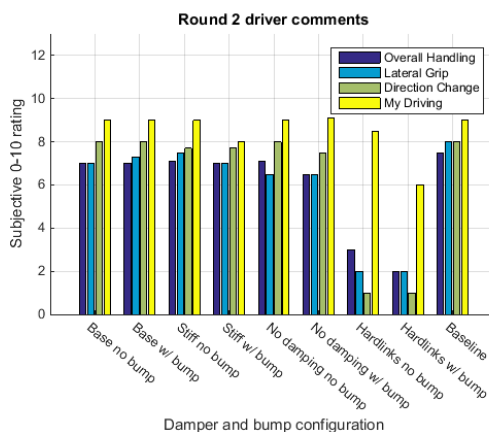


FIGURE 3.52: Subjective ratings from round 2 driver comments

3.3. Summary of system resonance

Changes in system resonance points can be seen by plotting the resonant frequency peaks against each simulation or test event. In this study we do not distinguish between very sharp peaks as seen in figure 3.53 and broader peaks covering a smooth range of frequencies. Thus, we cannot say which are more or less resonant, just how they move between frequencies.

Figure 3.54 shows the frequency response peaks of vertical tire load compared between simulations. Baseline, stiff and hardlinks each have one peak per simulation, while

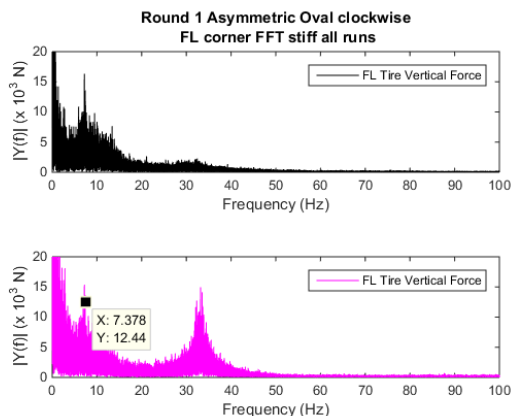


FIGURE 3.53: Example FFT highlighting resonant frequency

no damping has two. This can be seen clearly in figure 2.5 and others. The peak frequencies for no damping appear to be relatively constant across simulations, unchanged though changes in suspension spring rate (through addition of the anti-roll bar) and changes in mass (additional sprung mass due to load transfer), while there is some influence on the other dampers. Both stiff and no damping are unaffected by the addition of the anti-roll bar, but the hardlinks peak moves to the lower frequencies with the additional sprung mass in cornering, while the stiff peak is the most sensitive to sprung mass, moving 13 Hz higher between straightline and 2 g cornering. Baseline is the is affected by both the anti-roll bar and cornering, steadily moving the peak to the higher frequencies as the simulations progress.

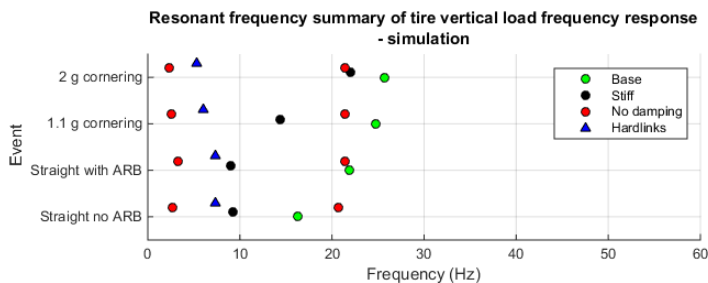


FIGURE 3.54: Summary of simulation resonant frequencies

The frequency peaks of vertical tire load from FFTs of round 1 logged data are shown in figures 3.55, and 3.56. Round 2 data is shown in appendix D4. Three things are immediately clear about the logged data: It is much noisier than the simulation, the frequency peaks span a larger range of frequencies, and in many cases many or all the dampers have peaks at the same frequencies.

In both rounds of testing there is a clear movement of the 8-10 Hz peak to lower frequencies, around 5-6 Hz in the skidpad and Asymmetric Oval events. The higher frequency peaks do not appear so clearly affected. It is unsurprising that many of the peaks appear in both vertical and lateral force.

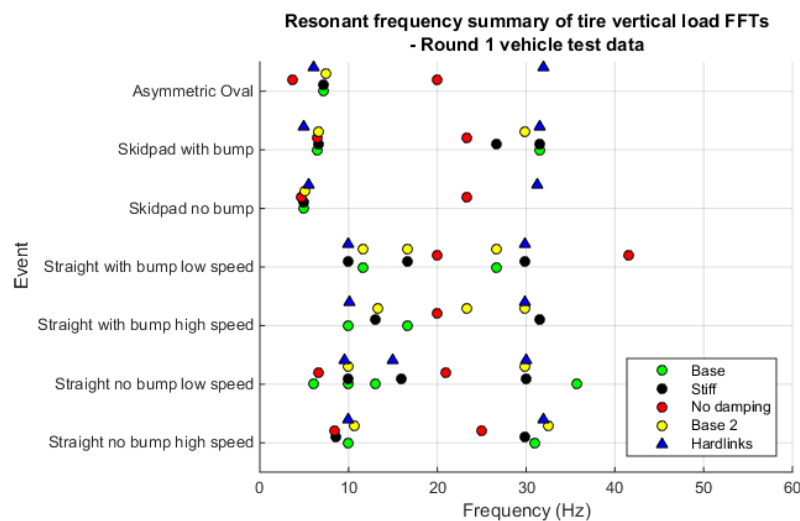


FIGURE 3.55: Summary of Round 1 vertical tire load resonant frequencies

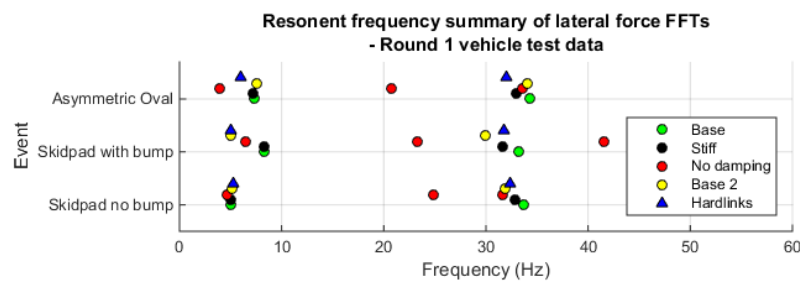


FIGURE 3.56: Summary of Round 1 lateral force resonant frequencies

4. DISCUSSION

4.1. The “best” damper

While extensive data has been collected, there is no clear “best” damper among those tested. It is clear hardlinks are not the right choice, with the worst performance in nearly every test, however in the full course tests the lap time difference was not as small as one would expect. No damping is best in Grip Factor in all runs without the bump, but oscillates excessively with the artificial bump, leading to poor Grip Factors. While artificial bump hits are not typical driving conditions, the resulting oscillation is indicative of the driver comments of control and ride quality without the bump as well. No damping also does worse than the Grip Factor would indicate in the Asymmetric Oval, the sprung mass bouncing vertically and oscillating in pitch (porpoising), particularly out of the low speed hairpin corner.

Stiff dampers fare well in lateral force and laptime of the skidpad and oval tests, but are often bested by one or both of the baseline dampers. Finally, there is good theoretical justification for the baseline dampers, and their performance is good across all tests. The large difference between the two baseline runs in each test however, is cause for caution, as is the lack of baseline 2 data in round 2 with bump testing.

The quarter car model suggests and physical data corroborates that simple linear damping is a compromise across frequencies, making none of the dampers tested ideal. Section 4.5. discusses the direction of future work damper builds utilizing these conclusions.

4.2. Validity of reducing vertical load variation

While it is very clear that dramatically increasing vertical load variation or decreasing Grip Factor reduces lateral force, as can be clearly seen in comparing any damper with hardlinks, the complete relationship between tire vertical load variation and lateral force is not so clear. As covered in the background, there is fundamentally good theoretical justification, but the data from this investigation only adds some additional evidence falling short of outright confirmation or characterization of the effect. The skidpad without bump tests appear to give the strongest relationship between Grip Factor and lateral force, but there is little if any evidence coupling Grip Factor and lap time in the Asymmetric Oval runs. More investigation is needed to better understand the relationship. In particular it may be non-linear or frequency dependent, which would help to explain the differences in conclusion between the skidpad and oval tests, the Asymmetric Oval having more activity in the 25+ Hz range.

4.3. Quarter car model

While the quarter car model does not closely predict the measured loads and frequency response found in physical testing, the simulation does seem to be useful for damper selection by giving a high level overview of general system behavior, including good representation of system natural frequencies. Figure 4.1 compares the frequency response of the simulation and FFTs from the Asymmetric Oval tests. Only no damping and hardlinks are shown from the logged data for clarity.

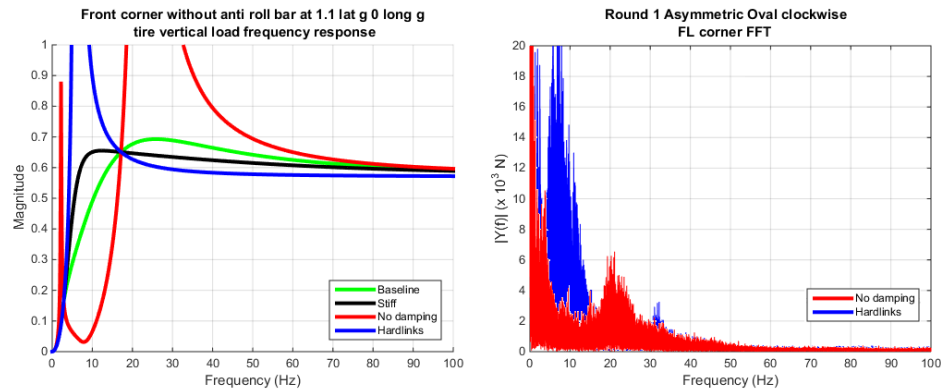


FIGURE 4.1: Comparison of frequency response of quarter car model and FFT of logged data

It is immediately clear that while the position of the peaks of no damping and hardlinks are mostly well represented in the model, the overall shape of the response is different, the activity in the logged data tapering off rapidly into the higher frequencies. This difference is to be expected - the model frequency response is typical of a bode plot which simply compares system output at each frequency, while logged data illustrates that there is substantially more force in the lower frequencies.

In the time domain, straightline with bump performance of the model is similar in overall shape, but differs in overestimating peak forces of all dampers and continued oscillation of the hardlinks. The overestimation of the peak tire load of the bump may well be due to the use of a step input to simulate the more complex interaction of the tire rolling onto and deforming around the bump, while the continual large oscillation of tire force with hardlinks is due to the absence of tire damping in the model. This was disregarded as is common in 2 DOF quarter car modeling [1, 2] but is clearly not appropriate where the suspension is rigid, as the only dynamics are both the sprung and unsprung masses vibrating on the undamped tire. The assumption appears to hold up when for all other dampers, note that no damping in both the simulation and physical testing retains a small amount of damping as noted in section 2.2.2. The model captures

the large oscillation of no damping at approximately 23 Hz, and there is some evidence that the stiff dampers respond faster and oscillate at higher frequency than the baseline dampers in both the simulation and logged data. Although the simulation also sees larger amplitude of the oscillation for the stiff dampers, this is far from clear in the test data.

Looking at Grip Factors in the step input and frequency response cases, the model does decently at representing the baseline and stiff dampers, predicting the similar results with the baseline dampers having a higher grip factor. Performance of no damping and hardlinks in the straightline with bump case is reasonably described by the model, showing poor Grip Factors for both and no damping performing better. However, in the frequency response case, the model of no damping and hardlinks does not well represent the test data.

In tests without the artificial bump no damping often had the largest Grip Factor, particularly in skidpad. In the model, this is not reflected as no damping has much larger frequency response areas, largely due to the extremely high peaks at 2.2 and 22 Hz which appear in logged data, but are not so severe. The presence of additional friction and damping in the true vehicle from the tire and suspension bearings could explain some of this difference.

Perhaps the largest drawback of the quarter car model is how clear and simple the results are. It is far too easy to fall into careful mathematical optimization of the model, trading response at some frequencies for others and justifying a claim of increased performance. The logged data reminds the prudent engineer that the model gives a general idea of system behavior, but reality is far from so smooth and definitive. This is particularly clear when looking at the artificial bump in testing, it is very difficult to determine what is “steady state” of vertical tire load because the real surface is so rough.

4.4. Noise in data - cloudiness of conclusions

As noted, the large variances in collected data makes interpretation of the results somewhat difficult. The tests were designed to make differences easy to see, using large differences in the dampers, many run repetitions, and two test sessions a year apart. Despite this there was still difficulty in seeing clear trends. The sources are believed to be primarily driver error and changing conditions of the course and vehicle. Driver error was primarily missing the artificial bump or incorrect speed when crossing the beacon, in particular a problem at the end of test runs as the driver would get bored, or in the case of no damping or hardlinks, uncomfortable in the car and would either speed up or slow down immediately after hitting the bump or crossing the beacon. The use of two baseline runs was done to allow comparison between the same vehicle run at difference stages of the test, allowing comparison of weather conditions, driver warm up and tire temperature. Differences between the baseline runs were large in a few of the tests, indicating a difference in conditions, but not helping to make conclusions to other dampers.

Another issue was reliability of the data logging system. Data was carefully processed to remove runs where the data dropped out as seen in figure 4.2, or suffered a logging error as seen in figure 3.20. It is believed that all these errors were caught and removed, however if any were included in the final results this could certainly add more spread to the data.

4.5. Designing a new damping curve

As the best damper differs between skidpad without bump, skidpad with bump and the Asymmetric Oval, there is more work left to develop the ideal damper for FS applications. There is evidence of different requirements to minimize vertical tire load

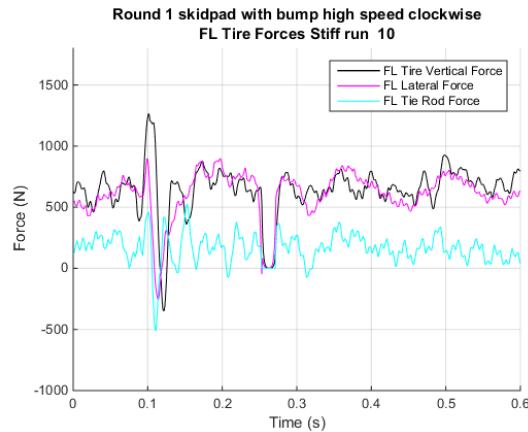


FIGURE 4.2: Example of strain gauge data dropping out

variation for individual wheel control vs body motions, both in damper speeds and suspension oscillation frequencies. References [20] and [1] give similar arguments that this is a compromise across frequencies. Quadrilinear, symmetric dampers would be a good first step, allowing the body control of the baseline dampers, with the bump absorption of no damping. A proposed damper force curve incorporating these characteristics is shown in figure 4.3 laid over the baseline damper curve.

A knee speed of $1 \frac{in}{s}$ was selected to capture most body motions in the baseline forces, while giving relatively low resistance to high speed motion. This should retain the characteristics of the no damping dampers tested giving good Grip Factors over rough pavement, but reduce the magnitude of oscillations due to hitting the artificial bump or other body motions. This speed matches that suggested in reference [18]. Section D5 shows selections of data illustrating damper speeds in skidpad with and without the artificial bump. Stiff and no damping are shown to give the full range of damper speeds found in testing.

This study has not found any justification for damper force asymmetry in compression and rebound, although this is common in racing dampers. Reference [5] suggests this is because compression damps the motion of the unsprung mass, while rebound damps the

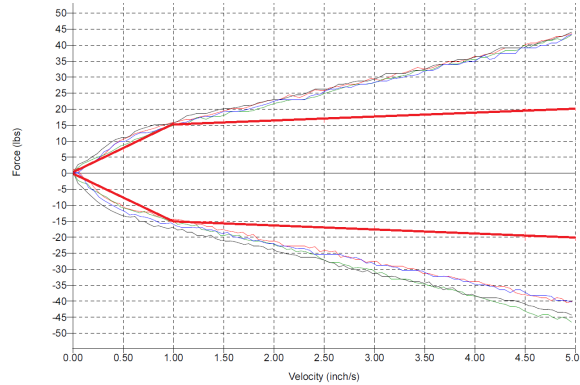


FIGURE 4.3: Proposed damper overlaying the baseline damper

motion on the sprung mass. Reference [8] cautions that any compression-rebound asymmetry can cause the car to *jack up* or *jack down* over a series of bumps, where the damper asymmetry cause a progressive change in ride height without time for the suspension to recover. More study is needed to determine differing requirements between compression and rebound, if any. This is covered in section 5.3.: Future work.

Looking at the frequency response output of the quarter car model, there is possibility for reduced vertical tire load variation by utilizing a composite damping curve. In the 0-3 Hz range infinite damping has the best performance, while no damping performs best in the 3-16 Hz range and infinite damping is again best in the 16-40 Hz range. A theoretical damper frequency response is shown alongside other dampers in the figure below.

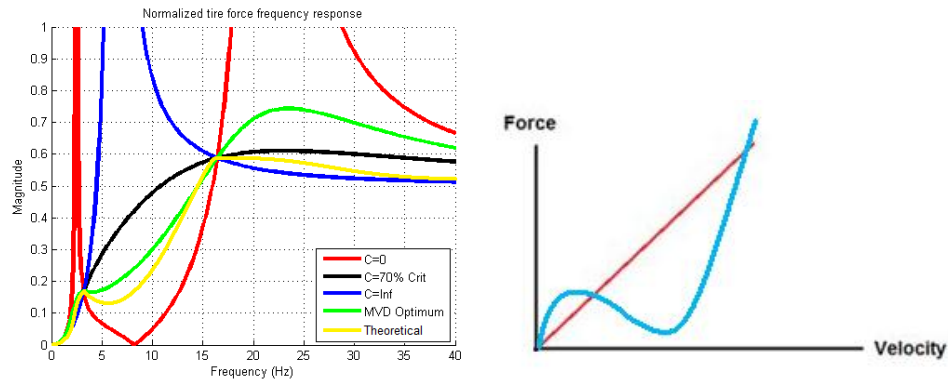


FIGURE 4.4: Theoretical damper frequency response and theoretical regressive damper

This damper would need regressive [33] or frequency dependent [34, 35] characteristics where damping forces decrease with speed or frequency in a certain range.

5. CONCLUSION

This study has attempted to put simple, clear use of engineering simulation and physical testing to better understand the problem or damping selection for racing cars. The validity and utility of the quarter car model was evaluated, the relationship between tire vertical load variation and in-plane grip was measured in full vehicle testing, and four damping configurations were compared in performance on typical FS courses. In summary, the quarter car model is a very simple but useful tool in understanding the major behavior of the vehicle's vertical dynamics and is a great tool to aid in selecting dampers. Model output is a large approximation of reality, but vehicle test data collected indicates minimal performance sensitivity to small changes in damping. That is, it is most important to be in the right range rather than calculated optimum to four or more significant figures.

There is some evidence that reducing tire vertical load variation improves lateral grip. This is most clearly seen in pure skidpad tests, though the data is not strongly conclusive. A metric to assess vertical load variation, called the Grip Factor was proposed

and proved useful throughout the analysis.

Finally, the vehicle testing performed has put data to vehicle behavior at the limits of damper tuning and shown the overall importance of the damper in the suspension system. Tire loading and vehicle behavior can be dramatically changed, though in a well sorted car with a trained driver the overall performance differences were smaller than many would expect. While there is much more to learn and develop, the quarter car model based linear symmetric damper selected to minimize tire vertical load variation over the 0-40 Hz range does well enough that we can rest at ease and put dampers aside until all but the smallest performance differences are sought out in reaching the upper echelons of performance.

5.1. Recommendations for FSAE teams

In FSAE where the overall understanding of dampers is generally limited and overall performance differences vary widely among the competitors, it would be appropriate to start with the basics of linear dampers in the correct force range before building out to complexities of non linearity and external adjustments.

For teams using double adjustable or other top end dampers, a complete set with shims can run \$4000, a significant portion of many teams budgets. Unless it is clear exactly what you want out of the damper and there is real evidence that these characteristics can only be achieved with the more expensive, high end dampers, most teams are better off using the extra money for tires and driver training.

As gross as it may seem, the data from this thesis serves to show that there is little practical difference between large adjustments in the damper as long as the damper is doing something. In that regard, it may not even be worth purchasing additional shims and custom valving shocks. The Penske 7800 quarter midget build shocks used in this

test came from the factory mismatched, but within 40% of the desired forces. As the difference between stiff and baseline was larger than this and they were very similar in performance, perhaps eliminating a \$1000 valve kit and expensive or time consuming dyno time could be a better use of resources for the cash strapped FSAE team.

As demonstrated by the large difference between baseline runs in some of the tests, driver and weather conditions look to have a larger effect than significant damper changes such as those between the base and stiff damper sets. Having a well sorted car for the conditions and well trained drivers will likely make a much larger difference than any changes to the dampers. Again as illustrated in this test even the best drivers in the most simple course (like a continuous skidpad) get better with more seat time.

5.2. Dampers for other applications

The conclusions reached in this investigation are representative of the environment - that is FS cars, tracks and drivers. Other forms of racing may have substantially different requirements and thus different results and conclusions. In particular in FS speeds are low, drivers are amateurs and the short schedule and educational nature of the competitions yield cars which are great in their own right, though far from perfect.

5.2.1 Ride

Little consideration has been made in this study for ride comfort as this is not of much concern due to the short driving stints and emphasis on performance. The data used in this test could be further processed with ride quality metrics to better understand the tradeoff between handling performance and ride.

5.2.2 Aero platform

In many types of road racing, particularly series with relatively smooth tracks and low speed variation throughout the lap, such as IndyCar or NASCAR Sprint Cup on oval tracks, aerodynamic effects may outweigh mechanical handling considerations and dampers can be used to help hold a stable aerodynamic platform [36] Figure 5.1 shows two NASCAR Sprint Cup cars on course; notice the extremely small distance between the front splitter and the ground. When sliding skirts were banned in Formula 1 for the 1981 season, Williams F1 tested a “no suspension” car [37] running at lower ride height to try and recoup some of the lost downforce. While they found potential for quicker lap times than the car with normal ride height and suspension (presumably due to the higher downforce from a lower car and more consistent ride height of the aerodynamic underbody), the car was noted to be virtually undrivable, driver Alan Jones suggesting a suspension for the seat should the design be used in a full length race.



FIGURE 5.1: 2006 NASCAR Sprint Cup cars. Photo courtesy of USAF

5.3. Future work

In any investigation there is always room for improvements on the current study and new directions in which to take the study emerge. This work has only scratched

the surface of a very deep topic, in this section potential expansions on this work are suggested.

5.3.1 Further analysis of existing data

In addition to the analysis presented here, there is much more study that could be done with the existing data. This would be the logical first step in any future work because the data is already collected, minimizing any additional effort or cost in better understanding the system. Looking at each of the four suspension corners would be interesting as interactions could be studied, such as pitch and roll motions resulting from hitting the artificial bump, or looking at the changes in vehicle balance over the undulating road. In addition to better understanding how damper selection influences balance, this analysis could be used to assess the merit of longitudinally interconnected suspension and the separation of the heave, pitch, roll, and warp modes it offers.

5.3.2 Softer than baseline dampers

Should another test be run, another linear symmetric damper should also be considered to compare with the baseline and stiff sets. While not completed, the test plan originally called for a 50% of baseline damper termed *soft*. This would give comparison with the baseline damper in two directions, giving a better understanding if the baseline was actually a good selection, rather than just *less than stiff and more than no damping*. This damper would also better fit to the 2 DOF quarter car *optimal* damping in the straightline cases. The additional damper would also give another spread of points to the Grip Factor vs. Lateral Force plots, giving more insight into the relationship between the two variables.

5.3.3 On track damper selection

Reference [5] and others recommend dampers be tuned on track to driver feedback on balance and grip. The most simple approaches usually add damping if the car oscillates

too much or is slow to respond, and to reduce damping if the car is harsh over bumps of skates across the track rather than gripping well. While this process isn't very analytical, it would be interesting to compare the results of this tuning method to that of dampers designed to minimize vertical load variation. Perhaps damping found through on track iteration will offer different performance strengths.

5.3.4 Bilinear dampers

A simple extension of this work would be to investigate bilinear dampers, which are linear, but not symmetric in compression and extension. Much literature suggests that Bilinear dampers should have higher performance than linear symmetric dampers [1, 5, 38] as road irregularities are likely not symmetric. It is well known that the force transmitted to the unsprung mass is harsher over bumps vs depressions as the force pushing the unsprung mass down into depressions only comes from the spring while the force from bumps comes from the spring, damper and inertia of the vehicle.

5.3.5 Quadrilinear dampers and airshocks

These are the typical norm in racing cars, based off the idea that damping is needed at low shaft speeds for body control, but damping forces should "blow off" at high speeds to limit ride harshness over bumps. Regressive dampers go further by actually reducing damping forces at high speeds below what they are at low speeds [33].

Air shocks combine a spring and damper into a single unit and are very popular in mountain biking for their reduction of part count, lower weight and higher adjustability than coil over spring - damper units. Airshocks typically have highly progressive spring rates [39] although this can be reduced with more complex valving in modern airshocks. In the mountain bike application it is acknowledged that coil springs and dampers are better from a pure dynamic standpoint[40] but not easily adjustable in spring rate for different riders. FS teams such as AMZ Racing from ETH Zurich have successfully used

airshocks, although the particular dampers used have been top of the line, comparable in price to the most expensive coilover spring dampers used in FS.

5.3.6 Inerters, mass dampers and other additional springing devices

As noted earlier, inerters give force output in relation to a difference in acceleration between their nodes. At the most basic level they could be beneficial as they are simply another tuneable parameter in the system and the previously missing mechanical analog of an ungrounded capacitor [41]. Inerters, also known as J dampers, were first used in Formula 1 in 2005 by McLaren [42] to reduce tire contact patch vertical load variation. Reference [2] shows how inerters can improve tire vertical load variation in a F1 quarter car model.

Mass dampers should be looked at for the same reason. They were famously used by Renault F1 in 2006 and subsequently banned from the sport. Reference [38] refers to a similar concept as a *Resonant vibration absorber*. Reference [1] refers to it as a dynamic vibration absorber.

5.3.7 Expansion of data acquisition

Although the vehicle used for testing was very well instrumented, there is more to learn with additional sensors.

Damper rod force

Direct measurement of damper rod force with load cell or strain gauges would allow comparison of the forces on track to those on a dyno. Things to look at would be:

- Force displacement dependence due to gas pressure or other effects
- Time delays and fluid/piston inertial effects
- Forces developed at very low displacements and high frequencies

A more advanced (pneumatic, not crank) shock dyno or a shaker rig might be a more economically viable intermediate step to sensors on the vehicle, although this is an additional abstraction from reality.

Sprung mass accelerations

To better evaluate ride comfort, vertical accelerometers on the sprung mass, and driver, as well as pitch and roll accelerometers on the sprung mass. would go a long way to seeing the true acceleration the driver is exposed to. It would be particularly interesting to look at the frequency content on vertical acceleration and jerk, and to consider the effects of porpoising and roll oscillation.

Optical slip angle sensors

Measuring tire forces directly as was done in this test is useful and focuses on the output performance which is of the most interest, but it does not well explain how these forces are developed. Two optical slip angle sensors like those from Corrsys-Datron [43] placed at the front and rear axles could be coupled with steer angle data to calculate individual tire slip angles [44]. This could be used to build an empirical tire model including dynamic load sensitivity effects and relaxation length. The system could also be used to put measured data to driver comments about turn in, balance and response over bumps.

High speed video

Particularly in the artificial bump tests there is a lot of activity, and it is difficult to fully understand what is occurring. High speed video would be helpful in looking at tire deformation around the bump and the vibration in vertical and lateral directions afterward. A test setup including a transparent road surface and video from below could be particularly interesting.

5.3.8 More advanced simulations

As noted in section 4.3. it is well recognized that the linear quarter car model is a large simplification, so more advanced simulations could improve the accuracy and utility. The nonlinear quarter car model is a simple extension and would be a necessary step to simulate the nonlinear damper proposed in section 4.5.. Adding an additional DOF of the tire vibrating internally could extend the application of the model past the natural frequency of the tires [1].

A 4 DOF *half car* model would allow investigation of heave and pitch modes and front-rear interaction of the road surface or hitting the bump with both front and rear wheels, while a 7 DOF model could include heave, pitch and roll of the sprung mass, and wheel displacements of the four unsprung masses. Both of these would be particularly interesting in looking at handling balance in skidpad.

5.3.9 Longitudinally interconnected suspensions

Connections between the front and rear suspensions show potential for traction improvements by separating suspension springing and damping for the four distinct modes. [26, 27] There is no need to have stiffness in the warp mode (other than limiting wheel travel at the extremes) so a vehicle with a soft warp mode could have higher traction over uneven surfaces while maintaining good body control.

BIBLIOGRAPHY

1. Giancarlo Genta. *Motor Vehicle Dynamics*. World Scientific Publishing Co. Pte. Ltd., 5 Toh Tuck Link, Singapore 596224, 1997.
2. Massimo Guiggiani. *The Science of Vehicle Dynamics: Handling, Braking, and Ride of Road and Race Cars*. Springer, 2014.
3. Christian Bourcier de Carbon. *Theorie mathematique et realisation pratique de la suspension amortie des vehicules terrestres*. Paris : impr. de Lang, Blanchong et Cie, 1951.
4. Peter Willem Anton ZEGELAAR. *The Dynamic Reponse of Tyres to Brake Torque Variation and Road Unevennesses*. PhD thesis, Delft University of Technology, 1998.
5. Carroll Smith. *Tune to Win*. Aero Publishers, Inc., 329 Aviation Road, Fallbrook, CA 92028, 1978.
6. Carroll Smith. *Engineer to Win*. MBI Publishing Company, 1984.
7. Carroll Smith. *Drive To Win*. Carroll Smith Consulting, Inc., 1996.
8. Paul Van Valkenburgh. *Race Car Engineering and Mechanics*. Dodd, Mead and Company, New York, 1976.
9. Allan Staniforth. *Competition Car Suspension*. Haynes Publishing, 2006.
10. Michael Royce, Suzanne Royce, John Bucknell, Pat Clarke, Mark Claywell, Steve Fox, David Gould, Dr. Michele Grimm, Dan Jones, Edward M Kasprzak, Jim Casprzak, Steve Lyman, Kim Lyon, Douglas L Milliken, WM C Mitchell, and David Redszus. *Learn & Compete: A Primer for Formula SAE, Formula Student and Formula Hybrid Teams*. Racecar Graphic Limited, 2012.
11. SAE International. 2014 FSAE rules. Technical report, SAE International, 2013.
12. William F. Milliken and Douglas L. Milliken. *Race Car Vehicle Dynamics*. SAE International, 400 Commonwealth Drive, Warrendale, PA 15096-0001, 1995.
13. Hans B. Pacejka. *Tire and Vehicle Dynamics*. Society of Automotive Engineers, Inc., 400 Commonwealth Drive, Warrendale, PA 15096-0001, 2006.
14. Paul Haney. *The Racing and High-Performance Tire: Using the Tires to Tune for Grip and Balance*. TV Motorsports and Society of Automotive Engineers, TV Motorsports, 31 Tophill Lane, Springfield, IL 62704 and Society of Automotive Engineers, 400 Commonwealth dr., Warrendale, PA 15096-0001, 2003.

15. John C. Dixon. *Tires, Suspension and Handling*. Society of Automotive Engineers, Inc., 400 Commonwealth Drive, Warrendale, PA 15096-0001, 1996.
16. Societe de Technologie Michelin. Grip on road surfaces. Technical report, Societe de Technologie Michelin, 2001.
17. Matt Giaraffa. Tech tip: Springs and dampers, part one: The phantom knowledge. Technical report, Optimum G, 2005.
18. Jim Kasprzak. Damping calculations: The proper damping for my vehicle. Presentation.
19. Jim Kasprzak. Shock testing & maintenance: The care & feeding of dampers. Presentation.
20. Samuel Philip Gacka and Christopher Gilles Doherty. Design analysis and testing of dampers for a Formula SAE race car. Technical report, SAE International, 2006.
21. Claude Rouelle. Vehicle dynamics and race car engineering seminar. Technical report, Optimum G, 2009.
22. Jim Kasprzak. Damper basics: Damper design, testing and tuning. Presentation.
23. Matt Giaraffa. Tech tip: Springs and dampers, part three: Revenge of the damping ratio. Technical report, Optimum G, 2005.
24. Fukashi Sugasawa, Hiroshi Kobayashi, Toshihiko Kakimoto, Yasuhiro Shiraishi, and Yoshiaki Tateishi. Electronically controlled shock absorber system used as a road sensor which utilizes super sonic waves. Technical Report 851652, SAE International, 1985.
25. Henri Kowalczyk. Damper tuning with the use of a seven post shaker rig. Technical report, SAE International, 2002.
26. Erik Zapletal. Balanced suspension. Technical report, SAE International, 2000.
27. Manuel Greiner. Basic interlinked suspension. *Racecar Engineering*, 23(3), March 2013.
28. Badin Jawad, Hassane El-Khoury, James Todd, and Mark Masen. Controlling weight transfer with active damping. Technical report, SAE International, 2001.
29. Min-Soo PARK, Takabumi FUKUDA, Tae gu KIM, and Setsuo MAEDA. Health risk evaluation of whole-body vibration by ISO 2631 5 and ISO 2631 1 for operators of agricultural tractors and recreational vehicles. *Industrial Health*, 51:364 – 370, 2013.

30. M. Fard, L. Lo, A. Subic, and R. Jazar. Effects of seat structural dynamics on current ride comfort criteria. *Ergonomics*, 57(10):1549–1561, 2014. PMID: 25017144.
31. International Organisation for Standardisation. Mechanical vibration and shock evaluation of human exposure to whole body vibration.
32. William S. Murray. Vehicle dynamic validation and analysis from suspension forces. Master’s thesis, Oregon State University, 2012.
33. Simon McBeath. Regression equation: Penske Racing Shocks’ latest development offers a new way of overcoming the age-old conundrum of hydraulic damping, with benefits for both lap time and tire wear. *Racecar Engineering*, 2009.
34. Mark Skews. Koni FSD damper. *Racing Line*.
35. Koni Group. Introduction to FSD technology for cars. Website.
36. David Caraviello. With ride height gone, options open up. Web article, July 2014.
37. Patrick Uden. Gentlemen, lift your skirts... TV Episode, March 1981.
38. John C. Dixon. *The Shock Absorber Handbook*. SAE International, 400 Commonwealth Drive Warrendale, PA 15096-0001, 2007.
39. Nick Anderson and Joe Graney. Shock rates v 1.0: Schooled by SCB Engineering, February 2015.
40. Richard Cunningham. Tech tuesday - what a negative spring is and why it makes the coil-spring nearly obsolete, May 2012.
41. Malcolm C. Smith. The inerter concept and its application. Technical report, University of Cambridge Department of Engineering, 2003.
42. Malcolm C. Smith. Inerters and Formula One. Technical report, University of Cambridge Department of Engineering, 2014.
43. Jennae Cohen. Corrsys-Datron sensor measures vehicle slip angle, November 2010.
44. Optimum G. On-track tire characterization. Technical report, Optimum G.

APPENDICES

A APPENDIX A Quarter car model

A1 Equation Derivations

Sprung and unsprung mass position, rigid dampers

$$0 = m\ddot{x} + (x - Y)k_t$$

$$0 = m\ddot{x} + xk_t - Yk_t$$

$$Yk_t = ms^2x + k_tx$$

$$Y = \frac{ms^2x + k_tx}{k_t}$$

$$x = \frac{k_t}{ms^2 + k_t}Y$$

Vertical tire load for rigid dampers

$$F_t = (Y - x)k_t$$

$$F_t = \left(Y - \frac{k_t}{ms^2 + k_t}Y \right) k_t$$

$$F_t = \left(1 - \frac{k_t}{ms^2 + k_t} \right) k_t Y$$

Equations of motion for 2 DOF system without tire damping

Force balance on sprung mass

$$0 = m_1 \ddot{x}_1 + k_1(x_1 - x_2) + c(\dot{x}_1 - \dot{x}_2)$$

$$0 = m_1 \ddot{x}_1 + c\dot{x}_1 + k_1 x_1 - c\dot{x}_2 - k_1 x_2$$

$$0 = (m_1 s^2 + cs + k_1)x_1 - (cs + k_1)x_2$$

Force balance on unsprung mass

$$0 = m_2 \ddot{x}_2 + c(\dot{x}_2 - \dot{x}_1) + k_1(x_2 - x_1) + k_2(x_2 - Y)$$

$$0 = -c\dot{x}_1 - k_1 x_1 + m_2 \ddot{x}_2 + c\dot{x}_2 + k_1 x_2 + k_2 x_2 - k_2 Y$$

$$0 = -csx_1 - k_1 x_1 + m_2 s^2 x_2 + csx_2 + k_1 x_2 + k_2 x_2 - k_2 Y$$

$$0 = -(cs - k_1)x_1 + (m_2 s^2 + cs + k_1 + k_2)x_2 - k_2 Y$$

$$k_2 Y = -(cs - k_1)x_1 + m_2 s^2 + cs + k_1 + k_2)x_2$$

Write equations in form $Ax = b$

$$\begin{bmatrix} m_1 s^2 + cs + k_1 & -(cs + k_1) \\ -(cs + k_1) & m_2 s^2 + cs + k_1 + k_2 \end{bmatrix} \begin{bmatrix} x_1 \\ x_2 \end{bmatrix} = \begin{bmatrix} 0 \\ k_2 Y \end{bmatrix} \quad (\text{A.1})$$

Use Cramer's Rule

$$A_1 = \begin{bmatrix} 0 & -(cs + k_1) \\ k_2 Y & m_2 s^2 + cs + k_1 + k_2 \end{bmatrix}$$

$$A_2 = \begin{bmatrix} m_1 s^2 + cs + k_1 & 0 \\ -(cs + k_1) & k_2 Y \end{bmatrix}$$

$$x_1 = \frac{\det(A_1)}{\det(A)}$$

$$x_1 = \frac{Y k_2 (cs + k_1)}{(m_1 s^2 + cs + k_1)(m_2 s^2 + cs + k_1 + k_2) - (cs + k_1)^2}$$

$$x_1 = \frac{Y k_2 (cs + k_1)}{m_1 m_2 s^4 + m_2 cs^3 + m_2 k_1 s^2 + m_1 cs^2 + k_1 cs + (k_1 + k_2)m_1 s^2 + (k_1 + k_2)cs + k_1(k_1 + k_2) - (cs + k_1)^2}$$

$$x_1 = \frac{Y k_2 (cs + k_1)}{m_1 m_2 s^4 + (m_2 + m_1)cs^3 + (m_2 k_1 + c^2 + (k_1 + k_2)m_1)s^2 + (2k_1 + k_2)cs + k_1(k_1 + k_2) - (cs + k_1)^2}$$

$$x_1 = \frac{Y k_2 (cs + k_1)}{m_1 m_2 s^4 + (m_1 + m_2)cs^3 + ((k_1 + k_2)m_1 + k_1 m_2 + c^2)s^2 + (2k_1 + k_2)cs + k_1(k_1 + k_2) - (cs + k_1)^2}$$

using

$$-(cs + k_1)^2 = -(c^2 s^2 + 2k_1 cs + k_1^2) \quad (\text{A.2})$$

the equation can be simplified to

$$x_1 = \frac{Y k_2 (cs + k_1)}{m_1 m_2 s^4 + (m_1 + m_2)cs^3 + ((k_1 + k_2)m_1 + k_1 m_2)s^2 + k_2 cs + k_1 k_2} \quad (\text{A.3})$$

$$x_2 = \frac{\det(A_2)}{\det(A)}$$

$$x_2 = \frac{Y k_2 (m_1 s^2 + cs + k_1)}{m_1 m_2 s^4 + (m_1 + m_2)cs^3 + ((k_1 + k_2)m_1 + k_1 m_2)s^2 + k_2 cs + k_1 k_2}$$

Load through the tire is then

$$\text{Tire Force} = k_2(Y - x_2)$$

$$\text{Tire Force} = k_2Y - k_2 \frac{Yk_2(m_1s^2 + cs + k_1)}{m_1m_2s^4 + (m_1 + m_2)cs^3 + ((k_1 + k_2)m_1 + k_1m_2)s^2 + k_2cs + k_1k_2}$$

$$\text{Tire Force} = Yk_2 \left(1 - \frac{k_2(m_1s^2 + cs + k_1)}{m_1m_2s^4 + (m_1 + m_2)cs^3 + ((k_1 + k_2)m_1 + k_1m_2)s^2 + k_2cs + k_1k_2} \right)$$

Acceleration of the sprung mass

$$\ddot{x}_1 = s^2x_1$$

$$\ddot{x}_1 = s^2 \left(\frac{Yk_2(cs + k_1)}{m_1m_2s^4 + (m_1 + m_2)cs^3 + ((k_1 + k_2)m_1 + k_1m_2)s^2 + k_2cs + k_1k_2} \right)$$

Vertical force transmitted between the unsprung and sprung masses

$$\text{susp. force} = (x_2 - x_1)k_1 + (\dot{x}_2 - \dot{x}_1)c$$

$$\text{susp. force} = (x_2 - x_1)k_1 + (x_2 - x_1)cs$$

$$\text{susp. force} = (k_1 + cs)x_2 - (k_1 + cs)x_1$$

$$\text{susp. force} = (k_1 + cs) \left(\frac{Yk_2(m_1s^2 + cs + k_1)}{m_1m_2s^4 + (m_1 + m_2)cs^3 + ((k_1 + k_2)m_1 + k_1m_2)s^2 + k_2cs + k_1k_2} \right) - (k_1 + cs)x_1$$

$$\text{susp. force} = (k_1 + cs) \left(\frac{Yk_2(m_1s^2 + cs + k_1) - Yk_2(cs + k_1)}{m_1m_2s^4 + (m_1 + m_2)cs^3 + ((k_1 + k_2)m_1 + k_1m_2)s^2 + k_2cs + k_1k_2} \right)$$

$$\text{susp. force} = Yk_2(k_1 + cs) \left(\frac{(m_1s^2 + cs + k_1) - (cs + k_1)}{m_1m_2s^4 + (m_1 + m_2)cs^3 + ((k_1 + k_2)m_1 + k_1m_2)s^2 + k_2cs + k_1k_2} \right)$$

$$\text{susp. force} = Yk_2(k_1 + cs) \left(\frac{m_1s^2}{m_1m_2s^4 + (m_1 + m_2)cs^3 + ((k_1 + k_2)m_1 + k_1m_2)s^2 + k_2cs + k_1k_2} \right)$$

Damper velocity

$$\text{damper velocity} = \dot{x}_2 - \dot{x}_1$$

$$\text{damper velocity} = s(x_2 - x_1)$$

A2 1 DOF Sprung mass equations of motion

Position of sprung mass

$$0 = m_1 \ddot{x}_1 + c(\dot{Y} - \dot{x}_1) + k_1(Y - x_1)$$

$$0 = -m_1 x_1 s^2 + c(Y - x_1)s + k_1(Y - x_1)$$

$$0 = -m_1 x_1 s^2 + cYs - cx_1s + k_1Y - k_1x_1$$

$$cYs + k_1Y = m_1 x_1 s^2 + cx_1s + k_1x_1$$

$$Y(cs + k_1) = m_1 x_1 s^2 + cx_1s + k_1x_1$$

$$Y \left(\frac{cs + k_1}{m_1 s^2 + cs + k_1} \right) = x_1$$

Vertical tire force

tire force = spring and damper force

$$\text{tire force} = m_1 \ddot{x}_1$$

$$\text{tire force} = m_1 x_1 s^2$$

$$\text{tire force} = m_1 \left(Y \left(\frac{cs + k_1}{m_1 s^2 + cs + k_1} \right) \right) s^2$$

$$\text{tire force} = Y m_1 s^2 \left(\frac{cs + k_1}{m_1 s^2 + cs + k_1} \right)$$

A3 Additional quarter car model output

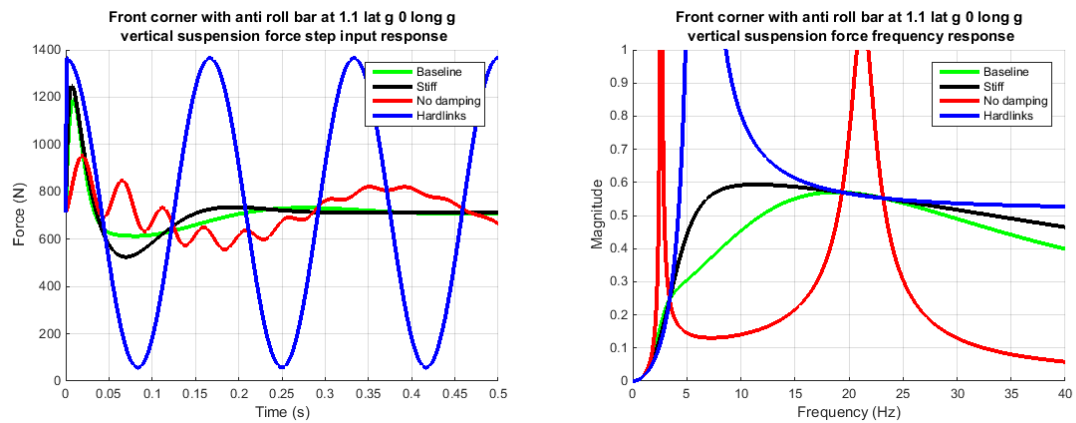


FIGURE 0.2: Cornering vertical suspension force frequency response

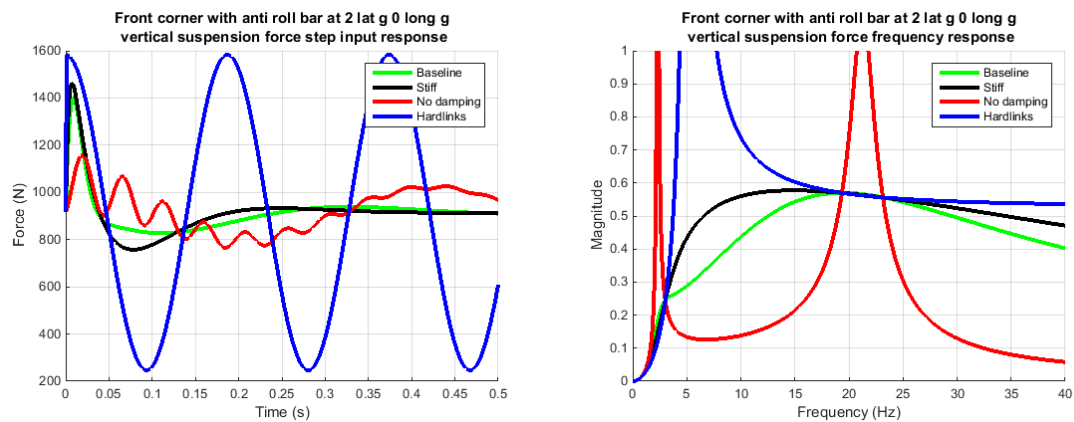


FIGURE 0.3: Cornering at 2 g vertical suspension force

B APPENDIX B Damper and Spring Force curves

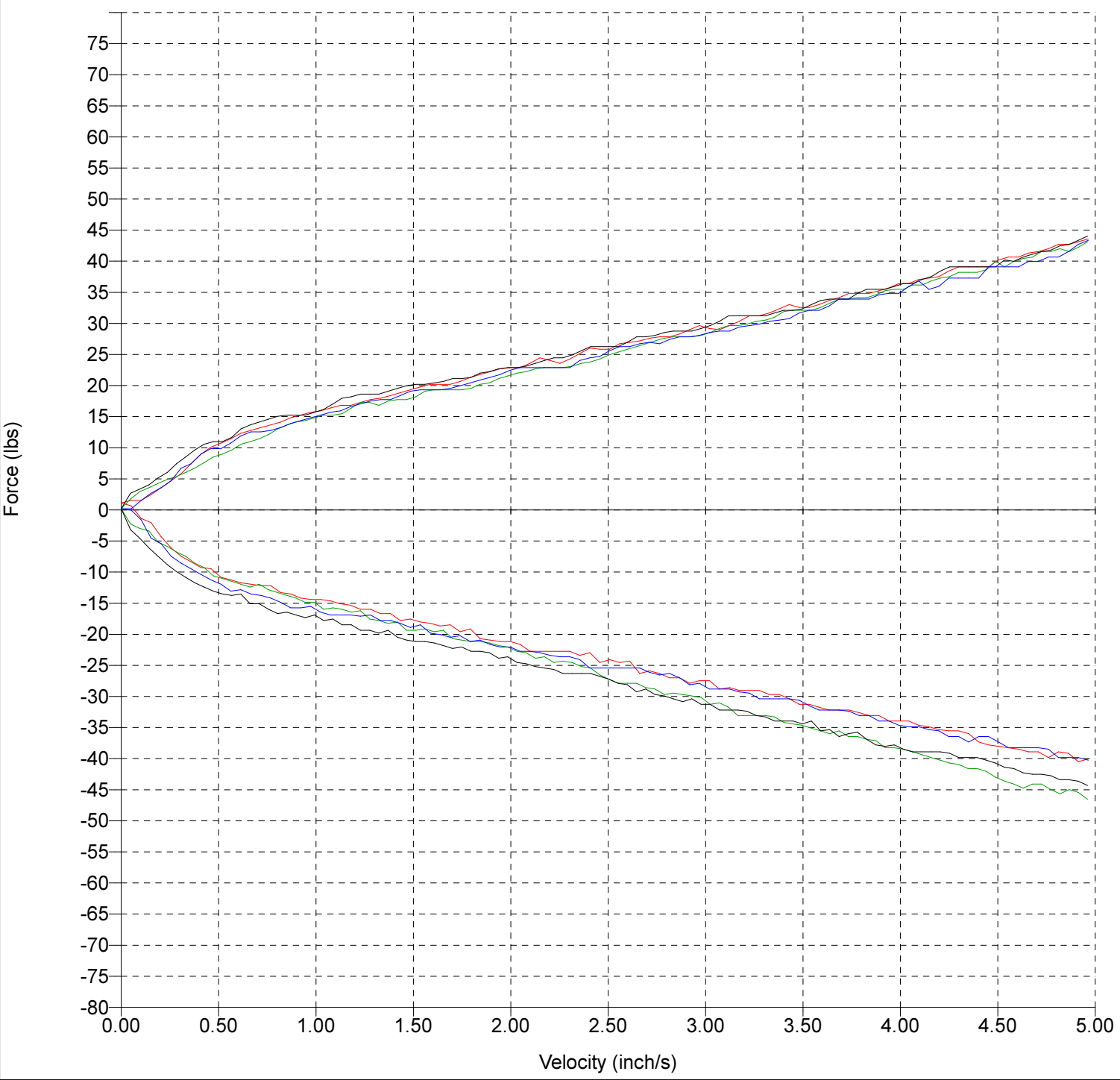
This appendix contains the raw force output from the SPA BTP 2000 shock dyno at the Shock Shop in Portland, Oregon. Plots are in order:

1. Baseline dampers
2. Stiff dampers
3. No damping dampers
4. 90 lb/in spring
5. 140 lb/in spring

All dampers were built using the Penske 2.5 weight VI-460 suspension fluid and charged to 100 psi gas pressure with nitrogen. Hardlinks were not run on the dyno as it is travel based and so essentially zero travel would damage the machine.



File: OSU FSAE 2 series shocks for testing 11-10-12.dat
 Shock model: P7800 Needle type: OSU FSAE 2 series shocks for testing 11-10-12
 Piston comp: degrees Jet checkball: Trace 1 is shock 21, 2 is shock 22, 3 is shock 23, 4 is 24
 Piston reb.: degrees Pressure: 75 psi
 Piston bleed: Valving C/R:



1 PV 5.23 inch/s @ 1.64Hz 28.0C
 B 0, 0 R 0, 0
 MaxF 48 MinF -44 lbs

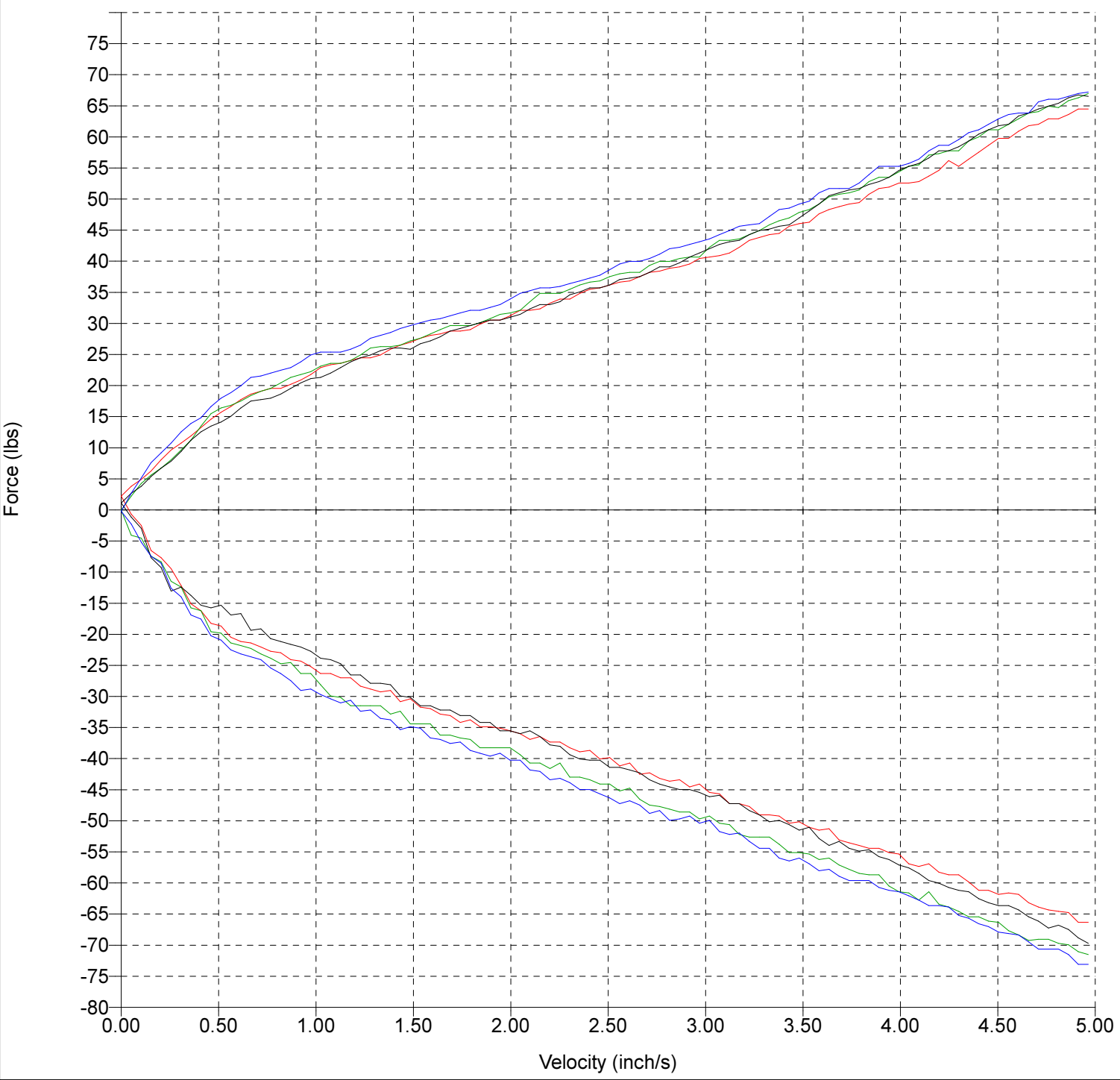
4 PV 5.12 inch/s @ 1.60Hz 27.5C
 B 0, 0 R 0, 0
 MaxF 46 MinF -43 lbs

2 PV 5.10 inch/s @ 1.60Hz 27.7C
 B 0, 0 R 0, 0
 MaxF 44 MinF -49 lbs

3 PV 5.11 inch/s @ 1.60Hz 27.5C
 B 0, 0 R 0, 0
 MaxF 46 MinF -48 lbs



File: OSU FSAE X (new) series shocks for testing 11-10-12.dat
 Shock model: Needle type: OSU FSAE X (new) series shocks for testing 11-10-12
 Piston comp: degrees Jet checkball: Trace 1 is shock X1, 2 is shock X2, 3 is shock X3, 4 is X4
 Piston reb.: degrees Pressure: psi
 Piston bleed: Valving C/R:



1 PV 5.24 inch/s @ 1.64Hz 28.1C
 B 0, 0 R 0, 0
 MaxF 68 MinF -72 lbs

4 PV 5.23 inch/s @ 1.64Hz 28.1C
 B 0, 0 R 0, 0
 MaxF 71 MinF -77 lbs

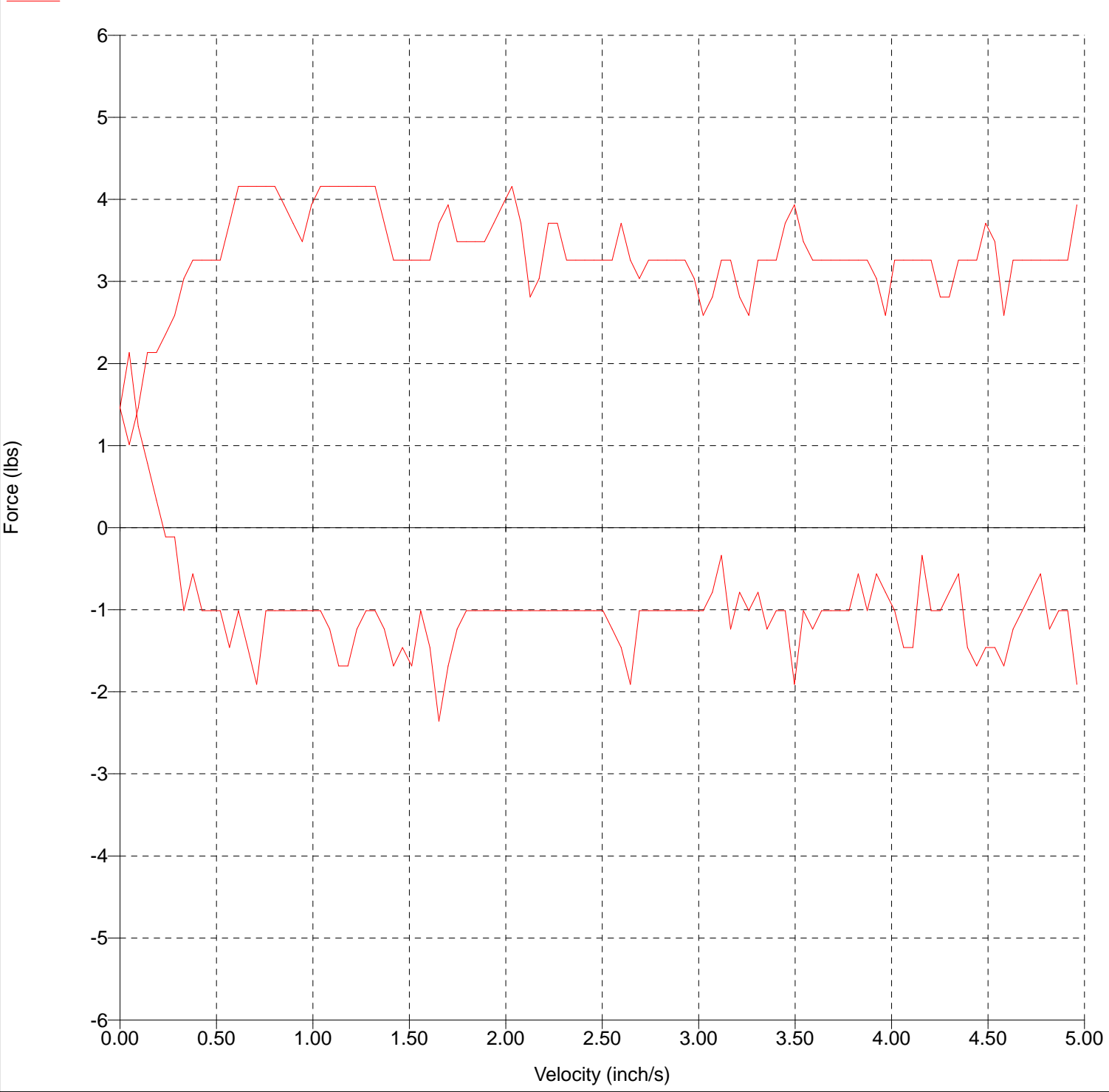
2 PV 5.25 inch/s @ 1.64Hz 28.0C
 B 0, 0 R 0, 0
 MaxF 70 MinF -77 lbs

3 PV 5.25 inch/s @ 1.64Hz 28.0C
 B 0, 0 R 0, 0
 MaxF 71 MinF -75 lbs



File: Penske 7800 with no shims 9-27-12.dat
Shock model: PS-7800 Needle type: Penske 7800 with no shims 9-27-12
Piston comp: degrees Jet checkball:
Piston reb.: degrees Pressure: psi
Piston bleed: Valving C/R: None!

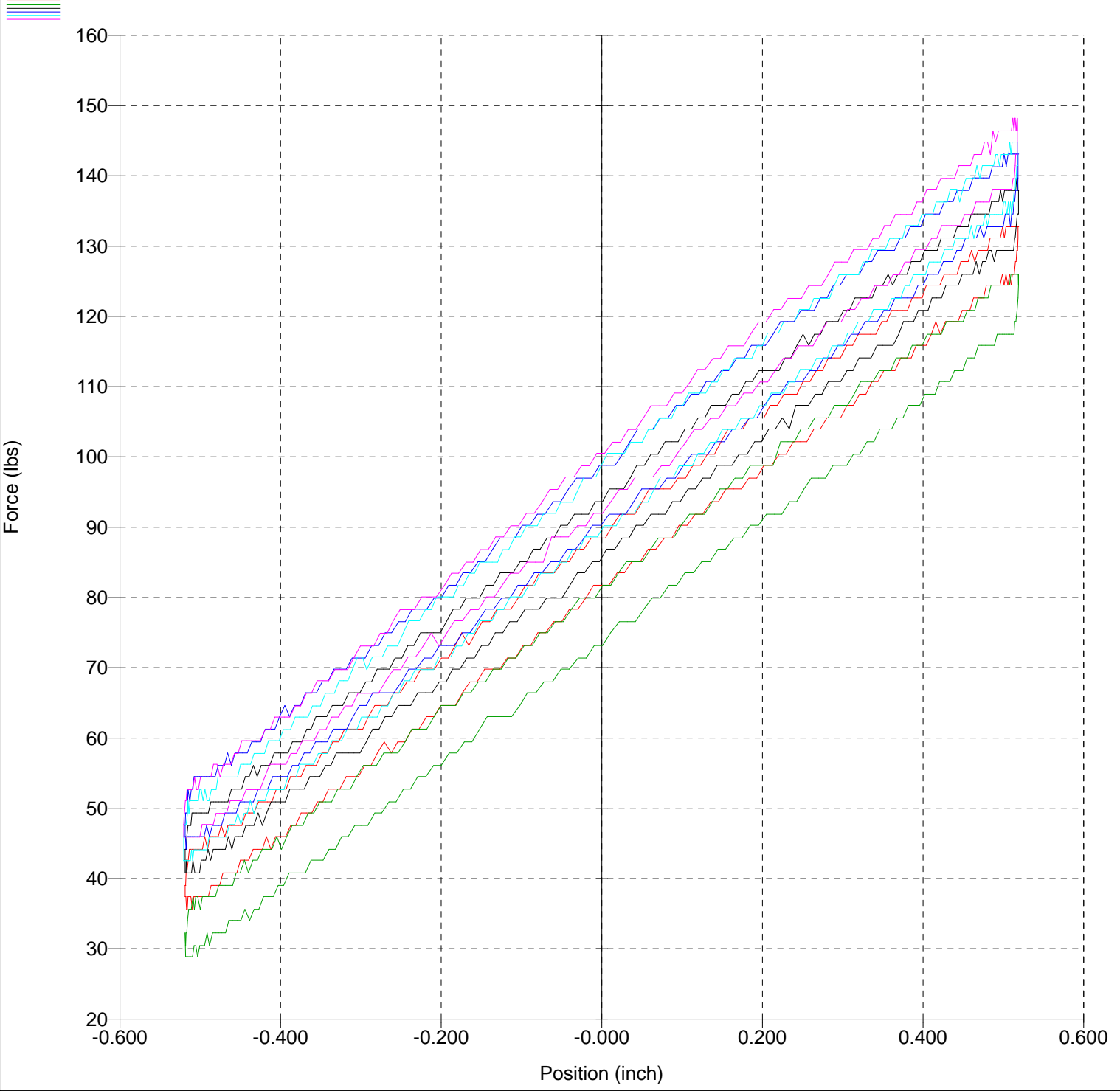
Shock Shop



1 PV 5.04 inch/s @ 1.57Hz 24.9C
B 0, 0 R 0, 0
MaxF 5 MinF -3 lbs



File: OSU FSAE 90# per in spring test 10-16-12.dat
 Shock model: Needle type: OSU FSAE 90#/in spring test 10-16-12
 Piston comp: degrees Jet checkball: Trace 1 is spring #1, etc. 1-4 are new springs
 Piston reb.: degrees Pressure: psi Traces 5 and 6 are used springs
 Piston bleed: Valving C/R:



1 PV 0.51 inch/s @ 0.15Hz 25.7C
 B 0, 0 R 0, 0 SPG
 MaxF 133 MinF 36 lbs

4 PV 0.54 inch/s @ 0.14Hz 26.0C
 B 0, 0 R 0, 0 SPG
 MaxF 143 MinF 44 lbs

2 PV 0.64 inch/s @ 0.18Hz 25.9C
 B 0, 0 R 0, 0 SPG
 MaxF 126 MinF 29 lbs

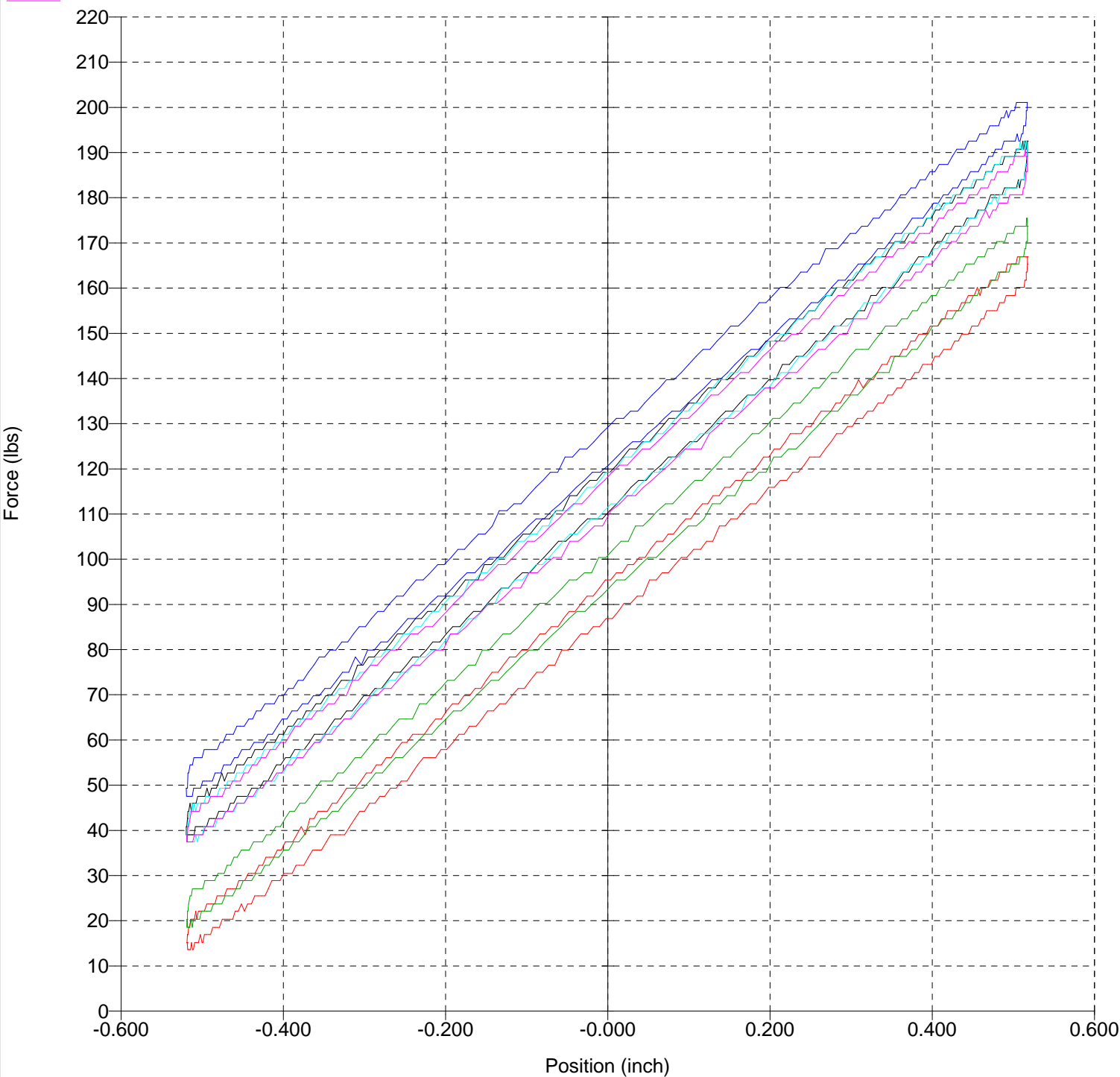
5 PV 0.42 inch/s @ 0.14Hz 25.4C
 B 0, 0 R 0, 0 SPG
 MaxF 145 MinF 43 lbs

3 PV 0.48 inch/s @ 0.14Hz 25.9C
 B 0, 0 R 0, 0 SPG
 MaxF 140 MinF 41 lbs

6 PV 0.56 inch/s @ 0.16Hz 25.7C
 B 0, 0 R 0, 0 SPG
 MaxF 148 MinF 46 lbs



File: OSU FSAE 140# per in spring test 10-16-12.dat
 Shock model: Needle type: OSU FSAE 140#/in spring test 10-16-12
 Piston comp: degrees Jet checkball: Trace 1 is spring #2, etc. 1-6 are new springs.
 Piston reb.: degrees Pressure: psi
 Piston bleed: Valving C/R:



1 PV 0.43 inch/s @ 0.11Hz 25.4C
 B 0, 0 R 0, 0 SPG
 MaxF 167 MinF 14 lbs

4 PV 0.51 inch/s @ 0.13Hz 25.5C
 B 0, 0 R 0, 0 SPG
 MaxF 201 MinF 48 lbs

2 PV 0.52 inch/s @ 0.15Hz 25.4C
 B 0, 0 R 0, 0 SPG
 MaxF 175 MinF 19 lbs

5 PV 0.53 inch/s @ 0.18Hz 25.5C
 B 0, 0 R 0, 0 SPG
 MaxF 193 MinF 37 lbs

3 PV 0.47 inch/s @ 0.13Hz 25.5C
 B 0, 0 R 0, 0 SPG
 MaxF 193 MinF 39 lbs

6 PV 0.59 inch/s @ 0.17Hz 25.7C
 B 0, 0 R 0, 0 SPG
 MaxF 191 MinF 37 lbs

C APPENDIX C Strain gauge calibration

Spreadsheet result in readable size

| GFR 2011 Susp Forces Test / Calibration | | | | | | Input | Calulated | |
|--|--|--------|--------------|---------|--|-----------------|-----------|---------|
| Date: | 15-Nov-2012 | | | | | Initial Results | | |
| Setup | Description | Corner | Applied Load | Applied | Expected Load Result | Result | Error | Error |
| Applied Weights On Wheels | | | | | | | | |
| 1 | FL Vertical Load Light | FL | -Dir-Z | -105.31 | FL susp Force Dir-Z = Applied Load | -99.2 | 6.11 | -5.80% |
| 2 | FL Vertical Load High | FL | -Dir-Z | -199.44 | FL susp Force Dir-Z = Applied Load 2 | -197.24 | 2.20 | -1.10% |
| 3 | FR Vertical Load Light | FR | -Dir-Z | -105.31 | FL susp Force Dir-Z = Applied Load | -91.4 | 13.91 | -13.21% |
| 4 | FR Vertical Load High | FR | -Dir-Z | -199.44 | FL susp Force Dir-Z = Applied Load 2 | -184.1 | 15.34 | -7.69% |
| 5 | RL Vertical Load Light | RL | -Dir-Z | -105.31 | FL susp Force Dir-Z = Applied Load | -110.54 | -5.23 | 4.97% |
| 6 | RL Vertical Load High | RL | -Dir-Z | -199.44 | FL susp Force Dir-Z = Applied Load 2 | -207.66 | -8.22 | 4.12% |
| 7 | RR Vertical Load Light | RR | -Dir-Z | -105.31 | FL susp Force Dir-Z = Applied Load | -109.96 | -4.65 | 4.42% |
| 8 | RR Vertical Load High | RR | -Dir-Z | -199.44 | FL susp Force Dir-Z = Applied Load 2 | -206.79 | -7.35 | 3.69% |
| Strap With Ratchet Induced | | | | | | | | |
| 9 | FL+RL Longitudinal Load Light 1 | FL | +/-Dir-X | -185.02 | -FL susp Force Dir-X = Applied Load | -189.143 | -4.13 | 2.23% |
| 10 | FL+RL Longitudinal Load Light 1 | RL | +/-Dir-X | 185.02 | RL susp Force Dir-X = Applied Load | 173.89 | -11.13 | -6.01% |
| 11 | FL+RL Longitudinal Load Light 2 | FL | +/-Dir-X | -155.59 | -FL susp Force Dir-X = Applied Load | -154.482 | 1.10 | -0.71% |
| 12 | FL+RL Longitudinal Load Light 2 | RL | +/-Dir-X | 155.59 | RL susp Force Dir-X = Applied Load | 150.98 | -4.61 | -2.96% |
| 13 | FL+RL Longitudinal Load High | FL | +/-Dir-X | -375.53 | -FL susp Force Dir-X = Applied Load 2 | -389.874 | -14.35 | 3.82% |
| 14 | FL+RL Longitudinal Load High | RL | +/-Dir-X | 375.53 | RL susp Force Dir-X = Applied Load 2 | 375.57 | 0.04 | 0.01% |
| 15 | FR+RR Longitudinal Load Light | FR | +/-Dir-X | -195.22 | -FL susp Force Dir-X = Applied Load | -205.32 | -10.10 | 5.17% |
| 16 | FR+RR Longitudinal Load Light | RR | +/-Dir-X | 195.22 | RL susp Force Dir-X = Applied Load | 202.603 | 7.38 | 3.78% |
| 17 | FR+RR Longitudinal Load High | FR | +/-Dir-X | -393.18 | -FL susp Force Dir-X = Applied Load 2 | -400.36 | -7.18 | 1.82% |
| 18 | FR+RR Longitudinal Load High | RR | +/-Dir-X | 393.18 | RL susp Force Dir-X = Applied Load 2 | 404.32 | 11.14 | 2.83% |
| Lateral Y Direction (Car On Side) | | | | | | | | |
| 19 | Lateral Load Right Base | FR | Dir-Y | 476.18 | FR susp Force Dir-Y = Front Axel Mass - FR Outboard | 454 | -22.18 | -4.66% |
| 20 | Lateral Load Right Light | FL | -Dir-Y | -180.95 | -FL susp Force Dir-Y = Applied Load + FL Outboard | -193.6 | -12.65 | 6.99% |
| 21 | Lateral Load Right Light | FR | Dir-Y | 581.49 | FR susp Force Dir-Y = Front Axel Mass - FR Outboard + Applied Load | 554.6 | -26.89 | -4.62% |
| 22 | Lateral Load Right High | FL | -Dir-Y | -275.07 | -FL susp Force Dir-Y = Applied Load 2 + FL Outboard | -282.1 | -7.03 | 2.55% |
| 23 | Lateral Load Right High | FR | Dir-Y | 675.61 | FR susp Force Dir-Y = Front Axel Mass - FR Outboard + Applied Load 2 | 647.1 | -28.51 | -4.22% |
| 24 | Lateral Load Right Base | RR | Dir-Y | 769.69 | RR susp Force Dir-Y = Rear Axel Mass - RR Outboard | 740.84 | -28.85 | -3.75% |
| 25 | Lateral Load Right Light | RL | -Dir-Y | -189.87 | -RL susp Force Dir-Y = Applied Load + RL Outboard | -198.87 | -9.00 | 4.74% |
| 26 | Lateral Load Right Light | RR | Dir-Y | 875.00 | RR susp Force Dir-Y = Rear Axel Mass -RR Outboard + Applied Load | 841.75 | -33.25 | -3.80% |
| 27 | Lateral Load Right High | RL | -Dir-Y | -284.00 | -RL susp Force Dir-Y = Applied Load 2 + RL Outboard | -292.82 | -8.82 | 3.11% |
| 28 | Lateral Load Right High | RR | Dir-Y | 969.13 | RR susp Force Dir-Y = Rear Axel Mass -RR Outboard + Applied Load 2 | 934.91 | -34.22 | -3.53% |
| 29 | Lateral Load Left Base | FL | Dir-Y | -480.59 | FL susp Force Dir-Y = Front Axel Mass - FL Outboard | -503.57 | -22.98 | 4.78% |
| 30 | Lateral Load Left Light | FR | -Dir-Y | 185.36 | -FR susp Force Dir-Y = Applied Load + FR Outboard | 181.8 | -3.56 | -1.92% |
| 31 | Lateral Load Left Light | FL | Dir-Y | -585.90 | FL susp Force Dir-Y = Front Axel Mass -FL Outboard + Applied Load | -602.7 | -16.80 | 2.87% |
| 32 | Lateral Load Left High | FR | -Dir-Y | 279.49 | -FR susp Force Dir-Y = Applied Load 2 + FR Outboard | 266.4 | -13.09 | -4.68% |
| 33 | Lateral Load Left High | FL | Dir-Y | -680.03 | FL susp Force Dir-Y = Front Axel Mass -FL Outboard + Applied Load 2 | -690.9 | -10.87 | 1.60% |
| 34 | Lateral Load Left Base | RL | Dir-Y | -769.69 | RL susp Force Dir-Y = Rear Axel Mass - RL Outboard | -698.84 | 70.85 | -9.21% |
| 35 | Lateral Load Left Light | RR | -Dir-Y | 192.13 | -RR susp Force Dir-Y = Applied Load + RR Outboard | 195.47 | 3.34 | 1.74% |
| 36 | Lateral Load Left Light | RL | Dir-Y | -875.00 | RL susp Force Dir-Y = Rear Axel Mass - RL Outboard + Applied Load | -804.4 | 70.60 | -8.07% |
| 37 | Lateral Load Left High | RR | -Dir-Y | 286.26 | -RR susp Force Dir-Y = Applied Load 2 + RR Outboard | 285.44 | -0.82 | -0.28% |
| 38 | Lateral Load Left High | RL | Dir-Y | -969.13 | RL susp Force Dir-Y = Rear Axel Mass - RL Outboard + Applied Load 2 | -902.27 | 66.86 | -6.90% |
| Static Car Weight Contributions | | | | | | | | |
| 39 | Full Car Vertical Static Test 1 | FL | -Dir - Z | 269.21 | FL Susp Force Dir-Z = FL Corner Weight | 279.16 | 9.95 | 3.70% |
| 40 | Full Car Vertical Static Test 1 | FR | -Dir - Z | 287.01 | FR Susp Force Dir-Z = FR Corner Weight | 283.24 | -3.77 | -1.31% |
| 41 | Full Car Vertical Static Test 1 | RL | -Dir - Z | 407.15 | RL Susp Force Dir-Z = RL Corner Weight | 464.58 | 57.43 | 14.10% |
| 42 | Full Car Vertical Static Test 1 | RR | -Dir - Z | 449.42 | RR Susp Force Dir-Z = RR Corner Weight | 466.06 | 16.64 | 3.70% |
| 43 | Full Car Vertical Static Test + Driver | FL | -Dir - Z | 516.17 | FL Susp Force Dir-Z = FL Corner Weight | 554.87 | 38.70 | 7.50% |
| 44 | Full Car Vertical Static Test + Driver | FR | -Dir - Z | 520.62 | FR Susp Force Dir-Z = FR Corner Weight | 534.16 | 13.54 | 2.60% |
| 45 | Full Car Vertical Static Test + Driver | RL | -Dir - Z | 596.27 | RL Susp Force Dir-Z = RL Corner Weight | 639.58 | 43.31 | 7.26% |
| 46 | Full Car Vertical Static Test + Driver | RR | -Dir - Z | 614.06 | RR Susp Force Dir-Z = RR Corner Weight | 646.7 | 32.64 | 5.31% |
| 47 | Full Car Vertical Static Test 2 | FL | -Dir - Z | 273.66 | FL Susp Force Dir-Z = FL Corner Weight | 286.08 | 12.42 | 4.54% |
| 48 | Full Car Vertical Static Test 2 | FR | -Dir - Z | 282.56 | FR Susp Force Dir-Z = FR Corner Weight | 302.37 | 19.81 | 7.01% |
| 49 | Full Car Vertical Static Test 2 | RL | -Dir - Z | 418.28 | RL Susp Force Dir-Z = RL Corner Weight | 459.82 | 41.54 | 9.93% |
| 50 | Full Car Vertical Static Test 2 | RR | -Dir - Z | 438.30 | RR Susp Force Dir-Z = RR Corner Weight | 466.68 | 28.38 | 6.48% |

D APPENDIX D Excerpts from logged data

D1 Driver comments

| Damper | Bump? | Overall handling | Lateral grip | Direction change | My driving | Comments |
|------------|-------|------------------|--------------|------------------|------------|---|
| Baseline | N | 7 | 7 | 8 | 9 | slow skidpad was easy to stay consistent. Easier to go left (outside lane) on skid pad cause you have more room. Track felt better the more laps I ran. Will try to be more consistent next run. |
| Baseline | Y | 7 | 7.3 | 8 | 9 | Turning right on skidpad felt more consistent [<i>sic</i>] by using the same throttle and more use of steering for race line corrections. I can definitely feel the front tires bump across more so than the rear. Which makes it more understeer over the bump rather than rear/oversteer unsettling. |
| Stiff | N | 7.1 | 7.5 | 7.7 | 9 | Mystery dampers :) car felt more stable, easier to make smaller adjustments after turn-in and during constant [<i>sic</i>] steering angles. Downshifts better when under braking. |
| Stiff | Y | 7 | 7 | 7.7 | 8 | The car reaction from bump wasn't as noticeable. The track felt faster, got up to higher rpm in 2nd gear. Natural bumps on the pavement seemed to unsettle the car more than the first runs. |
| No Damping | N | 7.1 | 6.5 | 8 | 9 | Felt like the whole car was on a trampoline or like a boat going over waves. The car would immediately spring up reacting to any bump on the pavement. Seemed like turn in was better but more difficult to keep car from oversteering. |
| No Damping | Y | 6.5 | 6.5 | 7.5 | 9.1 | High speed right skid pad was very noticeable going over the bump. It felt like the whole car jumped off the ground on the outside tires making more oversteer than understeer. Going over the bump straight at both high and low speeds I could definitely [<i>sic</i>] feel the car going over the bump. Didn't unsettle the car as much when turning left in skid pad. |
| Hardlinks | N | 3 | 2 | 1 | 8.5 | Really, really uncontrollably bumpy. The car would start skidding out (understeer) when trying to turn in. Car didn't [<i>sic</i>] feel stable at any point. Throttle control was difficult because of the jerky/bumps/twitches |
| Hardlinks | Y | 2 | 2 | 1 | 6 | The bump wasn't the most unstable or noticeable surface. It felt more bumpy going over the seams in the pavement. Overall it was pretty bouncy and hard vibrations. Especially under braking while downshifting. Throttle control was again difficult going over the natural bumps in the pavement but not so much over test bump. |
| Baseline | Y | 7.5 | 8 | 8 | 9 | Felt way better with actual dampers. Felt better as the temps increased with the sun. Seemed like everything got hotter quicker. Way more balanced after turn in and did not feel the pavement bumps or test bump as much. |

TABLE 0.1: Driver comments collected during round 2 testing

D2 Round 2 straight without bump FFTs

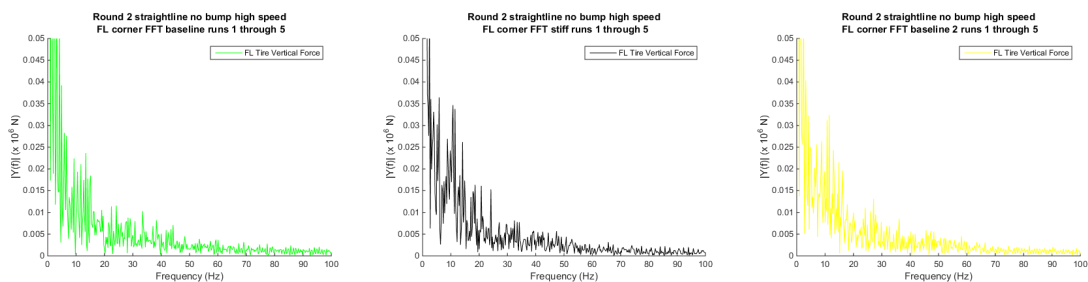


FIGURE 0.4: Round 2 straight no bump high speed FFTs

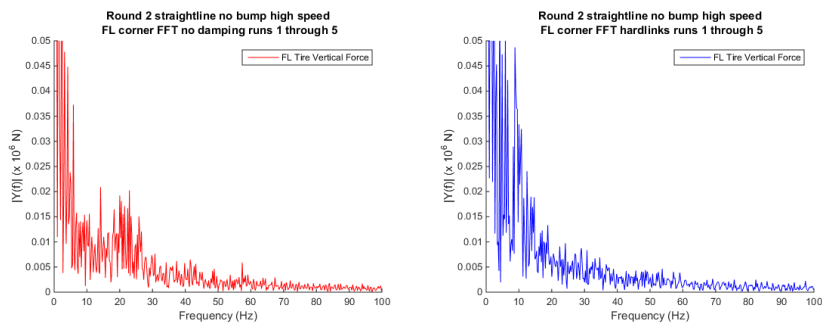


FIGURE 0.5: Round 2 straight no bump high speed FFTs

D3 Round 1 skidpad without bump FFTs

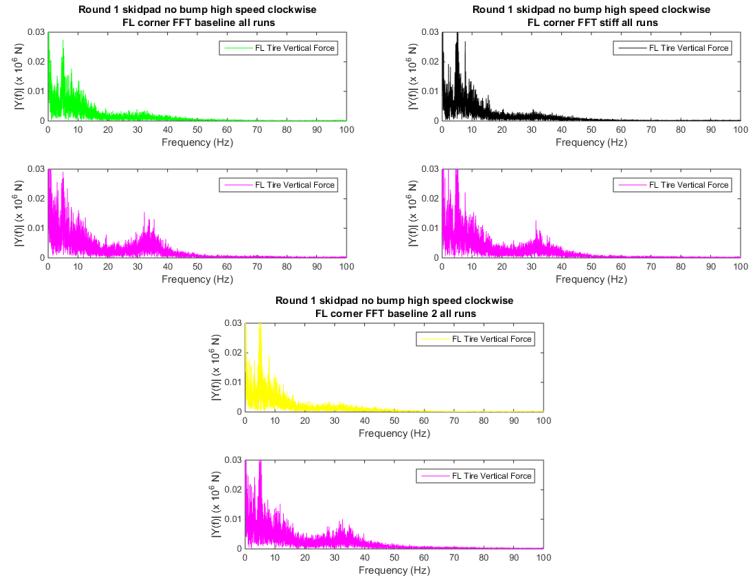


FIGURE 0.6: Round 1 skidpad FFT

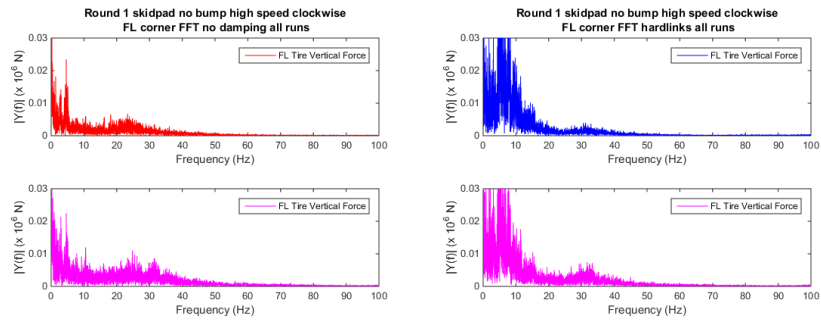


FIGURE 0.7: Round 1 skidpad FFT

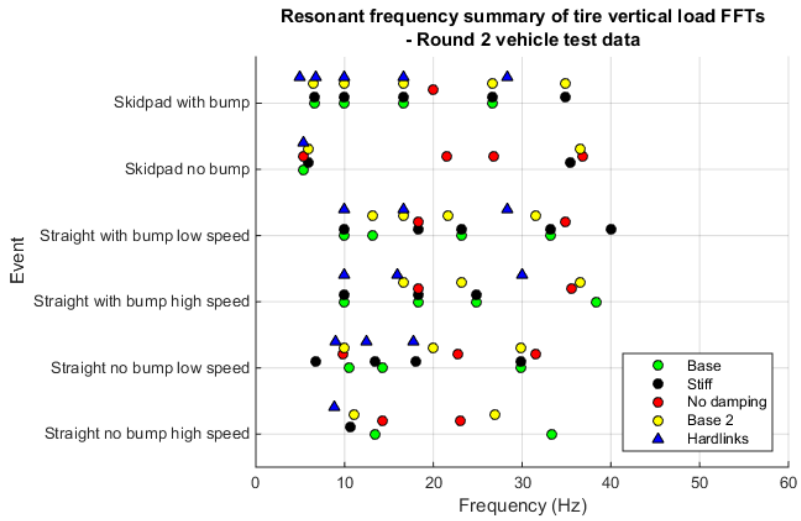


FIGURE 0.8: Summary of Round 2 vertical tire load resonant frequencies

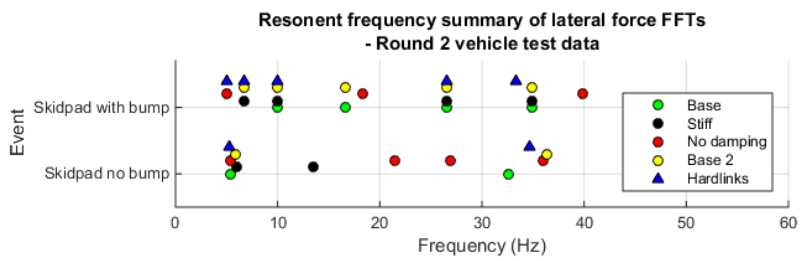


FIGURE 0.9: Summary of Round 2 lateral force resonant frequencies

D4 Round 2 resonant frequency summary

D5 Damper speeds

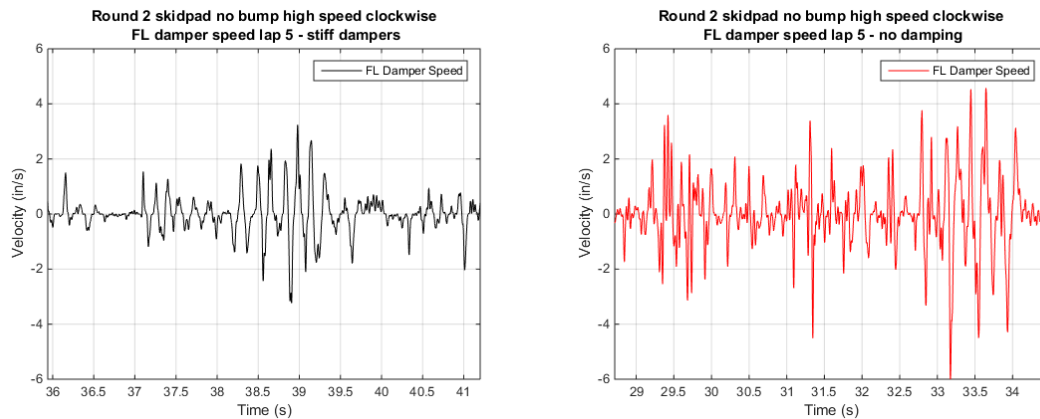


FIGURE 0.10: Damper speeds in round 2 skidpad without bump

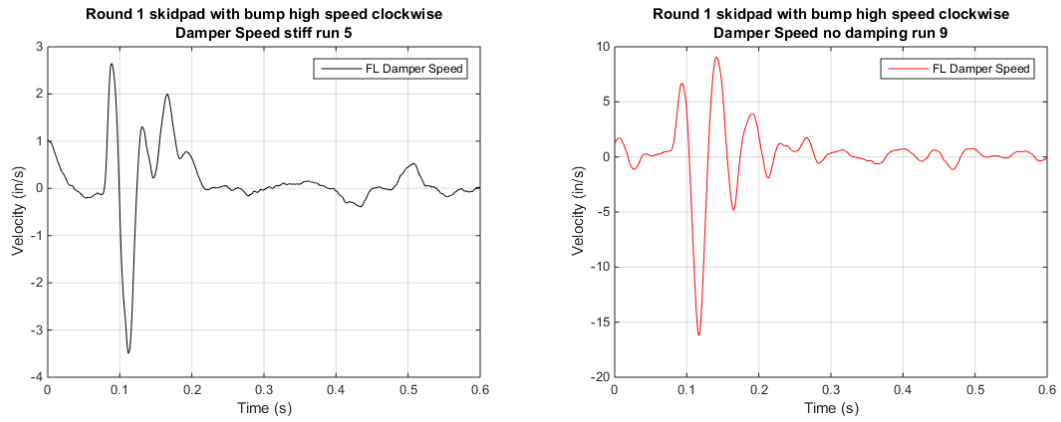


FIGURE 0.11: Damper speeds over bump in round 1

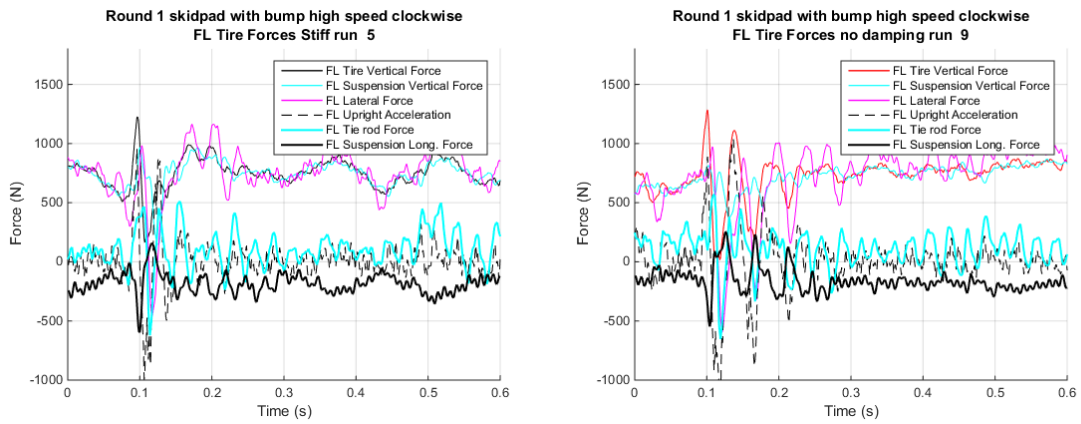


FIGURE 0.12: Tire forces over bump in round 1

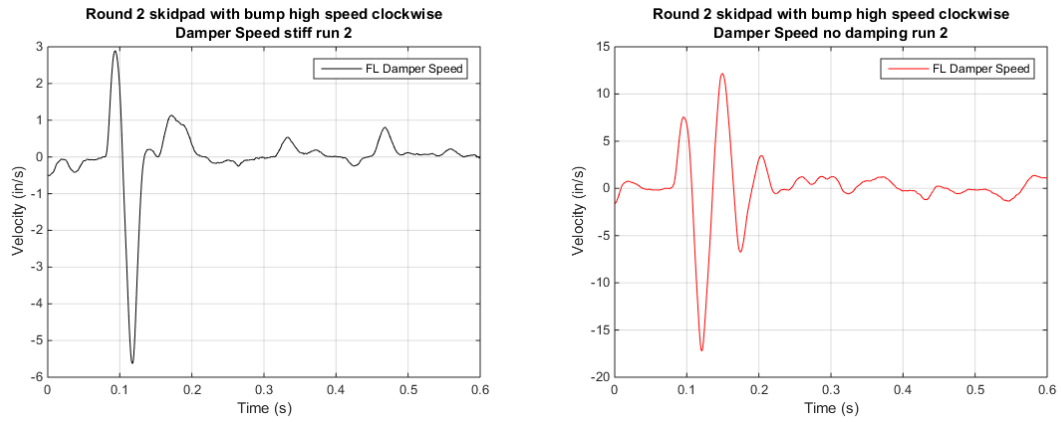


FIGURE 0.13: Damper speeds over bump in round 2

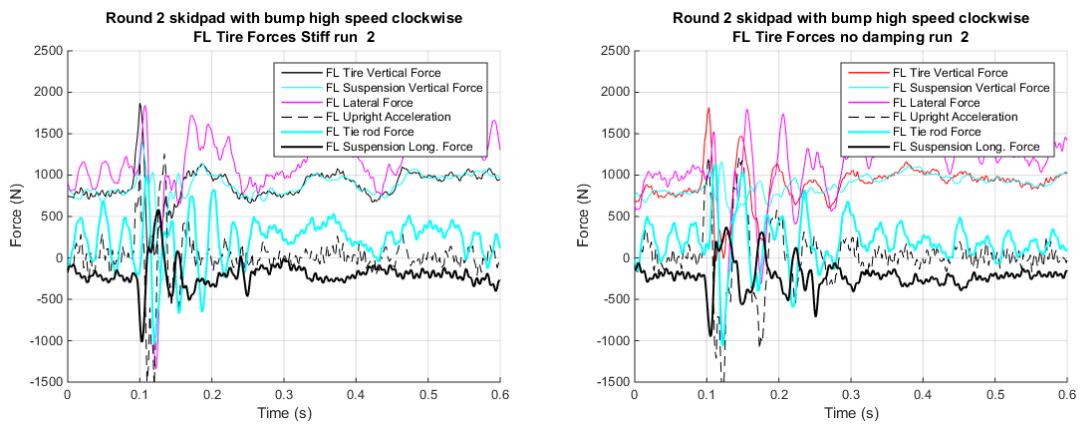


FIGURE 0.14: Tire forces over bump in round 2

D6 Driver inputs

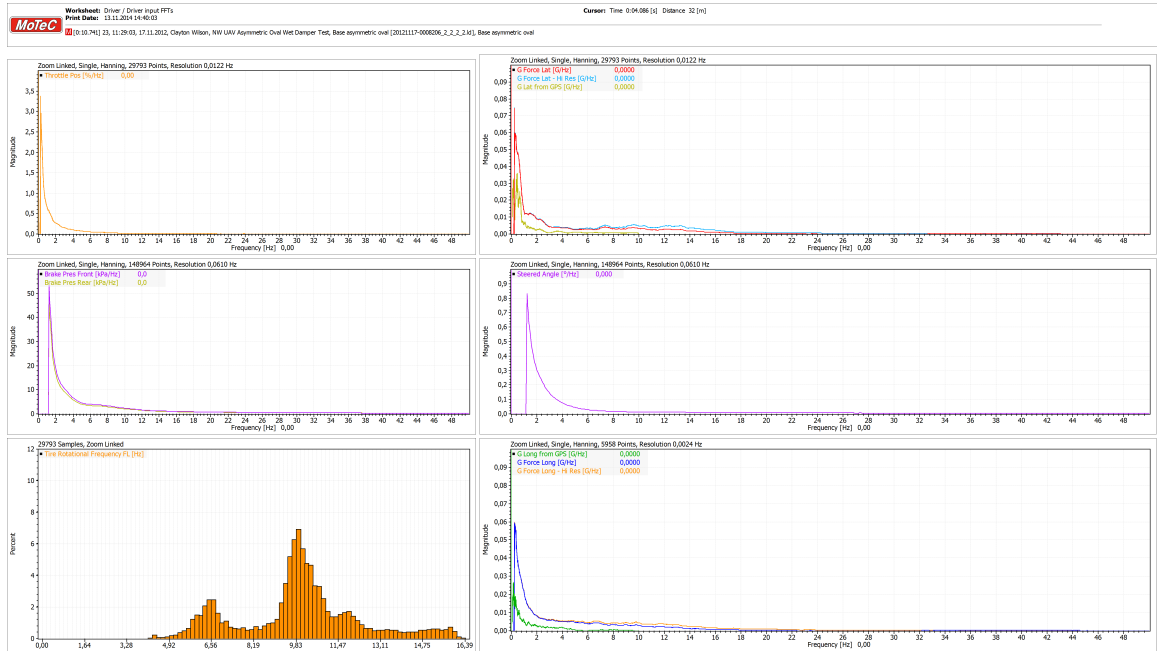


FIGURE 0.15: Driver input and vehicle acceleration FFTs used to determine tire vertical load variation filter cutoff frequency

E APPENDIX E Round 1 Test day photos



